Crustal structure of the SE Carpathians and its foreland from densely spaced geophysical data

Contents

CHAPTER I
INTRODUCTION

"Every known fact in natural science was divined by the presentiment of somebody, before it was actually verified."

Ralph Waldo Emerson

1.1. To-be's and to-do's

This thesis will examine what are the crustal structures of the south-eastern Carpathians, Vrancea Zone and Focsani Basin in Romania (Figure 1.1) and what are the implications of these to the past and present geodynamics of the region. This work has three objectives:

- first, to conduct novel methods of data acquisition, suitable to rough topography conditions and remarkably complicated shallow or deep rooted geological structures and to adopt specific (innovative) data processing flows and techniques;

- second, to model the data using geophysical forward and/or inverse methods and afterwards to interpret physically the models together with their resolution, robustness, error tests or estimation;

- and third, to integrate the results from different sets of data and to infer local and regional geotectonic interpretations.

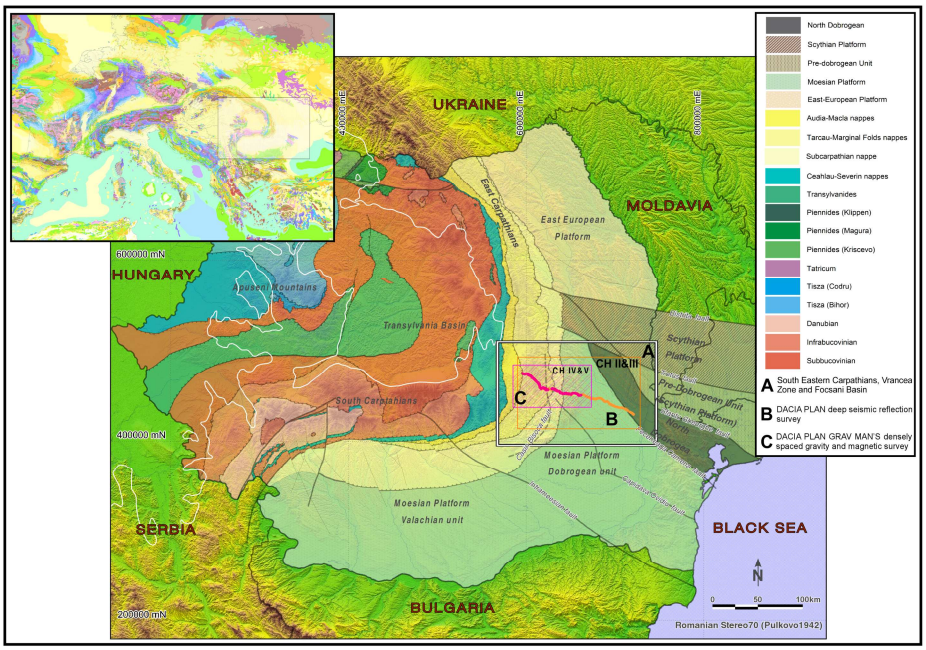

Fig.1.1. Tectonic map of Romania modified after Schmid et al. (2008) overlapping the 90 metres resolution Romanian DEM derived from the Shuttle Radar Topography Mission data sets (National Geospatial-Intelligence Agency - NGA and the National Aeronautics and Space Administration - NASA) and projected to the Pulkovo 1942 Romania Stereo70 system.

The south-eastern Carpathians represents a highly arcuate Alpine orogenic belt formed as a result of Triassic to Early Cretaceous rifting and passive margin evolution between European and Apulian plates (Schmid et al., 2008) followed by convergent movements from Late Cretaceous to Miocene. The Vrancea Zone represents a highly active seismic zone where crustal and intermediate mantle earthquakes occur with magnitudes up to 7.5, located beneath the external thin-skinned thrust belt of the south-eastern Carpathians at depths up to 220 km (Oncescu and Bonjer, 1997, Bala et al., 2003). The Focsani Basin is characterised by up to 13 km thick Middle Miocene to Quaternary sediments (Tarapoanca et al., 2003) that overlie older Palaeozoic-Mesozoic deposits (e.g., Visarion et al., 1988). These sediments are part of the Carpathians foreland, which is composed of two, internally complex, relatively stable areas, the East European/Scythian and the Moesian platforms, partly separated by the North Dobrogea orogen (e.g., Sandulescu and Visarion 1998). The latter is thought to comprise compressional structures of Mid-Jurassic age (Cimmerian orogeny) but the Alpine deformations dominate (Saintot et al. 2005).

A number of geodynamic models have been proposed for the area during its post-collisional stage (11-0 Ma): single or double subduction, slab detachment, oceanic or continental lithosphere delamination, thermal re-equilibration, other lithospheric instabilities and/or combinations of these (see e.g. discussions in

Heidbach et al., 2007, Matenco et al., 2007, and references therein). All of these models were developed in the context of the active present-day seismicity and observed high-velocity mantle anisotropy of the Vrancea seismogenic zone (Martin et al., 2006).

Two regional refraction/wide-angle surveys, VRANCEA99 and VRANCEA2001, were carried out in order to study the crustal and uppermost mantle structure of the Vrancea Zone and surroundings (cf. Hauser et al., 2002). The VRANCEA99 profile revealed an upper crust characterised by specific velocities (5.9–6.2 km/s) and a lower crust defined by higher velocities (6.7–7.0 km/s) separated by an intra-crustal discontinuity between 18–31 km depth (Hauser et al., 2001; Fig. 1.2). The depth to the Moho increases from 38 km at the northern end of the profile to 41 km beneath the Vrancea Zone (where it crosses the DACIA-PLAN profile - Danube and Carpathian Integrated Action on Processes in the Lithosphere and Neotectonics; Fig. 1.2) and furthermore decrease to about 30 km near the southern end of the profile (Hauser et al., 2002). The VRANCEA2001 profile (acquired in conjunction with DACIA PLAN; Fig. 1.2) indicates a thickening of the sedimentary cover of the Focsani Basin, from east to west (Hauser et al., 2007). The Moho depth under the Carpathians is about 40 km. Its presence was based partly on the occurrences of a strong reflection from the crust–mantle boundary. The Moho topography inferred from this seismic study was used as input information for the modelling of the gravity and magnetic data from the DACIA PLAN GRAV MAN'S profile (Danube and Carpathian Integrated Action on Processes in the Lithosphere and Neotectonics Gravity and Magnetic Survey; Fig. 1.2). Other deep reflection surveys (DRACULAs - Deep Reflection Acquisition Constraining Unusual Lithospheric Activity; Knapp et al., 2005; Fig. 1.2) were carried out during the summer of 2004 and shows reflectivity throughout the crust and upper mantle beneath the Carpathian hinterland (down 30 s TWT) and foreland (at 36 s TWT). High-resolution teleseismic body-wave tomography beneath the south-eastern Carpathians and surrounding showed travel times delays of up to 1.3 s and are caused by the almost 20-km thick layer of sediments in the Focsani Basin (Martin et al., 2005). A stand alone 3D upper crust tomographic velocity model (Landes et al., 2004) based on VRANCEA99 and VRANCEA 2001 data showed an upper crustal high-velocity zone, above the northern Vrancea seismic zone. The high-velocity zone below the flysch nappes is explained by an out-of-sequence thrust of the crystalline basement. Older DSS studies (Radulescu et al., 1976; Fig. 1.2) reveal lateral crustal heterogeneity across the Peceneaga–Camena and Capidava–Ovidiu faults whilst the succession of the sedimentary layers from Focsani Basin reaches a thickness of 12 km.

After revising the present and presented models and interpretations this thesis aims to formulate several general questions that are then attempted to be answered. What are the upper crustal structures that sustain the south-eastern Carpathians and its foreland basin architecture? Is the novel seismic acquisition

technique resolute enough to provide a robust interpretation? Are the previously known and constrained geological structures embodied by or consistent with seismic velocity models? What are the tectonic and geological processes behind the structures and their contacts? Does the geologically constrained and driven seismic ray tracing forward modelling offer sufficient information about the robustness of the coincidental seismic tomography model and does it provide additional information for structural interpretation? Do the gravity and magnetic models fit with the seismic models? Is there any physical evidence for crustal heterogeneity? Can the theoretically non-unique solution for any potential field model become a particularly unique materialisation for a model that integrates differently sourced, independent data? Do densely spaced geophysical data illuminate crustal structure?

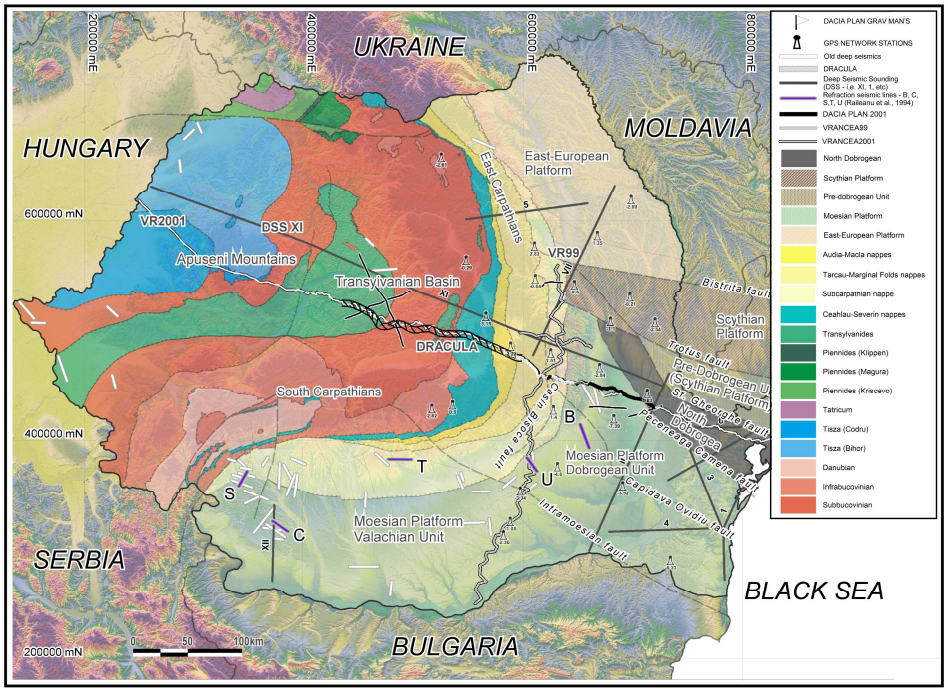

Fig. 1.2 Tectonic map of Romania modified after Schmid et al. (2008). Bottom layer shows the Romanian 90 m resolution Digital Elevation Model (Pulkovo 1942/Stereo70 coordinate system) derived from World Global SRTM. Overlay shows: fundamental deep reflection/refraction lines in Romania (i.e. Radulescu et al., 1976, Cornea et al., 1981, Raileanu et al., 1994, Hauser et al., 2001,2007, Bocin et al., 2005, Knapp et al., 2005, Panea et al., 2005,); and, Romanian GPS Network permanent stations (IGS and ISES) and multi annual vertical movement solutions (mm/year values; Hoeven et al., 2005).

All these questions arose while working with the data, consulting an endless number of publications about the origin of the Vrancea Zone and by consulting and discussing with various scientists. The mentioned questions where treated one after another through the thesis and though they elucidated some issues, the author is acutely

conscious that they raised others. The studies focused on what mainly could be expressed within the possibilities and stopped where the imagination took over scientific rigorousness.

The working progress of this thesis followed "*a developing story scenario*" when what was at first became an inverse seismic tomographic experiment then developed into an accompanying forward ray tracing structural and geophysical report on upper crustal structures. It continued by constraining the seismic information and by concluding through a gravity and magnetic modelling analysis the condition of the crustal scale geological structures and their interpretation in an historical and regional context.

1.2. Natural Laboratory

The south eastern Carpathians and the adjoined major units constitutes a complex geological system linked with the regional present/past Carpathian Pannonian region processes and evolution. The orogenic wedge and its surrounding areas associated with crustal movements and active seismicity represents a *natural laboratory* that examines the tectonic processes and their historicity and the correlation of these processes from landscape evolution to lithosphere dynamics. This thesis investigates geophysically and tectonically a number of major structures such as the Carpathians nappes, Moesian Platform or Focsani Basin but not excluding other adjacent units. The present section introduces the fundamentals of the Moesian Platform geology, its crustal architecture (i.e., controls on the Moho) and the numerous geodynamical models that defines the lithospheric structure beneath the south eastern Carpathians. That said and done it would provide to the readers (about this natural laboratory) the necessary basic regional geological geodynamical information.

1.2.1. The Moesian Platform

The previous studies in the northern and central Europe confirmed that the western margin of the East European craton is represented by the Trans-European Suture Zone (TESZ), the fundamental lithospheric boundary in Europe. This zone represents the contact between the crust of the East European craton, which is thicker and denser, and the Phanerozoic-accreted Europe. The East European craton has the base of the lithospheric mantle significantly deeper, too. The prolongation of this zone to the south eastern Europe (Romanian territory) remains blurred owed to the fact that the entire zone is overlain by the Carpathians and a thick foreland sedimentary basin. The Moesian Platform is located contingent and juxtaposed to the south western extremity of the East European craton margin. Across this margin there were accreted to Baltica two types of terranes: Eastern Avalonian terranes accreted during Late Ordovician-Early Devonian; and, terranes formed as Baltican during Cambrian,

displaced from it, and latter accreted along with Eastern Avalonian terranes. The Moesian Platform contains four distinct terranes, two with Baltican and two with Avalonian crustal affinities. A younger fifth terranes, the North Dobrogea (records Variscan accretion) lies between the Moesian Platform and the East European craton. Furthermore, the integration of present geological and geophysical information lead to the conclusion that the Moesian Platform is divided into three main units: the Dobrogean unit, the Valachian unit and the Danubian unit (Fig. 1.1 and 1.2). The Scythian Platform and Pre-Dobrogean unit to the north are separated from the East European craton by Bistrita fault and to the south from Nord Dobrogea unit by Sfantul Gheorghe and Trotus fault. The Dobrogean unit of the Moesian Platform is bounded to the east by the crustal scale Peceneaga-Camena fault. The Valachian and Dobrogean units are separated by the presently active Intramoesian fault.

The thick sedimentary cover of the Moesian Platform exceeding in some areas 10 km (i.e. Focsani Basin ~ 13 km; Tarapoanca et al., 2003) is traditionally split into four main mega sequences (Paraschiv et al, 1979). Figure 1.3 shows the Phanerozoic lithostratigraphy of the Moesian Platform for the Romanian territory. This lithostratigraphic column shows that within some major unconformities the following sequences are present: the Middle Cambrian-Upper Carboniferous, the Permian-Upper Triassic, the Jurassic-Senonian and the Palaeogene-Quaternary (Tari et al., 1997). Subsequently, the Middle Cambrian-Upper Carboniferous can be further subdivided into three main lithological subunits that reaches up to 5500 m in total thickness: the lower clastic group, the carbonate group and the upper clastic group. The Permian-Triassic sedimentary sequence, partially or completely missing in some areas due to post-deposition erosion (or non-depositional causes?), is separated into three units: the lower red clastic group (the thickest reaching up to 2700 m), the carbonate group and the upper red clastic group. Magmatic activity is recorded within this mega sequence whereas in the beginning of Permian and Middle-Upper Triassic boundary pyroclastites and effusive rocks are produced. The Jurassic-Cretacic mega sequence that reaches up to 3500 m thickness is separated too in three main depositional arrangements and characterised by carbonate development. Finally, the Palaeogene-Neogene mega sequence is split into three main sedimentary successions: Palaeocene and Eocene marls, sandstone and locally carbonates; a very thick Neogene succession greater than 5500 m in the inner parts of the Carpathians and north eastern sector of the platform composed from shallow water carbonates covered by deep water clastics, marls and sandstones; and the Quaternary formations up to 200 m thickness that contains continental clastics.

Figure 1.4 shows the Moesian Platform crustal structure in terms of seismic properties recorded in different areas. The deep seismic studies (DSS) suggest that the crust is highly heterogeneous in depth and composition. Within the Moesian Platform are differentiated seismically a middle-crust with short and subhorizontal

events, a crust-mantle transition zone in the western sector, and an variable visible Moho discontinuity and some subcrustal reflectivity.

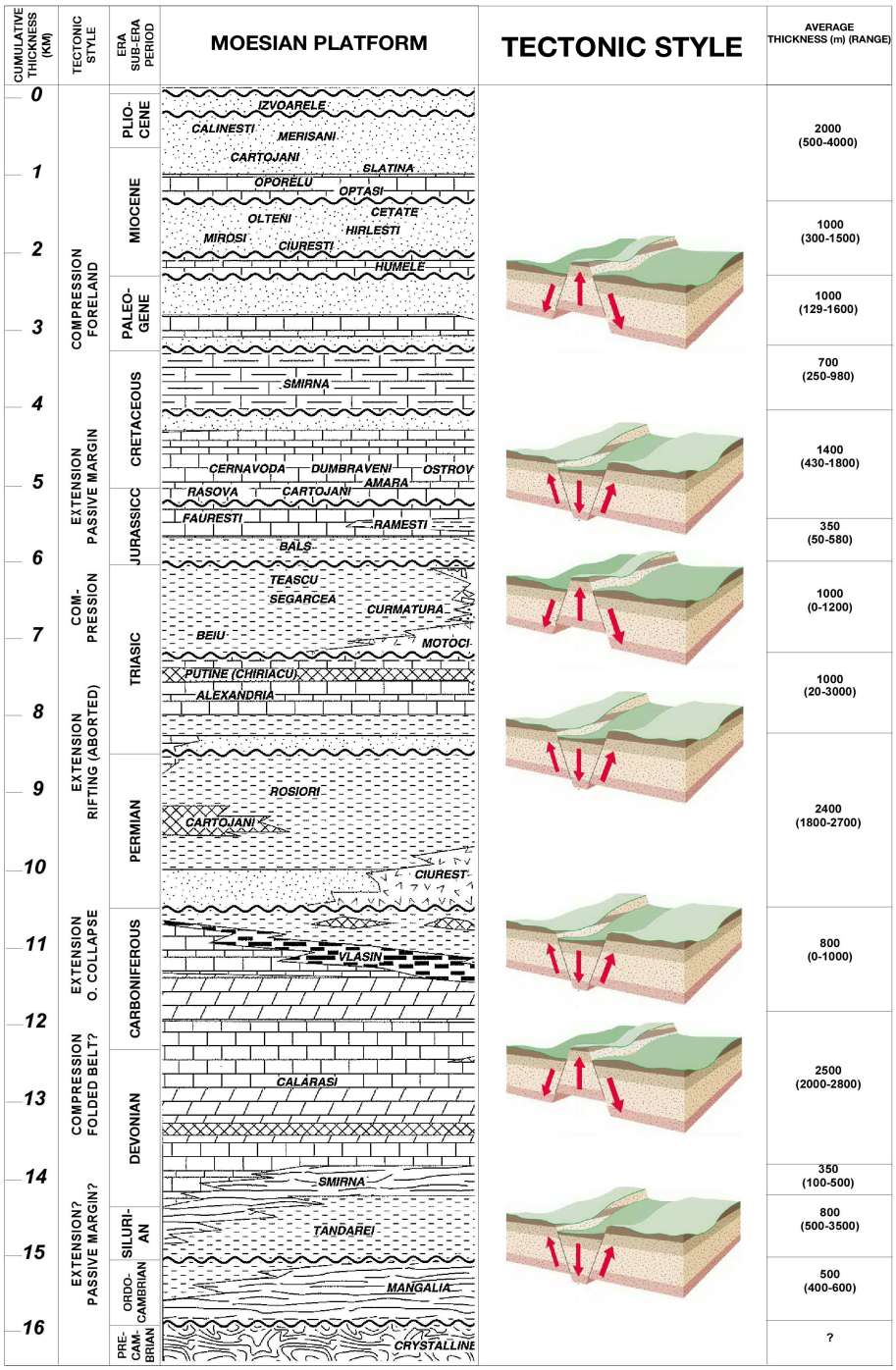

Fig. 1.3. Synthetic lithostratigraphic column for the Moesian Platform compiled from Tari et al. (1997).

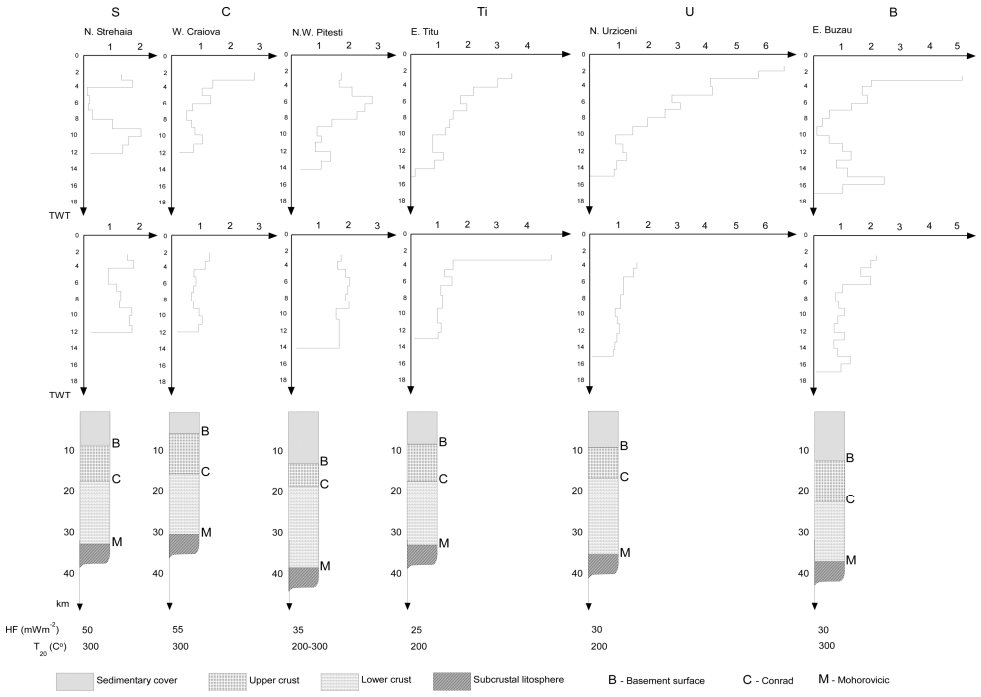

Fig. 1.4. Reflectivity histograms and crustal models for some lines belonging to the Moesian platform and southern Carpathian foredeep modified after Raileanu et al., 1994. The first row of graphs presents histograms with the density of reflections. The second row of graphs shows histograms with the average length of reflections. The third row shows synthetic columns of crustal composition (Radulescu, 1979, Talos et al., 1979, Radulescu et al., 1984, Raileanu et al., 1991,1992, Stanchevici 1992). Heat flow data (HF) after Demetrescu et al. (1991) and temperature at 20 km depth (T_{20}) after Demetrescu and Andreescu (1994).

The tectonic interpretation of the near vertical seismic reflection lines suggests that Moesian Platform has a brittle upper crust, a decoupling mid-crustal zone and a lower crust with brittle to ductile behaviour. The Moho topography infers a possible extensional or isostatic rebound process. The lower crust and upper mantle presents laminated zones with reduced viscosities.

1.2.2. Lithospheric models and geodynamic processes

In the area of the south eastern Carpathians it was identified a zone of active strong crustal and intermediate depth earthquakes. It is addressed within literature as the Vrancea Zone (or Window). This prone to earthquakes zone permitted to scientists that used various geological and geophysical data and constraints to infer a large number of geodynamical models. The development and availability of each scenario

lead to further understanding of the puzzle that reside within this intricate structure, from its upper crust substance to lithospheric fabric.

Radulescu and Sandulescu (1973) proposed a model that infers two major rifting phase in the southern margin of East European craton. Subsequently, it was suggested the presence of a westward plate subduction consumed below the orogeny that generated the Neogene magmas (Radulescu and Sandulescu, 1973). Girbarcea and Frisch in 1998 proposed a subduction model with delamination of the lower lithospheric mantle in order to explain the Pliocene to Quaternary tectonic evolution of the Carpathians. It is suggested that, after the continental collision, a slab break-off of the west-dipping subducting oceanic (eclogitic) slab occurred. Slab break-off is propagated eastward forcing a lithospheric delamination and movement of the Vrancea slab into its actual position. Knapp et al. (2005) suggests an alternative model for Vrancea zone seismicity that involves active continental lithospheric delamination, resulting from Miocene closure of an intra-continental basin and attendant lithospheric thickening. Gvirtzman (2002) introduced the idea that the seismically active Vrancea region is shifted approximately 50 km east of the place of maximum pull-down, indicating that lithospheric tearing is now occurring at one side of the detaching root and not above it in agreement with the interpretation of a lateral delamination of the lower lithosphere. Sperner et al. (2001) indicate the decoupling between the slab and the overlying crust due to a 'soft' elongation and later partially break off the subducted slab. Wortel and Spakman (2000) summarised the evolution and present state of the Vrancea Zone as a result of Africa-Eurasia convergence and its consequences, delamination of the lithospheric mantle and closely related mechanisms, and rollback in a land-locked basin setting.

Figure 1.5 presents the sum of the information inferred from the previous studies and it propose a working framework model for the crustal structure of the south eastern Carpathians and its foreland as well as for the heterogeneous lithospheric structure that lies beneath. The geological cross-section was updated with information from the seismic and potential field modelling, issues that will be latter discussed within the chapters of this thesis (Chapter II and III). The middle and lower crust boundaries derived from Hauser et al. (2007) were tested for robustness while used as a priori inputs in modelling seismic data. The Moho topography in the cross-section is constrained with the potential field modelling results (Chapter V). The two small insets represent the top and bottom view of the 3D interpolated seismic velocity perturbations (isosurface) values derived from Martin et al. (2006).

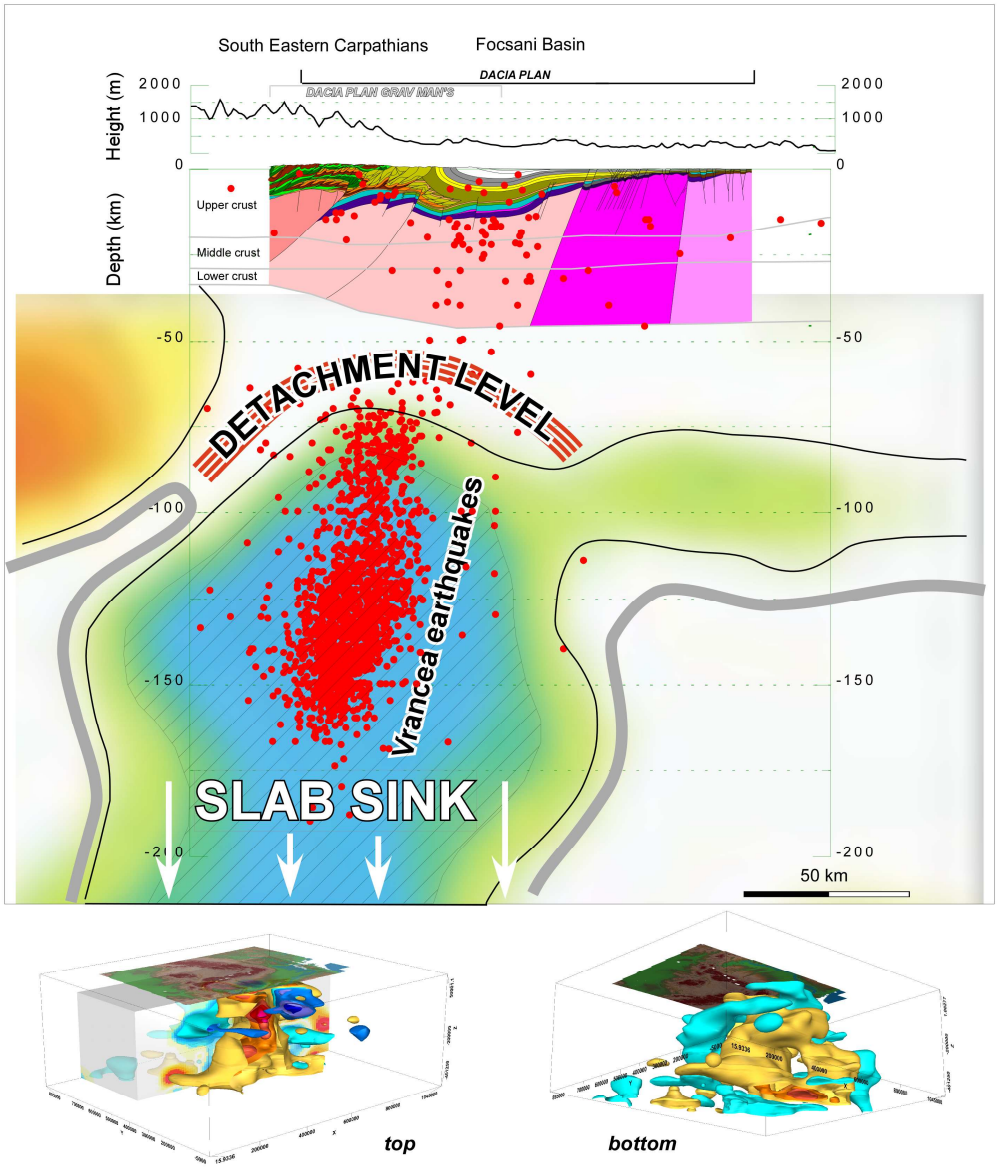

Fig. 1.5. Geological cross-section modified after Matenco et al. (2008) in the vicinity of the DACIA PLAN and the DACIA PLAN GRAV MAN'S profiles. The upper, middle and lower crust are inferred from Hauser et al. (2007). The lithospheric scale structure is interpreted from seismic velocity perturbations results Martin et al. (2006). 3D interpolation of seismic velocity perturbations (isosurface) inferred from Martin et al. (2006).

1.3. Overview of the chapters

Chapter II: The study presented in this chapter provides a firsthand seismic tomography modelling experiment based on seismic data recorded as part of DACIA PLAN survey acquired in 2001. The densely spaced deep reflection seismic profile supplied a set of first break seismic travel times that were inverted using PStomo_eq tomography algorithm (Tryggvason et al., 2002). The tomographic modelling and the work behind this experiment were led by Ari Tryggvason at Vrije Universiteit. The inversion was conducted iteratively, starting from a rough 2D initial model and running a couple of inversions (each comprising several iterations) whereas after each inversion was performed analysis that contributed to a new updated initial model. A final model was obtained with a very good RMS data fit and model robustness was validated through hit-ray cell coverage and checkerboard test.

The tomographic model correlates cogently with previous interpreted industry seismic reflection lines and complements the seismic section interpretation of the accompanying seismic experiment (Panea et al., 2005). Relevant meaningful knowledge was inferred from the model: depth to basement, lateral structural heterogeneity at the basement level or beneath the Focsani Basin and the structural embodiment of the foreland basin-thrust belt transition zone (previous interpretation was lacking in constraints). The related tectonic results revealed: in the Vrancea Zone a shallower pre-Tertiary basement; shallower than previously recognised (Landes et al., 2004) basement "uplift"; a detachment level well within sedimentary units underlying a thick Miocene and younger strata of the Focsani Basin.

Chapter III: The study presented in this chapter introduces a distinctive methodology of ray tracing seismic forward modelling in which the incorporation while modelling of known geology below the actual resolution of the seismic modelling methods, is a novel concept. The travel times used for modelling came from the same dataset of DACIA PLAN survey. Their use was established after a thorough investigation and tests. The modelling begins by inferring an initial seismic velocity model from travel times only (senso stricto *"seismological modelling"*) and then is perturbed in a subjective way by incorporation of independently known structural features. The model was perturbed also by using graphical velocity analysis on seismograms. The final model complements the tomographic image presented in Chapter II and supplements new information about geological mechanisms and structures in the area. A small subsection is provided for comparison between the final and previous tomographic model. Two new notions were identified and introduced, "*short wavelength*" and "*long wavelength*" features, which helped comprehend/render the modelling and afterwards the interpretation.

The model results refine basement structure beneath the south-eastern Carpathian nappe stack and Focsani Basin and led to the following conclusions: the supra-basement velocity perturbations (anomalous high velocity structures) indicate

faults or fault systems affecting basement and/or sedimentary layers; reverse faults on which crystalline rocks have been elevated to shallower depths; inferred faults appear to affect strata almost up to the surface; the velocity model suggests uplift in the south-eastern Carpathian and Vrancea Zone and subsidence in the adjacent foreland (post orogenic events); normal faults and flower structures are associated with the tectonic subsidence in the foreland; intracrustal earthquakes recorded on the faults suggest that topographic evolution is coupled with synchronous uplift-subsidence processes.

Chapter IV: This chapter presents the DACIA PLAN GRAV MAN'S data acquisition and processing. The chapter reviews previous measurements in the area and explains the motivation for acquiring new datasets. A small section called "*Instrumentation*" is included in order to provide information about the instruments and devices used for acquisition. Data acquisition is described in three subsections, documenting respectively the GPS (positioning), gravity and magnetic data acquisition. The data processing section follows the same logic and explains specific techniques/software used to correct and reduce the data necessary for the modelling and interpretation described in the following chapter.

Chapter V: This chapter presents a short review of DACIA PLAN GRAV MAN'S densely spaced gravity and magnetic data acquisition and processing and the modelling and interpretation of the first order potential field model. The model intentionally overlapped the previous deep seismic reflection profile in order to correlate and validate the previous results (Bocin et al., 2005; Panea et al., 2005; Hauser et al., 2007; Bocin et al., 2009). The modelling results allowed inferring information about basement composition, crustal affinity and crustal boundaries in the area of the south-eastern Carpathians and its foreland basin. Data processing was performed combining *in the field* procedures with software developed for commercial use, free downloaded sources and self developed algorithms.

The integrated gravity and magnetic shows the presence of shallow uplifted basement blocks or basement topography. The strong active crustal faults inferred from previous seismic velocity models interpretation or previous geological information are introduced in the gravity and magnetic model, modelled and tested for validity. One important conclusion represents the inference of crustal differentiation between crustal blocks. Subsequently, in the area the plate boundaries are subject to re-interpretation. Also the previously inferred Permo-Triassic rift (Panea et al., 2005) is better constrained. The boundary zone along with the general increase of the crustal thickness from west to east correlates with the presence of the Teisseyre Tornquist Palaeozoic zone that separates the Precambrian terranes of the East European Craton from the younger terranes.

Chapter VI: In the last Chapter, the outcomes of the work reported in this thesis are synthesized and a number of general conclusions are drawn on the geology

of the south-eastern Carpathians, Vrancea zone and Focsani Basin. Moreover, recommendations and suggestions are made for future scientific research in this subject area.

References

Bala, A., Radulian, M., Popescu, E., 2003. Earthquakes distribution and their focal mechanism in correlation with the active tectonic zones of Romania. Journal of Geodynamics 36: 129–145

Bocin, A., Stephenson, R., Tryggvason, A., Panea, I., Mocanu, V., Hauser, F., Matenco, L., 2005. 2.5 D seismic velocity modelling in the south-eastern Romainan Carpathians Orogen and its foreland, Tectonophysics, Volume 410, 273-291.

Bocin, A., Stephenson, R., Mocanu, V., Matenco, L., 2009. Tectonophysics. PII: S0040-1951(09)00419-3; DOI: 10.1016/j.tecto.2009.07.027

Cornea, I., Radulescu, F., Pompilian, A. and Sova, A., 1981. Deep seismic sounding in Romania. Pure Appl. Geophys., 119: 1144-1156.

Gîrbacea, R., and Frisch, W., 1998, Slab in the wrong place: Lower lithospheric mantle delamination in the last stage of the Eastern Carpathians subduction retreat: Geology, v. 26, p. 611-614.

Gvirtzman, Z., 2002, Partial detachment of a lithospheric root under the southeast Carpathians: Toward a better definition of the detachment concept: Geology, v. 30, p. 51-54.

Hauser, F., Raileanu, V., Fielitz, W., Bala, A., Prodehl, C., Polonic, G., Schulze, A., 2001. VRANCEA99-the crustal structure beneath the southeastern Carpathians and the Moesian Platform from a seismic refraction profile in Romania. Tectonophysics 340, 233 – 256.

Hauser, E., Prodehl, C., Landes, M., VRANCEA Working Group (A. Bala,V. Raileanu, J. Bribach, J. Knapp, C. Diaconescu, C. Dinu, V. Mocanu, W. Fielitz, S. Harder, G.R. Keller, E. egedus, and R.A. Stephenson), 2002. Seismic experiments target earthquake-prone region in Romania. EOS Trans. AGU 83457, 462–463.

Hauser, F., Raileanu, V., Fielitz, W., Dinu, C., Landes, M., Bala A., Prodehl, C., 2007. Seismic crustal structure between the Transylvanian Basin and the Black Sea, Romania. Tectonophysics.Volume 430, 1-25.

Heidbach, O., Ledermann, P., Kurfeß, D., Peters, G., Buchmann, T., Matenco, L., Negut, M., Sperner, B., Müller, B., Nuckelt, A. and Schmitt, G., 2007. Attached or not attached: slab dynamics beneath Vrancea, Romania, International Symposium on Strong Vrancea Earthquakes and Risk Mitigation. Oct. 4-6, 2007, Bucharest, Romania, pp. 4-20.

Hoeven van der A., Mocanu V., Spakman W., Nutto M., Nuckelt A., Matenco L., Munteanu L., Marcu C., Ambrosius B.A.C., 2005. Observation of present-day tectonic motions in the Southeastern Carpathians: Results of the ISES/CRC-461 GPS measurements. Earth and Planetary Science Letters 239: 177– 184.

Knapp, J.H., Knapp, C.C., Raileanu, V., Matenco, L., Mocanu, V., Dinu, C. 2005. Crustal constraints on the origin of mantle seismicity in the Vrancea Zone, Romania: the case for active continental lithospheric delamination. Tectonophysics, Volume 410, 311-323.

Landes, M., Fielitz, W., Hauser, F., Popa, M., CALIXTO Group, 2004. 3-D upper crustal tomographic structure across the Vrancea Seismic Zone, Romania. Tectonophysics, Volume 382, 85-102.

Martin, M., Ritter, J. R. R. and the CALIXTO working group. 2005. High-resolution teleseismic body-wave tomography beneath SE Romania - I. Implications for three-dimensional versus one-dimensional crustal correction strategies with a new crustal velocity model. Geophysical Journal International, Volume 162, Issue 46, pp. 448-460.

Matenco, L., G. Bertotti, K. Leever, S. Cloetingh, S. Schmid, M. Tarapoanca, and C. Dinu, 2007. Large-scale deformation in a locked collisional boundary: Interplay between subsidence and uplift, intraplate stress, and inherited lithospheric structure in the late stage of the SE Carpathians evolution, Tectonics, 26, TC4011, doi: 4010.1029/2006TC001951.

Oncescu, M. C., and K. P. Bonjer, 1997. A note on the depth recurrence and strain release of large Vrancea earthquakes, Tectonophysics, 272, 291 – 302, doi:10.1016/S0040-1951(96)00263-6.

Panea, I., Stephenson, R., Knapp, C., Mocanu, V., Drijkoningen, G., Matenco, L., Knapp, J., Prodehl, K. 2005. Near-vertical seismic reflection image using a novel acquisition technique across the Vrancea Zone and Foscani Basin, south eastern Carpathians. Tectonophysics, Volume 410, 293-309.

Radulescu, D., Sandulescu, M., 1973. The plate-tectonics concept and geological structure of the Carpathians. Tectonophysics 16, 155–161.

Radulescu, D.P., Cornea, I., Sandulescu, M., Constantinescu, P., Radulescu, F., Pompilian, A., 1976. Structure de la croute terrestre en Roumanie. Essai d'interpretation desetudes seismiques profondes. An. Inst. Geol. Geofiz. 50, 5 – 36.

Radulescu, F., 1979. Seismic studies on the structure of the crust in Romania. Ph.D. Thesis, Univ. Bucharest, 185 pp.

Radulescu, F., Raileanu, V. and Cornea, I., 1984. Contributions of the reflection seismic method to the crustal structure deciphering. Stud. Cercet. Geol. Geofiz. Geogr. Ser. Geofiz., 22: 11-17 (in Romanian).

Raileanu, V., Stiopol, D. and Mateciuc, D., 1991. Processing and interpretation of some reflection crustal lines of the depression in front of the Carpathians and of the Pannonian Depression. Intern. Rep., CFP-IFA, 31.915, CFP Archive, Bucharest, 38 pp. (in Romanian).

Raileanu, V., Stiopol, D., Barsan, M. and Mateciuc, D., 1992. Crustal reflection seismic profiling on a short line from NE area of Pannonian Depression. Stud. Cercet. Geofiz., 30: 29-39 (in Romanian).

Raileanu, V., Diaconescu, C.C., Radulescu, F., 1994. Characteristics of Romanian lithosphere from deep seismic reflection profiling. Tectonophysics, 239, 165-185.

Saintot, A., Stephenson, R., Stovba, S., Brunet, M-F., Yegorova, T., Starostenko, V., 2006. The south margin of the East European continent: its evolution during the Paleozoic and Early Mesozoic, in: Gee D.G. and Stephenson R.A. (Eds.), European Lithosphere Dynamics, Geological Society of London, Memoir 32: 277-289.

Schmid, S., Bernoulli, D., Fügenschuh, B., Matenco, L., Schefer, S., Schuster, R., Tischler, M. and Ustaszewski, K., 2008. The Alpine-Carpathian-Dinaridic orogenic system: correlation and evolution of tectonic units. Swiss Journal of Geosciences, 101(1): 139-183.

Sperner, B., Lorenz, F., Bonjer, K., Hettel, S., Muller, B., and Wenzel, F., 2001. Slab break-off - abrupt cut or gradual detachment? New insights from the Vrancea Region (SE Carpathians, Romania): Terra Nova, v. 13, p. 172-179.

Stanchevici, B., 1992. Seismic studies for deep seismic structure deciphering in the Eastern Carpathians and the Moesian Platform. Intern. Rep., Theme A. 3, Inst. for Geology and Geophysics, Bucharest, 16 pp. (in Romanian).

Talos, D., Radulescu, F., Pompilian, A., Popescu, M. And Ionescu, S., 1979. Some considerations upon velocity distribution in the Earth's crust of Romania. Rev. Roum. Geol. Geophys. Geogr. Ser. Geophys., 23: 63-75.

Tarapoanca, M., Bertotti, G., Matenco, L., Dinu, C., Cloetingh, S., 2003. Architecture of the Focsani Depression: a 13 km deep basin in the Carpathians Bend Zone (Romania). Tectonics, Volume 22, 1074.

Tryggvason, A., Rognvaldsson, S.Th., Flovenz, O. G., 2002. Three-dimensional imaging of the P-and S-wave velocity structure and earthquake locations beneath southwest Iceland. Geophys. J. Int. 151, 848 – 866.

Visarion, M., Sandulescu, M., Stanica, D., Veliciu, S., 1988. Contributions a la connaissance de la structure profonde de la plateforme Moesienne en Roumanie. St. Tehn. Econ., Geofiz., Volume 15, 68– 92.

Wortel, M.J.R., and Spakman, W., 2000, Subduction and Slab Detachment in the Mediteranean-Carpathian Region: Science, v. 290, p. 1910-1917.

CHAPTER II

2.5D SEISMIC VELOCITIES MODELLING IN THE SOUTH-EASTERN ROMANIAN CARPATHIANS OROGEN AND ITS FORELAND*

"It would be as useless to perceive how things 'actually look' as it would be to watch the random dots on untuned television screens."

Marvin Minsky

ABSTRACT

The DACIA-PLAN (Danube and Carpathian Integrated Action on Processes in the Lithosphere and Neotectonics) deep seismic reflection survey was performed in August–September 2001, with the objective of obtaining new information on the deep structure of the external Carpathians nappe system and the architecture of the Tertiary/Quaternary basins developed within and adjacent to the Vrancea zone, including the rapidly subsiding Focsani Basin. The DACIA-PLAN profile is about 140 km long,

This chapter is based on Bocin, A., Stephenson, R., Tryggvason, A., Panea, I., Mocanu, V., Hauser, F., Matenco, L., 2005. 2.5 D seismic velocity modelling in the south-eastern Romanian Carpathians Orogen and its foreland, Tectonophysics, Volume 410, 273-291.

having a roughly WNW–ESE direction, from near the southeast Transylvanian Basin, across the mountainous south-eastern Carpathians and their foreland to near the Danube River. A high resolution 2.5D velocity model of the upper crust along the seismic profile has been determined from a tomographic inversion of the DACIA-PLAN first arrival data. The results show that the data fairly accurately resolve the transition from sediment to crystalline basement beneath the Focsani Basin, where industry seismic data are available for correlation, at depths up to about 10 km. Beneath the external Carpathians nappes, apparent basement (material with velocities above 5.8 km/s) lies at depths as shallow as 3–4 km, which is less than previously anticipated on the basis of geological observations. The first arrival travel-time data show that there is significant lateral structural heterogeneity on the apparent basement surface in this area, suggesting that the high velocity material may be involved in Carpathian thrusting.

Keywords: Vrancea Zone, tomographic inversion, velocity model.

2.1. Introduction

A controlled source seismic experiment (DACIA-PLAN1) was carried-out in August–September 2001, in Romania, at the same time as a deep regional refraction survey (VRANCEA2001; cf. Hauser et al., 2002), as an international collaboration between the Netherlands Research Centre for Integrated Solid Earth Sciences (ISES, represented by the Vrije Universiteit, Amsterdam), the University of Bucharest, the Romanian National Institute for Earth Physics, the University of Karlsruhe, and the University of South Carolina. The DACIA-PLAN seismic profile is about 140 km long and has a NW–SE orientation, crossing the seismically-active Vrancea Zone of the south-eastern Carpathians orogenic belt and the foreland Focsani Basin (Fig. 2.1). The primary goal of DACIA-PLAN was the acquisition of a stacked deep seismic reflection image using a novel acquisition technique involving deployment of stand-alone seismic recorders ("Texans"). A description of the stacked seismic section and its geological interpretation is found in a companion paper to this one by Panea et al.(2005).

The Vrancea Zone, which is directly crossed by the DACIA-PLAN seismic profile, is known for its intense and persistent seismic activity comprising crustal and intermediate earthquakes, with magnitudes up to 7.5. The presence of the latter and the scarcity of earthquakes elsewhere along the Carpathian belt suggested to many researchers that the Vrancea Zone represents an isolated segment of the Eurasian Plate where a final stage of lithospheric subduction is still in process (e.g., Kiratzi, 1993). However, there remains considerable controversy as to the present-day geometry of such subduction, should it exist, and the exact mechanisms responsible for the neotectonic seismicity (Cloetingh and Burov, 1996; Girbacea, 1998; Wenzel et al., 1998a,b, 2002; Chalot-Prat and Girbacea, 2000; Wortel and Spakman, 2000; Sperner et al., 2001; Cloetingh et al., 2004; Sperner et al., 2004; Knapp et al., 2005; Panea et al., 2005).

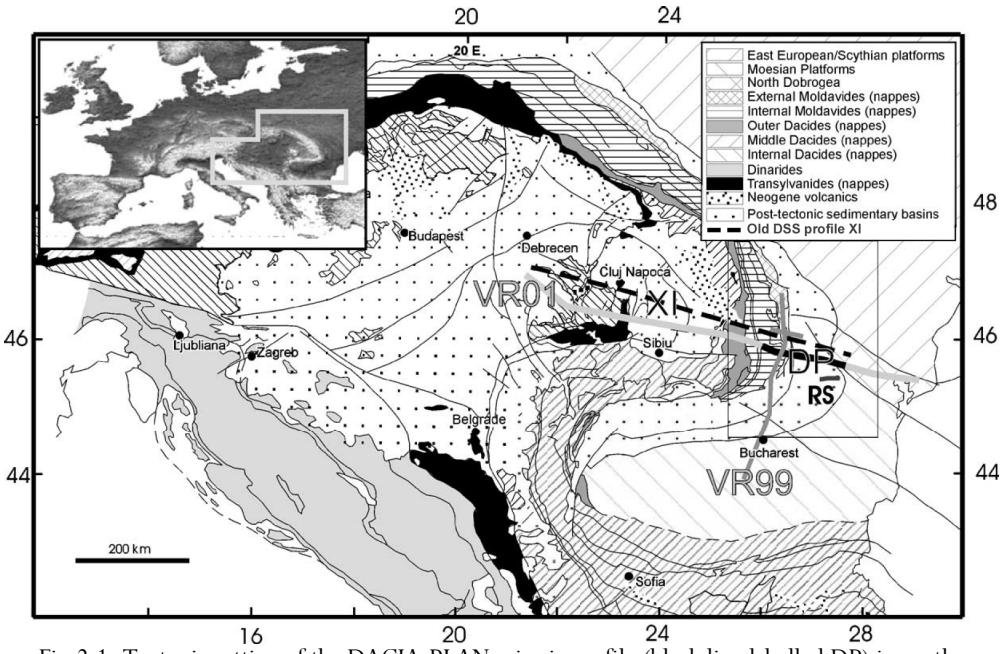

Fig.2.1. Tectonic setting of the DACIA-PLAN seismic profile (black line labelled DP) in south-eastern Europe, crossing the seismically active Vrancea Zone of the south-eastern Carpathian Orogen and its foreland basin, the Focsani Basin. Also shown are the locations of recently acquired seismic refraction/wide-angle reflection profiles VRANCEA-1999 (VR99) and VRANCEA-2001 (VR01). Add dashed line legend.

Two regional refraction/wide-angle surveys — VRANCEA99 and VRANCEA2001 (the latter acquired in conjunction with DACIA-PLAN) — were recently carried out in order to study the crustal and uppermost mantle structure of the Vrancea Zone and surroundings (cf. Hauser et al., 2002). The VRANCEA99 profile (Hauser et al., 2001), 300 km long running in NNE–SSW direction (Fig. 2.1), revealed an upper crust characterised by velocities of 5.9–6.2 km/s and a lower crust defined by a velocity range 6.7–7.0 km/s separated by an intra-crustal discontinuity between 18–31 km depth. The depth to the Moho increases from 38 km at the northern end of the profile to 41 km beneath the Vrancea Zone (where it crosses the DACIA-PLAN profile) and to about 30 km near the southern end. Preliminary analysis of the VRANCEA2001 profile (Hauser et al., 2002) indicates a thickening of the sedimentary cover of the Focsani Basin, from east to west and a Moho depth under the Carpathians of about 40 km. The latter was based partly on the presence of a strong reflection from the crust–mantle boundary although, in general, seismic energy was highly attenuated in the Carpathian belt, probably related to structural complexity in the supracrustal geology. Older DSS studies across the Vrancea Zone (Radulescu et al., 1976) indicate a thickness of 12 km for the Focsani Basin and reveal lateral crustal heterogeneity across the Peceneaga–Camena and Capidava–Ovidiu faults (Fig. 2.2).

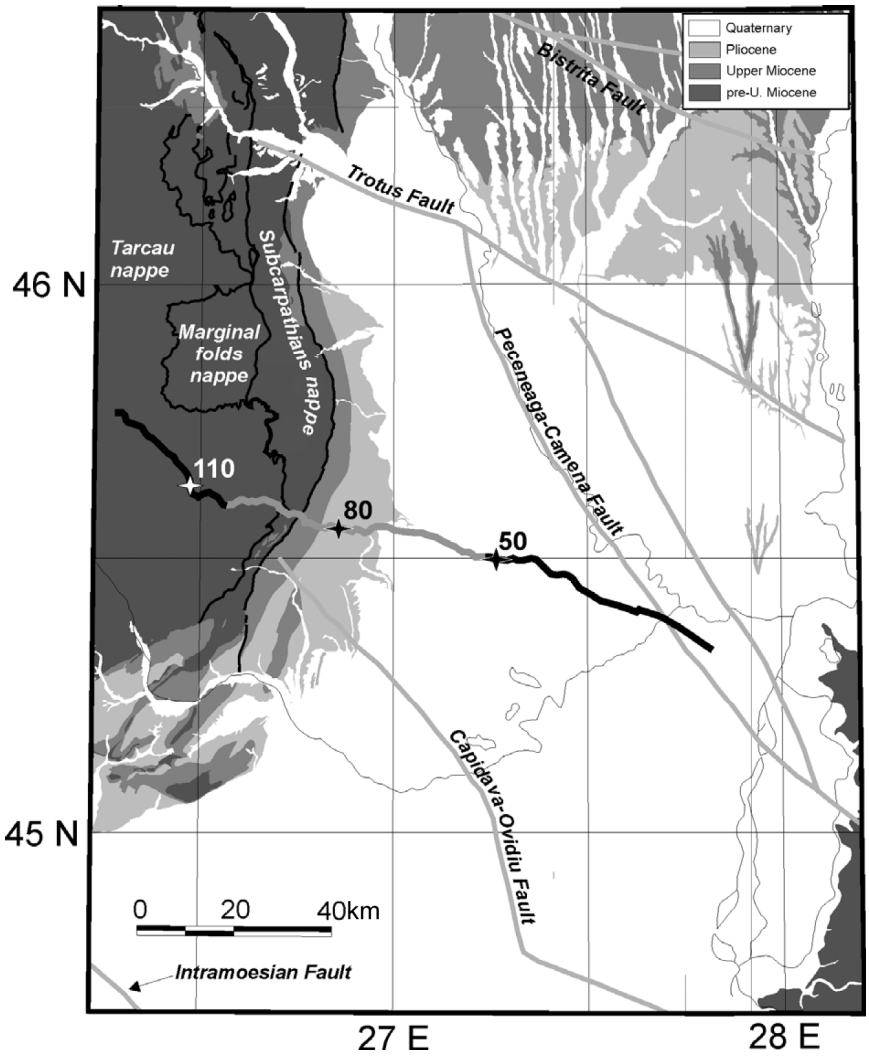

Fig.2.2. Geological map of the south-eastern Carpathians, from Matenco et al. (2003), with the location of the DACIA-PLAN seismic survey with the separate recorder deployments 1–3 indicated (black/grey/black segments). Shot gathers for shots 50, 80, and 110 (white and black stars) are shown in Fig. 2.3.

2.2. Regional geological setting

The DACIA-PLAN profile has a NW–SE orientation and crosses both the external part of the south-eastern Carpathians nappe stack and its foreland units. The traversed nappe pile is made up by the "external Moldavides system" (Sandulescu, 1988), viz. the Tarcau, Marginal Folds, and Subcarpathian nappes (cf. Fig. 2.2). To the southeast, the profile crosses the Moesian Platform and the westward extension of the North Dobrogean Platform, which are separated by the crustal scale Peceneaga–Camena Fault.

In general, the Carpathians comprise a highly arcuate Alpine orogenic belt formed between the European, Apulian, and related microplates during Triassic to Early Cretaceous extension and Late Cretaceous to Miocene contractional events (e.g., Burch-fiel, 1976; Sandulescu, 1988; Csontos, 1995 and references therein). The Romanian Carpathians consist of a nappe pile of crystalline rocks with Upper Palaeozoic to Mesozoic sedimentary cover and, in an external position, a Lower Cretaceous to Late Miocene thin-skinned thrust belt (e.g., Sandulescu, 1984). The highly arcuate shape of the orogen is considered to be a combined response to Late Cretaceous–Palaeogene oroclinal bending and to the passive filling of a thinned continental to oceanic embayment in the foreland of the advancing nappes (e.g., Csontos, 1995; Sandulescu, 1998; Schmid et al., 1998). The pre-existing arcuate shape induced different kinds of tectonic regimes throughout the orogen during Palaeogene– Miocene tectonic transport, post-dating the main Cretaceous docking phase. Three main post-docking deformational stages are recognised. During Palaeogene–Early Miocene times, the clockwise rotation of the Tizsa–Dacia block (senso Balla, 1986) caused NNE–SSW to ENE–WSW shortening in the internal Moldavides nappes of the East Carpathians (Matenco and Bertotti, 2000), large scale transtension/extension to core-complex formation in the South Carpathians (e.g., Schmid et al., 1998), and final collision of the Balkans with Moesia southwards (e.g., Doglioni et al., 1996). Collision with the stable foreland occurred during the Middle and Late Miocene (Badenian–Sarmatian) leading to large-scale deformation characterised by E–W shortening in the East Carpathians (e.g., Sandulescu, 1988; Matenco and Bertotti, 2000) and transpression/shortening in the South Carpathians (Matenco et al., 1997). Collision with the foreland culminated during Late Miocene (Sarmatian) times.

The foreland of the south-eastern Carpathians is made up of a complex puzzle of stable units, with different geometries and mechanical characteristics, inducing large lateral, along-arc variations in orogenic response (e.g., Matenco et al., 2003; Cloetingh et al., 2004). The structure of this foreland is composed of two, internally complex, relatively stable areas, the East European/Scythian and the Moesian platforms, partly separated by the North Dobrogea orogenic zone (Fig. 2.1; further details in Sandulescu and Visarion, 1988; Visarion et al., 1988). The East European and Scythian units are considered to be two crustal blocks developed north of the Trotus Fault, characterized by a thick crust (40–45 km, Enescu et al., 1992) developed below a thin, highly squeezed nappe pile (Matenco and Bertotti, 2000) or below typical, wedge-shaped foredeep sediments (e.g., Tarapoanca et al., 2003). South of the Trotus and west of the Peceneaga–Camena faults (Fig. 2.1), the Moesian block comprises a 35–40 km thick (Radulescu, 1988) Precambrian-aged crustal unit (Sandulescu, 1984), buried below up to 13 km of Middle Miocene to Quaternary sediments. The North Dobrogea zone, located between the Scythian and Moesian platforms (Fig. 2.1) has a complex polydeformed basement and a heterogeneous Triassic–Cretaceous sedimentary cover. West of the Danube the basement and

Mesozoic sediments are covered by a thick succession of Tertiary deposits, forming the pre-Dobrogean depression (e.g., Visarion et al., 1988). The Peceneaga–Camena Fault separates the North Dobrogea and Moesian units, with an estimated decrease in the crustal thickness of the later of 10 km, as indicated by profile XI (Radulescu et al., 1976). This fault has been repeatedly displaced during the late Alpine evolution of the overlying foredeep (e.g., Tarapoanca et al., 2003) and is currently active as part of a broad normal fault system with Moesia as the hanging-wall (e.g., Matenco et al., 2005), with events occurring from its Black Sea prolongation all the way to the junction with the Trotus Fault system.

The Focsani Basin contains up to 13 km of sediments deposited in a foredeep type setting. However, as a foredeep, the Focsani Basin is unusual in that more than half of its sedimentary succession was deposited after the cessation of active foreland tectonics and also in the symmetrical development of the two basin flanks rather than the typical wedge-shape foredeep (see Bertotti et al., 2003; Tarapoanca et al., 2003 for a more detailed description). The contact zone between orogen and foredeep in the study area has been traditionally considered as a blind thrust unconformably overlain by post-tectonic cover, the latter being indicative of the end of thrusting. However, the overall position and tilting of the sediments and, particularly, the eastward dip of the Upper Sarmatian unit suggest that this surface is a backthrust (Matenco and Bertotti, 2000). As a result, in the frontal area a triangle zone is formed, with the backthrust compensating displacement on a basal sole thrust called the Pericarpathian fault.

Post-orogenic, Pliocene–Quaternary deformation is variable within the area of the DACIA-PLAN profile. In the nappe stack, a small-scale, late stage, out-of sequence N–S contractional event led to E–W oriented thrusts (e.g., Hyppolite and Sandulescu, 1996), while the Moesian foreland is characterised by large scale extensional deformation, mostly localised on the eastern flank of the Focsani Basin (Tarapoanca et al., 2003). A short, ~50 km wavelength couple/fold between accelerated subsidence in the centre of the Focsani Basin (Bertotti et al., 2003) and rapid uplift of its neighbouring western flank (Sanders et al., 1999) tilted post-orogenic Pliocene–Quaternary beds into a sub-vertical position with up to 1 km of foredeep topography.

The Tarcau and Marginal Folds nappes are made up mainly of Cretaceous to Lower Miocene turbidites, while the Subcarpathian Nappe consists mainly of Palaeogene–Upper Miocene clastic mollasse-type deposits (e.g., Ionesi, 1994). A particular feature in the study area is the presence of two evaporitic layers of Early and Middle Miocene age. The first of these forms large-scale diapiric structures related to the main thrust faults (e.g., Sandulescu, 1998; Matenco and Bertotti, 2000). Previous geological and geophysical studies have suggested a thickness of about 8 km for the nappe stack in the area crossed by the DACIA-PLAN profile (e.g., Matenco and Bertotti, 2000). This was based on limited industry reflection seismic

data and magnetotelluric surveys as well as geological cross-sections derived from the surface geology and some borehole data (Cornea et al., 1981; Radulescu and Raileanu, 1981; Demetrescu, 1982; Oncescu, 1982, 1984; Radulescu et al., 1984; Stanica et al., 1986; Enescu et al., 1988, 1993; Radulescu, 1988; Raileanu et al., 1994; Matenco and Bertotti, 2000). The subsurface structure of the nappes is generally still under debate.

2.3. DACIA-PLAN seismic data

The DACIA-PLAN seismic data were recorded using approximately 640 autonomous one-compo-nent digital seismographs, mainly REFTEK-125s ("Texans") from the University of Texas at El Paso and PASSCAL (Program for Array Seismic Studies of the Continental Lithosphere). These were set out at (nominally) 100 m intervals on three successive deployments ("Deployments 1–3" west to east; cf. Fig. 2.2), using 334 recorders on Deployment 1 and the full contingent of recorders on Deployments 2 and 3 (637 and 632), recording 29, 47, and 55 explosive shots, respectively (cf. Tables 1 and 2). As such the respective lengths of deployments 1–3 were 22.1, 55.8, and 55.9 km, which included some overlap of recordings between deployments 1 and 2 and 2 and 3. The total acquisition length was about 140 km, and the farthest offset used in the tomography was 59 km. Nominal shot spacing was 1 km but varied according to the availability of appropriate drilling and shooting circumstances. Shot point attributes are summarised in Table 2. Elevations along the line vary from about 1240 m, in the mountainous Deployment 1, to about 40 m in the eastern foreland part of the profile. Positioning (including elevations) and timing was accomplished using differential GPS measurements for most shot points and some recorder sites. Non-differential GPS measurements were used for determining the remaining co-ordinates (cf. Table 2).

In total, 127 successfully detonated shots were recorded on 67,951 seismic traces. Three typical shot gathers are shown in Fig. 2.3. A minimum phase bandpass filter (4–16 Hz) and AGC were applied to all shot gathers (cf. Panea et al., this volume). Although the signal to noise ratio is highly variable, with better results generally achieved in the foreland (Fig. 2.3c), the first breaks used in the tomographic inversion study described here are typically clearly seen. The first-arrival picking uncertainty was ~30 ms. Of the 67,951 traces recorded, 46,235 were considered clear enough to be used in the inversion (cf. Table 2). As an estimate for data-related errors (mainly positioning), a total of 1394 reciprocal travel time pairs were identified showing an RMS reciprocity of 0.073 s.

Table 1

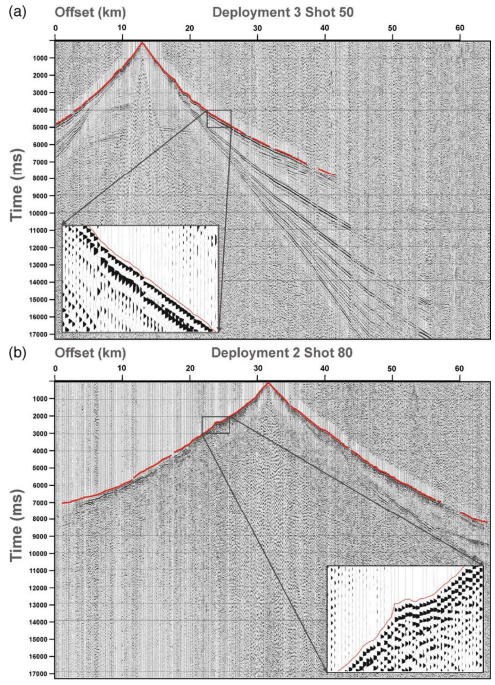

DACIA-PLAN acquisition parameters	
Source	28 kg dynamite
Nominal source spacing	1 km
Shot depth	20 m
Recorders	Reftek 125
Nominal receiver spacing	100 m
Number of channels	334 - deployment 1 637 - deployment 2 632 - deployment 3
Number of shots	29 - deployment 1 47 - deployment 2 55 - deployment 3
Sampling interval	5 ms

Fig.2.3. (a) Shot gather 50 recorded as part of DACIA-PLAN Deployment 3 (cf. Fig. 2.2), (b) shot gather 80 recorded as part of Deployment 2, and (c) shot gather 110 from Deployment 1. The signal-to-noise ratio is clearly better in the third, from the sedimentary foredeep area (Focsani Basin), than in the first, which was recorded in the Carpathian nappe belt, although first breaks are easily distinguished in all of them. Only a subset of traces used in the tomographic velocity analysis is shown.

Table 2

DACIA-PLAN shot table (DPGS — differential GPS positioning for shot point latitude, longitude, and elevation; GPS — non-differential GPS positioning for shot point latitude, longitude, and elevation)

Shot number	Easting UTM	Northing UTM	Source	Elevation (m)	Number of traces	Number of traces used
131	444652.0	5068804.0	DGPS	1062.0	326	178
130	445303.0	5068748.0	DGPS	1069.0	326	192
129	446352.0	5068410.0	DGPS	1088.0	326	226
128	446828.0	5067303.0	DGPS	1114.0	326	250
127	447978.0	5066606.0	DGPS	1154.0	324	258
126	449180.0	5066104.0	DGPS	1200.0	324	253
125	449818.0	5065811.0	DGPS	1222.0	324	233
124	450384.0	5065264.0	DGPS	1212.0	324	268
123	450789.0	5064440.0	DGPS	1182.0	324	284
122	451210.0	5063915.0	DGPS	1164.0	324	232
121	451731.0	5063730.0	DGPS	1155.0	322	223
120	452656.0	5063028.0	DGPS	1142.0	324	200
119	453428.0	5062185.0	DGPS	1128.0	324	265
118	454272.0	5061595.0	DGPS	1113.0	324	295
117	454976.0	5060541.0	DGPS	1096.0	324	251

116	456138.0	5059807.0	DGPS	1083.0	324	285
115	456721.0	5058884.0	DGPS	1072.0	322	303
114	457057.0	5058480.0	DGPS	1069.0	323	313
113	457816.0	5057595.0	DGPS	1044.0	323	231
112	458544.0	5057030.0	DGPS	995.0	323	264
111	458974.0	5055991.0	DGPS	956.0	323	221
110	459532.0	5054605.0	DGPS	918.0	323	297
109	459516.0	5054008.0	DGPS	902.0	323	284
108	459699.0	5052840.0	DGPS	871.0	323	246
107	460712.0	5051628.0	DGPS	830.0	322	269
106	461035.0	5051370.0	DGPS	820.0	322	313
105	462040.0	5051844.0	DGPS	892.0	322	260
104	462918.0	5052270.0	DGPS	954.0	322	277
103	464640.2	5051721.5	GPS	1049.8	322	262
102	466472.0	5049770.0	DGPS	999.0	622	412
101	468191.0	5049967.0	DGPS	1207.0	622	379
100	468718.0	5050558.0	DGPS	1233.0	622	375
99	470072.0	5051096.0	DGPS	1119.0	624	424
98	471577.0	5050698.0	GPS	1026.0	622	448
97	472228.0	5050338.0	DGPS	985.0	621	269
96	474119.0	5050963.0	DGPS	783.0	621	336
95	474602.0	5050786.0	DGPS	745.0	621	369
94	475767.0	5050253.0	DGPS	788.0	620	373
93	476570.0	5050177.0	DGPS	788.0	620	399
92	477094.0	5049339.0	DGPS	766.0	620	397
91	477923.0	5048749.0	DGPS	767.0	620	382
90	479324.4	5048251.5	GPS	634.8	620	248
89	480323.0	5048085.0	DGPS	521.0	620	334
88	481413.0	5048018.0	DGPS	487.0	620	389
87	481878.4	5047473.0	DGPS	489.3	620	425
86	482069.0	5046739.0	DGPS	487.0	620	378
85	483173.0	5046156.0	DGPS	444.0	620	436
84	483831.5	5045839.5	GPS	429.5	620	461
83	485403.0	5045217.0	DGPS	405.0	624	441
82	486006.0	5045150.0	DGPS	397.0	622	572
81	487187.0	5045508.0	DGPS	385.0	622	525
80	488207.0	5045558.0	DGPS	372.0	622	560
79				Misfired		
78	490872.0	5044775.0	GPS	341.0	621	529
77	491697.0	5044406.0	GPS	334.0	621	527
76	492466.0	5044599.0	GPS	327.0	620	545
75	492974.0	5044824.0	GPS	322.0	620	532
74	493789.0	5044421.0	DGPS	315.0	620	542
73	494737.0	5044107.0	DGPS	339.0	620	543
72	495542.0	5044682.0	DGPS	418.0	620	490
71	495895.0	5045400.0	DGPS	467.0	620	465
70	496839.0	5045523.0	DGPS	439.0	620	526
69	498747.0	5045397.0	DGPS	407.0	624	525
68	499316.0	5045275.0	DGPS	392.0	622	526
67	500210.0	5044836.0	DGPS	385.0	623	563
66	502166.0	5044403.0	DGPS	335.0	622	565
65	503523.0	5044150.0	DGPS	288.0	621	315
64				Misfired		
63	505979.0	5044188.0	DGPS	193.0	620	438
62	507064.0	5043683.0	DGPS	138.0	620	495
61	508245.0	5043335.0	GPS	119.0	620	321
60	509509.0	5042847.0	GPS	115.0	620	386
59	510150.0	5042370.0	GPS	114.0	620	383
58	511010.0	5041899.0	DGPS	111.0	620	388
57	511865.7	5041638.0	DGPS	108.0	620	368
56	512641.0	5041213.0	DGPS	104.0	620	408
55	514951.0	5040314.0	DGPS	95.0	621	436

54	515734.5	5039922.0	DGPS	93.0	621	389
53	516332.0	5039177.0	DGPS	91.0	621	393
52	517380.5	5039009.5	DGPS	87.5	621	407
51	518285.0	5039200.0	DGPS	84.0	621	339
50	519223.0	5039076.0	DGPS	76.0	621	354
49	520315.0	5038912.0	DGPS	75.0	621	372
48	521210.0	5038769.0	DGPS	71.0	621	382
47	522142.0	5038767.5	DGPS	68.0	621	338
46	523358.0	5038761.0	GPS	68.0	621	380
45	524677.0	5038753.0	DGPS	66.0	621	361
44	525610.0	5038746.5	GPS	63.0	621	375
43	526344.9	5038741.5	DGPS	61.4	621	377
42	527849.0	5038732.5	DGPS	59.0	621	414
41	528892.0	5038667.0	DGPS	60.0	621	425
40	529683.2	5038026.8	DGPS	59.0	621	416
39	530171.0	5037388.0	DGPS	57.0	621	463
38	530933.0	5036588.0	GPS	58.0	621	368
37	531818.0	5035804.0	DGPS	59.0	621	366
36	532420.0	5035531.0	GPS	57.0	621	318
35	533305.0	5035596.0	DGPS	54.0	621	377
34	534685.0	5035841.0	DGPS	51.0	621	344
33	535364.0	5035437.0	DGPS	50.0	621	401
32	536189.0	5034650.0	GPS	50.0	621	469
31	536942.0	5033805.0	GPS	49.0	621	444
30	537378.0	5033109.0	GPS	48.0	621	416
29	538492.0	5032505.0	GPS	48.0	621	404
28	539408.0	5031815.0	DGPS	47.0	621	512
27	540232.0	5031259.0	DGPS	48.0	621	445
26	541021.0	5030846.0	DGPS	47.0	622	475
25	541945.0	5030459.0	GPS	45.0	622	393
24	542986.0	5030112.0	DGPS	45.0	622	455
23	543842.0	5029821.0	GPS	45.0	622	394
22	544883.0	5029473.0	DGPS	45.0	622	364
21	545571.0	5029239.0	GPS	45.0	622	405
20	546739.0	5028877.0	DGPS	45.0	622	420
19	547568.0	5028591.0	GPS	45.0	622	438
18			Misfired			
17	549598.0	5028629.0	DGPS	44.0	622	436
16	550575.0	5028480.0	GPS	44.0	622	382
15	551502.0	5028177.0	DGPS	43.0	621	335
14	552643.0	5027794.0	DGPS	42.0	621	272
13			Not drilled			
12	554427.0	5027051.0	DGPS	42.0	621	316
11	555180.0	5026637.0	GPS	42.0	622	259
10	556050.0	5026061.0	DGPS	41.0	622	387
9	556573.0	5025721.0	GPS	41.0	623	211
8			Misfired			
7			Misfired			
6	559233.0	5023982.0	DGPS	42.0	624	193
5	560083.0	5023411.0	DGPS	42.0	624	208
4	561175.0	5022700.0	DGPS	41.0	625	328
3	561936.0	5022220.0	DGPS	40.0	625	265
2	562772.0	5021665.0	DGPS	43.0	625	336
1	564113.0	5020790.0	DGPS	45.0	627	333

2.4. First arrival tomography model

2.4.1. Modelling method PStomo_eq

PStomo_eq is a travel time tomography algorithm (Tryggvason et al., 2002) which handles both controlled (known time and location) and earthquakes sources. There are several features of the code that are particularly well suited for using controlled source data — the possibility to control which maximum offsets to use in the inversion (allows building the model from the top to the bottom) without changing the input travel time files, and the possibility to simultaneously invert for receiver statics (or source statics — but not both) along the model (Bergman et al., 2004). The latter is very useful, as there is commonly substantial near surface heterogeneity (Quaternary sediments) that otherwise might get smeared into the part of the model representing consolidated rocks, given that the model parameterisation is rarely fine enough to handle the shallowest (thin) layers of sediments. The algorithm also allows for changing model parameterisation (block size) with depth, as the resolving power of the data generally decrease with depth, and a model block size suitable for the near surface layers might be too small for the deeper parts of the model. Smoothing constraints are utilised in order to control the amount of velocity variation. In cases where the velocity is discontinuous, smoothing may not be desired. PStomo_eq allows the use of a priori constraints on the inversions, including allowing specific velocity discontinuities and limiting velocities within certain ranges. This can be very useful, for example, in inferring the presence of a basement structure with a basement rock/sediment velocity contrast.

The forward part of the algorithm computes a time field from a source (or station) to all cells in the model (Hole and Zelt, 1995). The travel times to all receivers (or shots) are computed from this time field and ray tracing is performed "backwards" perpendicular to isochrons (Hole, 1992). For computational efficiency travel times can be computed either from the shots or from the receivers, whichever is fewer in number.

The drawback in this approach is that no secondary phases, such as reflections, can be used in the modelling. The strengths are that a first arrival is always found and that the finite difference time and ray tracing computations are very fast and stable. The inversion is performed with the conjugate gradient solver LSQR (Paige and Saunders, 1982).

2.4.2. Modelling parameterisation and procedure

The model was parameterised as shown in Fig. 2.4. Due to the crookedness of the line the tomography was performed in a 2.5D manner, implying that the travel time computations and ray tracing were done in 3D, but the velocities only vary in 2D — with depth and along the profile. The inversion cells were also allowed to vary with

depth to reflect the decrease in resolution power of the first arrival travel time field with depth. In the near surface the inversion cell dimensions were 0.5 km along the profile (x), 0.25 km vertically (z), and 5 km perpendicular to the profile(y). At 1 km depth the cell dimensions were 0.5, 5.0, and 0.5 km in x, y, and z, respectively, and at 5 km depth 2, 1, and 5 km, respectively. The forward travel times were computed on a 250 m uniform grid. Various other modelling parameters are listed in Table 3.

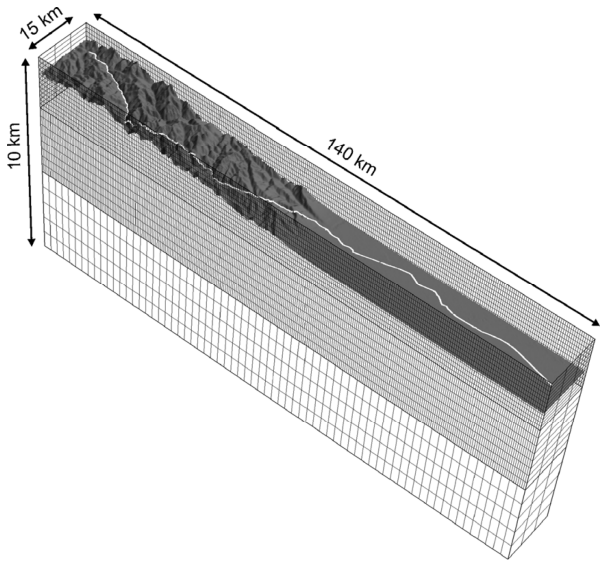

Fig.2.4. Three-dimensional geometry of the tomography model, with computation cells increasing in size with depth, showing the trace of the DACIA-PLAN profile with respect to topography.

Table 3

Summary of parameters for the tomographic inversion

Number of model blocks in x, y and z directions	135, 3, 40
Ray tracing block size (km)	0.25
Inversion grid size (number of ray tracing blocks)	4, 20, 2
Weight on the Laplacian of the velocity perturbations (0 — no smoothing, 200 — very	200, 100, 50, 20
Maximum allowed P-wave travel time residual (seconds)	0.4–0.2
Number of sources	124
Number of receivers	1574
Number of travel times	46000
Maximum offset for the tracing (km)	5, 15, 65
Top of model (km, from sea level, negative up)	-2.0
Max conditional number in LSQR (controlling when no more iterations should be done)	500, 1000
Max number of LSQR-iterations	500

The inversion was conducted iteratively. Travel time curves from five different locations along the profile were analysed and a rough 2D initial model was constructed from these (Fig. 2.5a). A tomographic inversion was performed using all travel time data and the data fit and deviations from the initial model were then analysed. The initial model was updated, based on this analysis, and another tomographic inversion was performed. Each tomographic inversion itself comprised

several iterations, typically 10 to 12, using the shorter offsets and larger weight on the smoothing constraint equations during the earlier iterations. After each iteration, new ray paths were computed in the updated velocity model. When no further improvement in the RMS data fit was observed the procedure was stopped.

The reason for this iterative procedure is the non-linearity of travel time inversion — the velocities are updated where the rays are located, and consequently if the rays are in the "wrong" places, convergence to a reliable model is not guaranteed. This is especially important for geometries where all the receivers and sources are located on the surface; in this case the ray paths are strongly dependent on the velocity gradients in the model.

From the analysis of the various travel time curves, a starting model consisting of three sedimentary layers and a basement layer was adopted (cf. Fig. 2.5a). The top layer, with velocities in the 2.0–2.7 km/s range, is almost absent west of km 50 in the profile. The next layer, having velocities in the 3.0–3.6 km/s range, occurs along the entire profile but is very thin in places. A layer with velocities in the 4.0–4.6 km/s range, occurring along the entire profile, follows. The basement layer has velocities in the range 5.8–6.1 km/s and its surface shows pronounced topography. In fact, whereas identifying the different sedimentary layers and their velocities was relatively straight forward, identifying the basement topography was the most time consuming part of the modelling, as only first arrivals and no reflected phases were used. At the sedimentary–basement interface a velocity discontinuity had to be included to fit the travel times. The smoothing constraints incorporated in the inversions favours a smooth velocity model, however, and, accordingly, the inversion was done with two additional constraints: the first disallowed velocities to fall in the 4.8–5.6 km/s range, thus favouring models preserving the velocity discontinuity at the top of the basement, and the second impeded velocities above 6.3 km/s. Both constraints favoured (but did not require) basement topography over laterally varying velocities in modelling variations in the travel time curves.

The final model is shown in Fig. 2.5b. The cell "hit-rate" — the accumulated ray length in each inversion cell — is shown in Fig. 2.5c. The RMS data fit was reduced by 59% from 0.164 s for the initial model in Fig. 2.5a to 0.068 s for the final model shown in Fig. 2.5b. The final RMS data fit of the model is very similar to the RMS data fit of the reciprocal data pairs, indicating that the model fits the data to the level that could be expected. Selected observed compared to calculated travel-times can be seen in Fig. 2.5d and final residual travel-times distributed on all receivers on the profile in Fig. 2.5e.

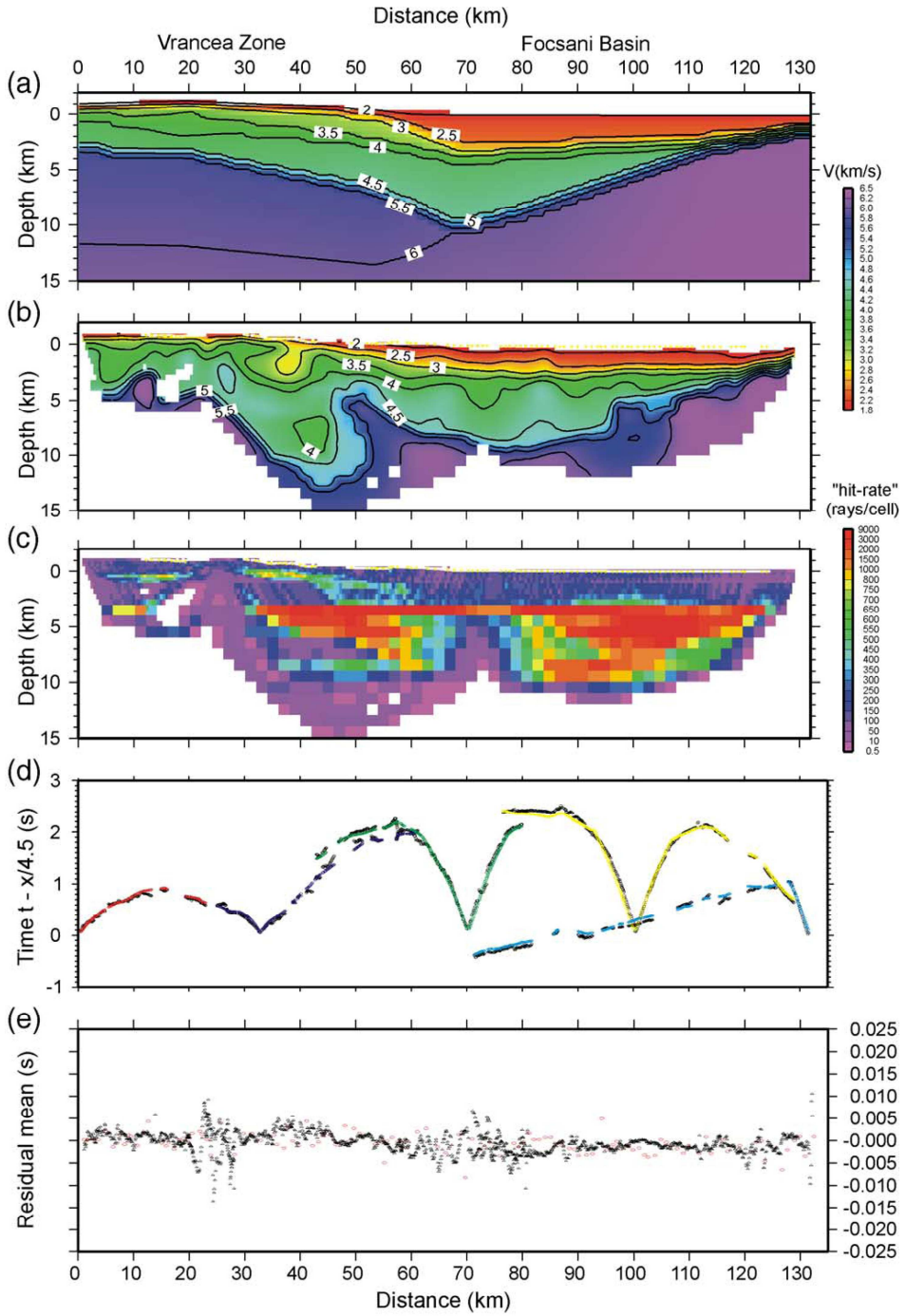

Fig.2.5. (a) The initial model adopted for tomographic inversion based on first-arrival phase velocities; (b) the final P-wave velocity model, shown only for the region which is affected by the seismic rays during the final inversion step; (c) the cell hit-rate for the final model after tomographic inversion of all the 46,000 travel times; (d) recorded travel times (coloured symbols) for a subset of data that were used in the forward modelling compared to computed travel times (black symbols) for the same shots for the final P-wave velocity model; and (e) the final mean data residual distributed on all receivers along the profile.

2.4.3. Modelling results

The resulting velocity model shows a near-surface layer with velocities of 1.8–2.2 km/s that reaches a maximum depth of 2 km. It is substantially thinner west of 50 km along the profile. This is underlain by material with velocities in the range of 3 to 4.6 km/s. The base of this "layer" is marked by velocities generally exceeding 5.8 km/s. At km 10–15 there is an abrupt change of depth (~2.5 to ~5 km). This occurs in a part of the model obtained with data having a maximum offset of 22 km, implying that the dataset is on the limit of inferring velocity at this depth. The evidence for basement velocities at the depth of 3 km in this area comes from the few shots recording offsets larger than about 20 km. The anomalously high receiver residuals between 24 and 29 km along the profile (Fig. 2.5e) are explained by the discontinuity in the travel time curves caused by the sharp variation in basement topography at km 5–20, and the difficulty obtaining a model that fits this discontinuity well on all data. Eastwards, depth to basement increases to more than 10 km at about km 45. This is accompanied by a profound velocity inversion at depths of 5 to 10 km at km 50. The velocity distribution at these depths is constrained by the lack of rays travelling at basement velocities between km 25 and 50. A shallow, low velocity (2.6–3 km/s) anomaly is in evidence between km 35–42 at depths 1–3 km. Further to the east, the top of the basement shallows significantly, showing some complexity, between km 95 and 125.

2.4.4. Checkerboard test and model robustness

In order to evaluate the reliability of the obtained model, a checkerboard test was performed. A ±10% velocity perturbation was superimposed on the final model in blocks commensurate with the inversion grid cell sizes. Noise with 0.07 s standard deviation was added to the synthetic travel times computed through (km 45–65 and 80–110). The reconstructed model has features of poor vertical resolution (smeared checkerboard cells) were ray coverage is unidirectional (not crossing), typically at the ends of the profile, but also at km 22 and 75 (the transition points between deployments). Resolution quickly falls off with depth, but the larger checkerboard blocks are still well reconstructed in the range km 80–120. Along the top of the basement rays are mainly travelling horizontally; therefore the checkerboard cells are substantially smeared out along this interface.

Generally, any numerical test as shown in Fig. 2.6 will provide information only where there is ray coverage. For the present acquisition style, where all sources and receivers are at the surface, the geometry of the inversion problem is very non-linear. This implies that the dataset also carries information where the rays do not travel. For example, between km 30 and 50 the checkerboard indicates that there is essentially no information below 5 km depth. This is not true, because models having

faster velocities in this region did not fit the data, and were consistently rejected by the inversion process. This was a feature of the dataset. Although the velocity inversion at km 50 along the profile was very robust in terms of starting models, it cannot be "proved" or "disproved" by a checkerboard test. It follows that the resolution matrix is also not necessarily a reliable measure of the robustness of certain features of the velocity model.

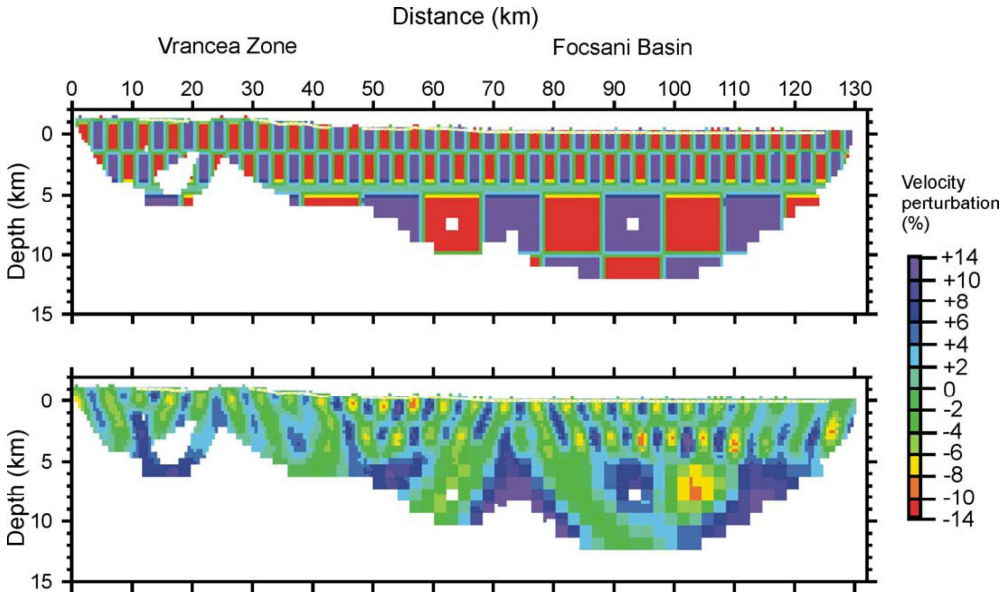

Fig.2.6. Checkerboard test and model robustness. See text for explanation and discussion.

2.5. Geological interpretation and discussion

The overall structure of the velocity model suggests a close correlation with regional geological structure inferred from industry seismic data and other geophysical surveys (e.g., Stanica et al., 1999; Tarapoanca et al., 2003; Tarapoanca, 2004). Fig. 2.7 shows the superposition of the main features of the present velocity model (Fig. 2.5b) with a compatible geological cross-section, modified from Cloetingh et al. (2004) according to the present results.

Two main zones can be identified on the velocity section. The eastern zone (km 55–125) closely follows the regional synclinal pattern of the Focsani Basin, where a thick Miocene Quaternary package develops in the foreland of the south-eastern Carpathians. Within this regional pattern, local variations (slightly higher velocities at depths 4–8 km in the km 95–115 range) may reflect the effects of normal faults organised in horsts and grabens, recognised in industry seismic reflection data especially in the eastern Focsani Basin as affecting strata as young as Upper Miocene (Tarapoanca et al., 2003; Tarapoanca, 2004). Some heterogeneity

within the sedimentary succession in the easternmost part of the basin (km 115–125) may be related to basement involving deformation on the well defined Peceneaga–Camena Fault (Fig. 2.2) that marks the transition between the North Dobrogean and Moesian blocks of the East Carpathians foreland and is recognised at the crustal level in potential field data (Radulescu et al., 1976).

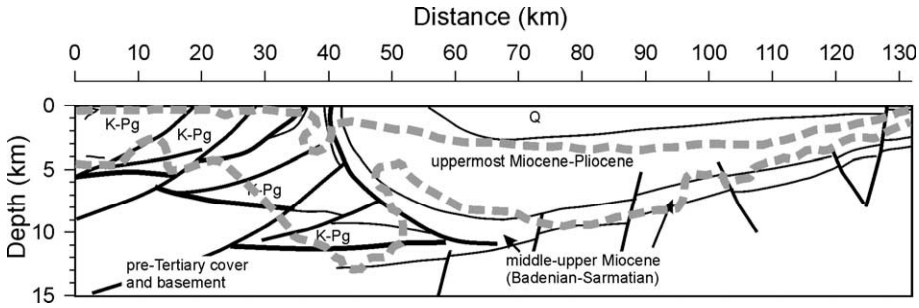

Fig.2.7. The main features of the final velocity model (Fig. 2.5c) — thickest dashed line corresponding to the ~4.5–5.5 km/s velocity transition (~base of sedimentary succession along the profile), thinnest dashed line to the ~4.5–5.0 km/s velocity transition near the south-eastern end of the profile, and the intermediate thickness dashed line to the ~2.5–3.0 km/s velocity transition (~base of Quaternary) — superimposed on a geological cross-section modified from Cloetingh et al. (2004; cf. Matenco and Bertotti, 2000, cf. Tarapoanca et al., 2003).

The western zone of the velocity section corresponds to the external thin-skinned thrust belt of the East Carpathians (Vrancea Zone km 0–50). On the basis of the computed velocity field no detailed internal structure can be definitively interpreted along the profile. However, a general feature that appears to be robust even on the basis of a qualitative assessment of the observed travel-time curves, is the presence of high velocities (>5.5 km/s) at quite shallow levels (<5 km). Such velocities likely correlate with Carpathians pre-Tertiary rocks and can be considered as "basement" in respect of Carpathian thrusting and nappe development. Anomalously shallow basement has also been inferred in the area of the western DACIA-PLAN profile by recent 3D velocity models derived from VRANCEA99 refraction data (e.g., Landes et al., 2004). Thus, a large basement block apparently lies at shallow levels in the external parts of the Tarcau Nappe, possibly resulting from basement thrusting into the thin-skinned nappe pile (Landes et al., 2004). Complexities inherent to the travel-time data within the western 40 km of the DACIA-PLAN profile suggest that there may be a degree of structural dislocation along the inferred basement "horizon". In fact, Roure et al. (1993) and Ellouz et al. (1996) suggested, from geological mapping, that a large basement block from the lower plate was involved in the development of the thin-skinned thrust stack. It is also noted that thrusts involving basement reactivation of earlier normal faults developed in the lower plate elsewhere in the Carpathians (e.g., Ziegler et al., 1995;

Krzywiec, 2001). However, any interpretation of basement involvement in Carpathian thrusting in this area does not exclude subsequent late stage post-orogenic lower plate basement uplift below the nappe pile as a result of the some coupling between subsidence in the Focsani Basin and uplift in the western neighbouring area of the Vrancea Zone (Matenco and Bertotti, 2000).

The most striking feature of the velocity model is the tabular high velocity zone developed at depths of 5–10 km near the contact between the thrust-sheets and Focsani Basin, at distances of 45–70 km along the DACIA-PLAN profile. Continuity of this high velocity zone eastwards at deeper levels and the apparent lower velocities developed westwards and below support an interpretation that it implies large scale backthrusting along the western flank of the Focsani Basin, compatible with the presence of a large scale triangle zone developed in the frontal part of the south-eastern Carpathians (Matenco and Bertotti, 2000). To the west (35–40 km) and at shallower levels (b2 km) a low velocity anomaly can be seen near the main Carpathian thrust. This anomaly likely represents the presence of an Early Miocene-aged salt structure formed during Late Miocene frontal thrusting, the existence of which is indicated by salt exposures in this area (L. Matenco, personal communication).

2.6. Summary and conclusions

As part of a seismic survey (DACIA-PLAN) crossing the Vrancea Zone in the south-eastern Carpathians and its foreland (Focsani Basin), designed primarily for recording reflected seismic phases suitable for CDP stacking, first arrival travel-time data have been inverted using tomographic techniques to derive a first-order velocity model along the profile at shallow depths.

Velocity structure in the resulting 2.5D model is imaged to a depth of about 5 km within the western part of the DACIA-PLAN profile, where it crosses the external thin-skinned thrust belt of the East Carpathians (Vrancea Zone), and up to about 10 km further to the east, beneath the thick Tertiary Focsani Basin. Depth to basement, as well as lateral structural heterogeneity at the basement level, beneath the Focsani Basin resolved by the tomographic model is highly correlatable with structure in this area based on the interpretation of numerous industry seismic reflection lines. Accordingly, the tomographic velocity structure implied for the foreland basin-thrust belt transition zone and the external thrust belt itself, where independent seismic constraints on geological architecture at depth are essentially lacking, are considered to be fairly robust. The results in this area strongly imply that pre-Tertiary basement in the Vrancea Zone is shallower (<5 km) than previously deduced in published geological cross-sections (where it is taken to be as deep as 8–10 km) and indeed shallower than the less resolved basement "uplift" in the same and surrounding areas inferred from regional refraction data (Landes et al., 2004). Further, complexities observed in the travel-time data and their implications for the

velocity modelling suggest that basement material (in any case, material characterised by velocities greater than 5.5 km/s) is likely involved in Carpathian thrusting. In particular, the degree of basement involved in large scale back-thrusting along the western flank of the Focsani Basin appears to be significant and implies a detachment level well within sedimentary (or other) units underlying the ~12 km thick Miocene and younger strata of the Focsani Basin.

Acknowledgments

The authors of this paper represent only a subset of those who worked on the acquisition, processing, and modelling of the DACIA-PLAN seismic dataset or who facilitated this work, including Nicolae Cazan, Marcela Haldan, Ionelia Panea, Ion Dumitru, and Paul Georgescu (all of the Department of Geology and Geophysics, University of Bucharest, Romania) as well as many University of Bucharest students who assisted in the field; Victor Raileanu (National Institute for Earth Physics, Bucharest); Claus Prodehl and others, including Hanna-Maria Rumpel and Michael Landes (University of Karlsruhe, Germany); Guy Drijkoningen (Delft University, Netherlands); Camelia Knapp (Department of Geological Sciences, University of South Carolina, Columbia, USA); and Steve Harder (Department of Earth Sciences, University of Texas at El Paso, USA). Corneliu Dinu of the University of Bucharest is specifically thanked for personal and logistical support. Direct financing of DACIA PLAN was provided by the Netherlands Research Centre for Integrated Solid Earth Sciences and by Forest Oil International, Denver. Tim Berge of the latter is personally thanked for his role, support, and understanding. Further, the acquisition programme could not have taken place without the logistical coordination with and support of the VRANCEA2001 refraction/wide-angle seismic project, which was funded by the German Science Foundation (DGF) through Collaborative Research Centre 461 "Strong Earthquakes: a Challenge for Geosciences and Civil Engineering", based at the University of Karlsruhe.

References

Balla, Z., 1986. Paleotectonic reconstruction of the central Alpine–Mediteranean belt for the Neogene. Tectonophysics 127, 213 – 243.

Bergman, B., Tryggvason, A., Juhlin, C., 2004. Seismic tomography using static corrections in a till-covered bedrock environment. Geophysics 69 (4), 1082 – 1090.

Bertotti, G., Matenco, L., Cloetingh, S., 2003. Vertical movements in and around the SE Carpathian foredeep: lithospheric memory and stress field control. Terra Nova 15, 299 – 305.

Burchfiel, B.C., 1976. Geology of Romania. Spec. Paper, 158. Geological Society of America. 82 pp.

Chalot-Prat, F., Girbacea, R., 2000. Partial delamination of continental mantle lithosphere, uplift-related crust–mantle decoupling, volcanism and basin formation: a new model for the Pliocene–Quaternary evolution of the southern East-Carpathians, Romania. Tectonophysics 327, 83 – 107.

Cloetingh, S., Burov, E.B., 1996. Thermomechanical structure of European continental lithosphere; constraints from rheological profiles and EET estimates. Geophys. J. Int. 124, 695 – 723.

Cloetingh, S., Burov, E., Matenco, L., Toussaint, G., Bertotti, G., Andriessen, P.A.M., Wortel, M.J.R., Spakman, W., 2004. Thermo-mechanical controls on the mode of continental collision in the SE Carpathians (Romania). Earth Planet. Sci. Lett. 218, 57 – 76.

Cornea, I., Radulescu, F., Pompilian, A., Sova, A., 1981. Deep seismic sounding in Romania. Pure Appl. Geophys. 119, 1144 –1156.

Csontos, L., 1995. Tertiary tectonic evolution of the intra-Carpathian area: a review. Acta Vulcanol. 7, 1– 13.

Demetrescu, C., 1982. Thermal structure of the crust and upper mantle of Romania. Tectonophysics 90, 123 – 135.

Doglioni, C., Busatta, C., Bolis, G., Marianini, L., Zanella, M., 1996. On the structural evolution of the eastern Balkans (Bulgaria). Mar. Pet. Geol. 13 (2), 225 – 251.

Ellouz, N., Roure,F., Sandulescu, M., Badescu, D., 1996. Balanced cross-sections in the Eastern Carpathians (Romania): a tool to quantify Neogene dynamics. In: Roure, F., Ellouz, N., Shein, V.S., Skvortsov, I. (Eds.), Geodynamic Evolution of Sedimentary Basins. International Symposium Moskow 1992 Proceedings. Technip, Paris, pp. 305 – 325.

Enescu, D., Pompilian, A., Bala, A., 1988. Distributions of the seismic wave velocities in the lithosphere of some regions in Romania. Rev. Roum. Geol. Geophys. Geogr. Ser. Geophys.32, 3–11.

Enescu, D., Danchiv, D., Bala, A., 1992. Lithosphere structure in Romania II. Thickness of Earth crust. Depth-dependent propagation velocity curves for P and S waves. Stud. Cercet. Geol. Geofiz. Geogr. Ser. Geofiz. 30, 3 – 19.

Enescu, D., Diaconescu, C., Diaconescu, M., 1993. Lithosphere structure in Romania: III. Results on the deep structure of Vrancea zone. Rev. Roum. GE OPHYSIQUE, Bucarest 37, 51– 60.

Girbacea, R., Frisch, W., 1998. Slab in the wrong place: lower lithospheric mantle delamination in the last stage of the Eastern Carpathian subduction retreat. Geology 26, 611 – 614.

Hauser, F., Raileanu, V., Fielitz, W., Bala, A., Prodehl, C., Polonic, G., Schulze, A., 2001. VRANCEA99-the crustal structure beneath the southeastern Carpathians and the Moesian Platform from a seismic refraction profile in Romania. Tectonophysics 340, 233 – 256.

Hauser, E., Prodehl, C., Landes, M., VRANCEAWorking Group (A. Bala,VRaileanu, J. Bribach, J. Knapp, C. Diaconescu,C. Dinu, V. Mocanu, W. Fielitz, S. Harder, G.R. Keller, E. egedus, and R.A. Stephenson), 2002. Seismic experiments target earthquake-prone region in Romania. EOS Trans. AGU 83457, 462–463.

Hippolyte, J.C., Sandulescu, M., 1996. Paleostress characterization of the "Wallachian" phase in its type area, southeastern Carpathians, Romania. Tectonophysics 263, 235 – 249.

Hole, J.A., 1992. Nonlinear high-resolution three-dimensional seismic travel time tomography. J. Geophys. Res. 97, 6553 – 6562. Hole, J.A., Zelt, B.C., 1995. 3-D finite-difference reflection travel times. Geophys. J. Int. 121, 427 – 434. Ionesi, L., 1994. Geologia unitatilor de platforma si a orogenului Nord-Dobrogean. Ed. Tehnica, Bucuresti.

Kiratzi, A.A., 1993. Active deformation in the Vrancea Region, Rumania. PAGEOPH 140, 392 – 402.

Knapp, J.H., Knapp, C.C., Raileanu, V., Matenco, L., Mocanu, V., Dinu, C. 2005. Crustal constraints on the origin of mantle seismicity in the Vrancea Zone, Romania: the case for active continental lithospheric delamination. Tectonophysics, Volume 410, 311-323.

Krzywiec,P., 2001. Contrasting tectonic and sedimentary history of the central and eastern parts of the Polish Carpathian foredeep basin— results of seismic data interpretation. Mar. Pet. Geol. 18, 13–38.

Landes, M., Fielitz, W., Hauser, F., Popa, M., CALIXTO Group, 2004. 3-D upper crustal tomographic structure across the Vrancea Seismic Zone, Romania. Tectonophysics 382, 85– 102.

Matenco, L., Bertotti, G., 2000. Tertiary tectonic evolution of the external East Carpathians (Romania). Tectonophysics 316, 255 – 286.

Matenco, L., Zoetemeijer, R., Cloetingh, S., Dinu, C., 1997. Lateral variations in mechanical properties of the Romanian external Carpathians: inferences of flexure and gravity modelling. Tectonophysics 282, 147 – 166.

Matenco, L., Bertotti, G., Cloetingh, S., Dinu, C., 2003. Subsidence analysis and tectonic evolution of the external Carpathian-Moesian platform region duringTertiary times. Sediment. Geol. 156, 71–94.

Matenco, L., Tilita, M., Cloetingh, S., Dinu, C., 2005. Coupling between foreland and backarc basins post-orogenic vertical movements: neotectonic deformations in the SE Carpathians-Transylvania basin corridor. Geophys. Res. Abstr. 7 (05363).

Oncescu, M.C., 1982. Velocity structure of the Vrancea region, Romania. Tectonophysics 90, 117 – 122.

Oncescu, M.C., 1984. Deep structure of the Vrancea region, Romania, inferred from simultaneous inversion for hypocenters and 3D velocity structure. Ann. Geophys. 2, 23 – 27.

Paige, C.C., Saunders, M.A., 1982. LSQR: an algorithm for sparse linear equation and sparse least square. ACM. Trans. Math. Softw. 8, 43 – 71.

Panea, I., Stephenson, R., Knapp, C., Mocanu, V., Drijkoningen, G., Matenco, L., Knapp, J., Prodehl, K. 2005. Near-vertical seismic reflection image using a novel acquisition technique across the Vrancea Zone and Foscani Basin, south eastern Carpathians. Tectonophysics, Volume 410, 293-309.

Radulescu, F., 1988. Seismic models of the crustal structure in Romania. Rev. Roum. Geol. Geophys. Geogr. Ser. Geophys. 32, 13 –17 (in Romanian).

Radulescu, F., Raileanu, V., 1981. Reflection records with prolonged times. Studies on the Crustal and Upper Mantle Structure in the S and W of Romania. Intern. Rep. CSEN/CFP, 31.81.3, CFP Archive, Bucharest. 35 pp.

Radulescu, D.P., Cornea, I., Sandulescu, M., Constantinescu, P., Radulescu, F., Pompilian, A., 1976. Structure de la croˆute terrestre en Roumanie. Essai d'interpretation desetudes seismiques profondes. An. Inst. Geol. Geofiz. 50, 5 – 36.

Radulescu, F., Raileanu, V., Cornea, I., 1984. Contributions of the reflection seismic method to the crustal structure deciphering. Stud. Cercet. Geol. Geofiz. Geogr. Ser. Geofiz. 22, 11–17 (in Romanian).

Raileanu,V., Diaconescu,C.,Radulescu,F., 1994. Characteristicsof Romanian lithosphere from deep seismic reflection profiling. Tectonophysics 239, 165 – 185.

Roure, F., Roca, E., Sassi, W., 1993. The Neogene evolution of the outer Carpathian flysch units (Poland, Ukraine and Romania)" kinematics of a foreland/fold-and-thrust belt system. Sedimentary Geology, 86: 177-201.

Sanders, C., Andriessen, P., Cloetingh, S., 1999. Life cycle of the East Carpathian Orogen: erosion history of a doubly vergent critical wedge assessed by fission track thermochronology. J. Geophys. Res. 104, 112 (095–29).

Sandulescu, M., 1984. Geotectonica Romaniei (Geotectonics of Romania). Ed. TehnicA, Bucharest (450 pp.).

Sandulescu, M., 1988. Cenozoic tectonic history of the Carpathians. In: Royden, L.H., Horvath, F. (Eds.), The Pannonian Basin, A Study in Basin Evolution. AAPG memoir, pp. 17 – 25.

Sandulescu, M., Visarion, M., 1988. La structure des plate-formes situees dans l ′avant-pays et au-dessous des nappes du flysch des Carpathes orientales. St. Tehn. Econ., Geofiz. 15, 62 – 67.

Schmid, S.M., Berza, T., Diaconescu, V., Froitzheim, N., Fuegenschuh, B., 1998. Orogen-parallel extension in the South Carpathians during the Paleogene. Tectonophysics 297, 209 – 228.

Sperner, B., Lorenz, F.P., Bonjer, K.-P., Hettel, S., Mu¨ ller, B., Wenzel, F., 2001. Slab break-off — abrupt cut or gradual detachment? New insights from the Vrancea Region (SE Carpathians, Romania). Terra Nova 13 (3), 172 – 179.

Sperner, B., Ioane, D., Lillie, R.J., 2004. Slab behavior and its surface expression: new insights from gravity modelling in the SE-Carpathians. Tectonophysics 382, 51– 84.

Stanica, D., Stanica, M.,Visarion, M., 1986. The structure of the crust and upper mantle in Romania as deduced from magneto-telluric data. Rev. Roum. Geol. Geophys. Geogr.Ser.Geophys. 30, 25 –35.

Stanica, D., Stanica, M., Zugravescu, D., 1999. Geodynamic evolution of the Vrancea seismogenic volume revealed by magneto-telluric tomography. St. cerc. GEOFIZICA, tomul 37, 61 –69 (Bucuresti).

Tarapoanca, M. 2004. Architecture, 3D geometry and tectonic evolution of the Carpathians Foreland Basin. [PhD Thesis]: Amsterdam. The Netherlands, Vrije Universiteit, 120 pp.

Tarapoanca, M., Bertotti, G., Matenco, L., Dinu, C., Cloetingh, S., 2003. Architecture of the Focsani Depression: a 13 km deep basin in the Carpathians Bend Zone (Romania). Tectonics 22, 1074. doi:10.1029/2002TC001486.

Tryggvason, A., Rognvaldsson, S.Th., Flovenz, O. G., 2002. Three-dimensional imaging of the P-and S-wave velocity structure and earthquake locations beneath southwest Iceland. Geophys. J. Int. 151, 848 – 866.

Visarion, M., Sandulescu, M., Stanica, D., Veliciu, S., 1988. Contributions a` la connaissance de la structure profonde de la plateforme Moesienne en Roumanie. St. Tehn. Econ., Geofiz. 15, 68 –92.

Wenzel, F., Achauer, U., Enescu, D., Kissling, E., Russo, R., Mocanu, V., 1998a. The final stage of plate detachment: international tomographic experiment in Romania aims to a high-resolution snapshot of this process. EOS.

Wenzel, F., Lorenz, F.P., Sperner, B., Oncescu, M.C., 1998b. Seismotectonics of the Romanian Vrancea area. In: Wenzel, F., Lungu, D. (Eds.),Vrancea Earthquakes. Kluwer Academic Publishers, Dordrecht, Netherlands.

Wenzel, F., Sperner, B., Lorenz, F., Mocanu, V., 2002. Geodynamics, tomographic images and seismicity of the Vrancea region (SE–Carpathians, Romania). Stephan Mueller Special Publication Series 3, 95 – 104.

Wortel, M.J.R., Spakman, W., 2000. Subduction and slab detachment in the Mediterranean–Carpathian Region. Science 290, 1910 – 1917.

Ziegler, P.A., Cloetingh, S., van, W.J.D., 1995. Dynamics of intra-plate compressional deformation: the Alpine Foreland and other examples. Tectonophysics 252, 7 – 59.

CHAPTER III

ARCHITECTURE OF THE SOUTH-EASTERN CARPATHIANS NAPPES AND FOCSANI BASIN (ROMANIA) FROM 2D RAY TRACING OF DENSELY-SPACED REFRACTION DATA*

"Truth in science can be defined as the working hypothesis best suited to open the way to the next better one."

Konrad Zacharias Lorenz

ABSTRACT

A velocity model of the upper crust (maximum depth 10-15 km) of the earthquake-prone Vrancea area (Romania) from 2D forward ray tracing of densely-spaced refraction data is presented. The model is derived from more than 11000 travel times recorded at stations 100 m apart picked from 42 shot gathers along a 140 km line crossing the south-eastern Carpathian bending zone and the adjacent deep (foreland) Focsani Basin. The model refines basement structure beneath the south-eastern Carpathian nappe stack and Focsani Basin and documents reverse faults on which crystalline rocks or highly metamorphosed Mesozoic sedimentary cover of the crystalline basement have been elevated to depths as shallow as 3.5-4 km (with a vertical displacement of at least 2-2.5 km) beneath the external

* This study is based on Bocin, A., Stephenson, R., Mocanu, V., Matenco, L., 2009. Architecture of the south-eastern Carpathians nappes and Focsani Basin (Romania) from 2D ray tracing of densely-spaced refraction data, Tectonophysics, doi:10.1016/j.tecto.2009.07.027

Carpathian nappes in the Vrancea Zone. Fault systems (flower structures) and normal faults associated with the overall tectonic subsidence of the foreland basin are also inferred. Some of the basement fault systems appear to be recently active, since they involve overlying young (Tertiary-Quaternary) sedimentary layers, and may be associated with intracrustal earthquakes recorded in the area.

Keywords: south-eastern Carpathians, Focsani Basin, 2D ray tracing, velocity model, Vrancea Zone.

3.1. Introduction

DACIA-PLAN is a WNW-ESE running 140 km seismic profile that crosses the south-eastern Carpathian nappes, partly overlain by the Brasov/Targu Secuiesc Basin in the hinterland in the west, and their foreland, the Focsani Basin in the east (Fig. 3.1). This is the part of the Carpathian Orogen referred to in Romania as its "bending zone". DACIA-PLAN aimed to use a novel (at the time) acquisition technique (Panea et al., 2005) in rough terrain conditions for revealing crustal scale structure beneath the south-eastern Carpathians nappe stack and Focsani Basin and, in so doing, help solve the crustal structure and active deformation puzzle associated with the seismicity of the Vrancea Zone, one of the most seismically active region in continental Europe (Landes et al., 2004).

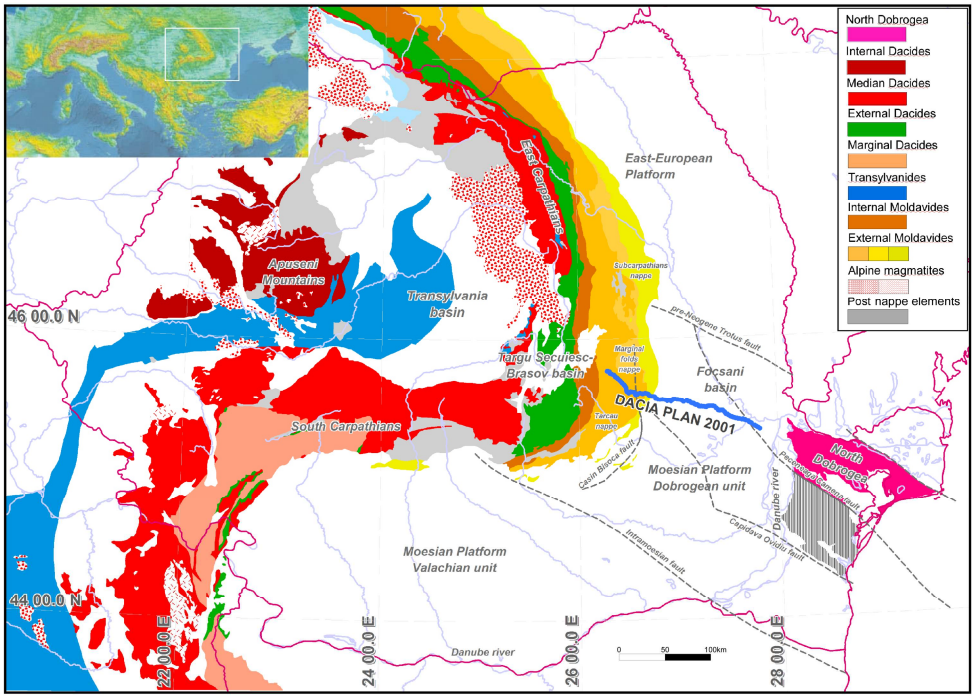

Fig.3.1. Tectonic setting of the DACIA-PLAN seismic profile crossing the Vrancea Zone and the Focsani Basin (modified from Sandulescu, 1984; the major syn-orogenic units terminology is adapted from Burchfield (1976); inset – topographic map of south-eastern Europe showing the location of study area.

A deep seismic reflection stack was obtained and interpreted by Panea et al. (2005). This displays, though the quality of the image is not high, a succession of thrusts and nappes, a thick foreland sedimentary basin (where reflected events are clearer than in the thrust domain). Some of the geometry of the complex contacts between these units and the accompanying basement faults and other systems of faults can also be seen. An accompanying tomographic first-order seismic velocity model (Bocin et. al, 2005) revealed a thick sedimentary basin (~10km) with underlying basement structural features suggesting a number of previously unresolved fault patterns and processes. The tomography model also suggested that thrusting was shallower than previously thought (<5km) and that it incorporated an ensemble of basement units with regional uplift.

Here, the tomography based velocity model has been extended and refined by ray-tracing. The degree of independent geological and geophysical constraint for the upper crust along the DACIA-PLAN profile, combined with the high density nature of the dataset, has allowed the development of a ray trace velocity model that is subject to an additional degree of structural interpretation. The approach was to derive first a seismic velocity model that conformed objectively to the observed travel times (this in itself based in part on the previously developed and published tomography model; Bocin et al., 2005) and, as such, would obey the usual rules of such modelling. This objective model was then perturbed in a subjective way by the incorporation of independently known structural features (within the supra-basement sedimentary velocity layers, as known from geological mapping and industry seismic reflection profiling) but only in such a way that the expression of these features remained within the resolving power of the ray-trace modelling methodology and its limits as concerning parameterisation. Regarding the latter, this means that such structures, including, for example, low-angle thrusts and near-vertical fault zones, could only be defined in terms of simplifying velocity layer geometries. As such, the inferred structural/velocity model presented here not only complements the earlier tomographic image (Bocin et al., 2005) but supplements it to provide a better resolved geological interpretation with new information on structural relationships occurring in the Vrancea Zone of the south-eastern Carpathians.

3.2. Geological overview

3.2.1. Tectonic setting

The Carpathians formed during the Alpine orogeny, as a result of Triassic to Early Cretaceous extension between the European and Apulian plates and related microplates (Schmid et al., 2008) followed by convergent movements from the Late Cretaceous to Miocene. The Miocene evolution (20-11 Ma) is commonly associated with the existence of a concave embayment in the Carpathians foreland, invaded by

previously stacked basement and cover nappes during the Neogene retreat (roll-back) of a European subducting slab (e.g., Royden, 1993a, 1993b). A number of mechanisms have been proposed to have affected the area during its post-collisional stage (11-0 Ma). These include slab detachment, oceanic or continental lithosphere delamination, thermal re-equilibration, other lithospheric instabilities and/or combinations of these (see discussions in Heidbach et al., 2007, and Matenco et al., 2007, and references therein).

All of these models were developed in the context of the active present-day seismicity and observed high-velocity mantle anisotropy of the Vrancea seismogenic zone (Martin et al., 2006). All of them place the peak of crustal deformation, which is limited to the Carpathians bending zone, near the Pliocene-Quaternary boundary. These deformations are characterised by coeval vertical movements in the orogen and in the foreland (uplift and subsidence, respectively) with similar amplitudes in the order of 2-4 km (e.g. Cloetingh et al., 2004; Matenco et al., 2007).

3.2.2. Geology along the profile

The Romanian part of the Carpathians consists of a nappe pile of crystalline rocks overlain by Upper Palaeozoic to Mesozoic sediments and, in an external position, by a thin-skinned succession of Lower Cretaceous to Upper Miocene nappes originating from the same thrust belt ("External Moldavides"; Fig. 3.1). A very deep foreland basin (the Focsani Basin) was formed (Tarapoanca, 2004), after the main stages of thrusting, in front of the south-eastern Carpathians bend, from the Miocene until present.

The thin-skinned orogenic wedge comprises a number of thrust nappes, whose emplacement age is gradually younger towards the foreland (e.g., Sandulescu and Visarion, 1988). These nappes record an estimated 140-160 km of shortening during the Miocene (Roure et al., 1993; Ellouz et al., 1994; Morley, 1996).. The DACIA-PLAN profile crosses part of this south-eastern Carpathians nappe complex, specifically the Tarcau, Marginal Folds and Subcarpathian nappes (Fig. 3.2, Sandulescu, 1984).

The Tarcau nappe (Sandulescu, 1984) is widely exposed. It has a minimum width of 40 km and a NE-SW orientation. The Marginal Folds nappe unit, which corresponds in location with the Vrancea Zone, has a rectangular shape (Fig. 3.2) and comprises Cretaceous, Palaeogene and Miocene successions. The extent of this unit to the south is a matter of debate, being covered by the Tarcau nappe. The Subcarpathian nappe ("thrusted internal foredeep"; Sandulescu and Visarion, 1988) cross-thrusts the undeformed foreland basin and is characterised mainly by the presence of middle Eocene to late Miocene sediments. These sediments were

tectonically deformed during the late Miocene, followed by salt structure emplacement during the Pliocene-Quaternary.

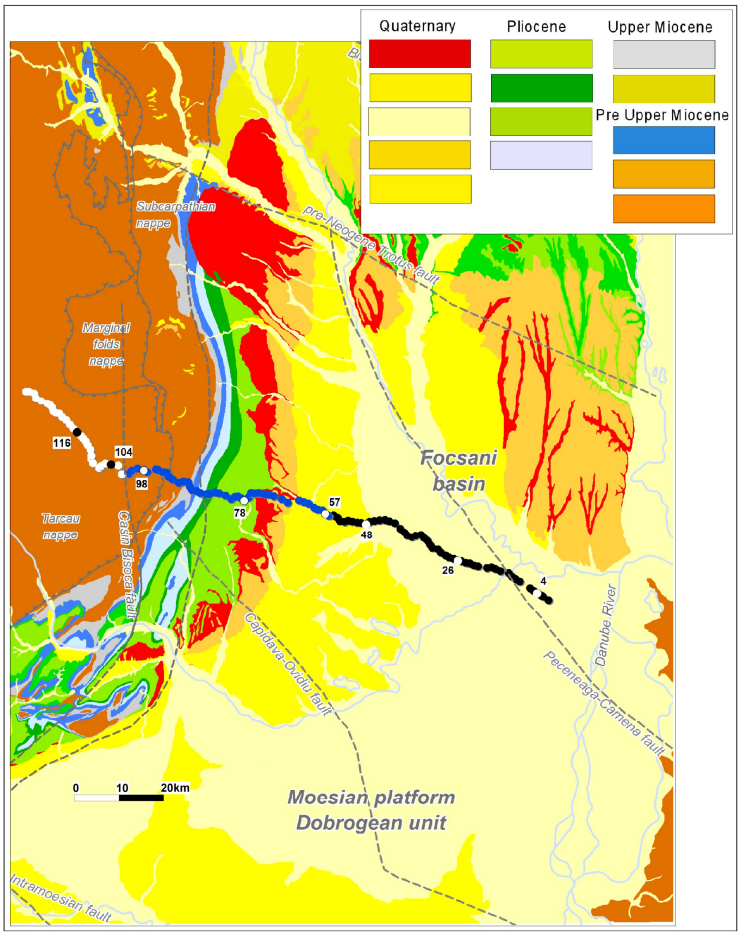

Fig.3.2. Geological map of the south-eastern Carpathians nappe complex and Focsani Basin sedimentary cover (modified after Matenco et al., 2003), with the location of the DACIA-PLAN seismic survey. The individual lengths of deployments I-III were 22.1, 55.8 and 55.9 km; some overlap exists between the deployments (about 5.3 km between deployment I and II and 10.3 km between Deployment II and III).

To the east, the thick Focsani foreland basin was developed (Fig. 3.2), overlying autochthonous Palaeozoic-Mesozoic sedimentary rock complexes (Visarion et al., 1988). Its maximum thickness is roughly 13 km to the north of the bending zone (Tarapoanca et al., 2003), gradually decreasing towards the ENE and SSE. The westward limit of the Focsani syncline is conventionally considered to be the Casin-Bisoca fault, active during post-Miocene times (Fig. 3.1). Although its kinematics are unclear below the nappes to the north (Dicea, 1995; Hippolyte and Sandulescu, 1996), it appears to be the direct prolongation of basement involved thrusts interpreted from foredeep velocity structure and geometry (Bocin et al., 2005;

Leever et al., 2006). To the north, the Subcarpathian nappe is thrusted over the foreland, while to the south of the pre-Neogene Trotus fault, the Carpathians front is outlined by a recumbent fold, which is overlain by Upper Sarmatian-Quaternary sediments (Dicea, 1995). The basement structure of the foreland basin includes two large stable platforms, the East European Platform and the Moesian Platform, separated by what is called the North Dobrogean zone (Fig. 3.1; cf. Saintot et al., 2006). It is limited to the north by the Trotus fault, to the south by the Intramoesian Fault and neighbours the North Dobrogean zone along the basement scale Peceneaga-Camena fault.

3.3. DACIA-PLAN data

3.3.1. Seismic data acquisition

A set of 90 s long seismic records were registered using single-component digital seismographs (REFTEK-125s; "Texans") on a transect crossing the main tectonic units of the south-eastern Carpathians and its foreland (Fig. 3.2). Seismographs were placed at 100 m intervals on three overlapping deployments (from west to east, "Deployments I-III") using 334 recorders on Deployment I and 632 recorders on both Deployments II and III, recording 29, 45, and 53 explosive shots respectively (cf. Table 1). The individual lengths of deployments I-III were 22.1, 55.8 and 55.9 km, with a nominal shot spacing of 1 km that varied due to rough terrain, drilling and shooting circumstances. The overlap between deployment I and II was 5.3 km; between deployment II and III it was 10.3 km. Because of road access, the geometry of the seismic line is crooked. The highest elevation reached was 1240 m, in the mountainous Deployment I. The lowest elevation (40 m) occurs in the foreland basin at the eastern end of the line. Positioning and timing was accomplished using differential GPS measurements for most of the shot points and some recorder sites (see Bocin et al., 2005 for details). A total of 127 shots were fired and 67,951 seismic traces were recorded (see Bocin et al., 2005 and Table 2 for shot locations and other details).

Table 1 DACIA-PLAN acquisition parameters

Source	***28 kg dynamite***
Nominal source spacing	***1 km***
Shot depth	***20 m***
Recorders	***Reftek-125 s***
Nominal receiver spacing	***100 m***
Number of channels	***334 — deployment 1***
	637 — deployment 2
	632 — deployment 3
Number of shots	***29 — deployment 1***
	45 — deployment 2
	53 — deployment 3
Record length	***90 s***
Sampling interval	***5 ms***

Table 2. List of seismic shots used for ray tracing modelling (see Bocin et al., 2005 for other details of shotpoints).

Shot	Easting	Northing	Elevation	Positioning	Number	Data fit
131	444566.33	5068808.90	1061.00	DGPS	422	0.090
127	448044.97	5066571.41	1157.00	DGPS	386	0.080
124	450554.54	5065009.77	1201.00	DGPS	472	0.080
120	452859.40	5062772.69	1138.00	DGPS	502	0.100
116	456269.51	5059412.47	1078.00	DGPS	446	0.100
113	458307.87	5057225.17	1007.00	DGPS	546	0.180
110	459527.69	5053999.40	1011.00	DGPS	501	0.120
108	459891.98	5052246.97	857.00	DGPS	532	0.170
104	463941.47	5052049.21	1064.00	DGPS	512	0.160
101	468158.86	5049917.44	1207.00	DGPS	589	0.290
98	471542.27	5050697.86	1026.00	GPS	535	0.170
95	474836.86	5050745.81	745.00	DGPS	583	0.180
93	476718.37	5050134.70	788.00	DGPS	564	0.240
91	478140.39	5048592.47	767.00	DGPS	571	0.190
87	482048.31	5046920.86	489.00	DGPS	623	0.190
84	484407.73	5045500.74	430.00	GPS	559	0.220
81	487766.96	5045639.93	385.00	DGPS	583	0.190
78	491511.51	5044141.01	334.00	GPS	644	0.220
75	493796.72	5044328.42	315.00	DGPS	598	0.290
72	496036.44	5045546.37	418.00	DGPS	585	0.410
69	499227.69	5045255.95	407.00	DGPS	682	0.080
66	503085.16	5044155.67	335.00	DGPS	668	0.150
62	508111.00	5043461.80	138.00	DGPS	677	0.135
60	510506.59	5042085.09	115.00	GPS	655	0.131
57	513061.34	5040846.74	108.00	DGPS	648	0.117
54	515877.36	5039920.83	93.00	DGPS	651	0.160
51	518305.42	5039204.07	84.00	DGPS	673	0.163
48	521284.39	5038697.36	71.00	DGPS	670	0.130
45	524304.65	5039126.04	66.00	DGPS	656	0.128
42	527686.91	5039070.62	59.00	DGPS	670	0.123
38	531067.18	5036476.17	58.00	GPS	652	0.142
35	533717.01	5035649.41	54.00	DGPS	653	0.137
32	536460.46	5034453.81	50.00	GPS	660	0.138
29	538794.73	5032473.76	48.00	GPS	647	0.100
26	541324.66	5030654.14	47.00	DGPS	636	0.195
23	544191.56	5029745.18	45.00	GPS	643	0.202
20	547058.06	5028755.95	45.00	DGPS	633	0.183
16	551087.76	5028357.93	44.00	GPS	607	0.152
12	555024.23	5026987.75	42.00	DGPS	561	0.104
9	557515.48	5025114.13	41.00	GPS	481	0.072
4	561636.98	5022408.46	41.00	DGPS	634	0.088
2	562772.00	5021665.00	43.00	DGPS	622	0.045

3.3.2. Data used

Along the seismic line the quality of data varies according to acquisition circumstances and thus strongly differs from the foreland basin to the nappe system (e.g. Panea et al., 2005). The signal-to-noise ratio is relatively low, especially at large offsets. There are surface wave cones for shots situated in the Carpathians (see Fig. 3.3). Nevertheless, picking first-arrival travel times provided sufficient data for ray tracing. The uncertainty for first-arrival refracted phase picks lies in the range 30-50 ms. A top mute and a minimum phase band-pass filter (4-16 Hz) were applied prior to picking.

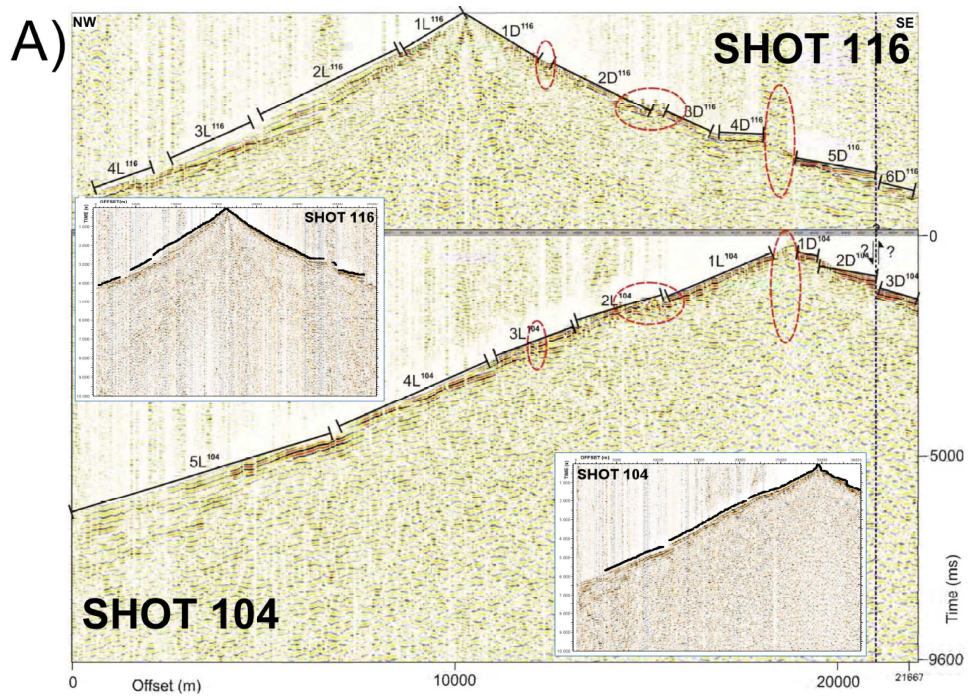

Fig.3.3. Identification of refracted phases from shot gathers and recurrent variations of seismic attributes due to velocity perturbations or seismic ray illumination (see text for extended explanations): a) deployment I shot gathers 116 and 104.

The number of shots used for forward modelling was 42 (every third shot was chosen; Table 2). Where the signal to noise ratio and/or positioning was poor, an adjacent shot gather was used instead. Some representative shot records, illustrating the signal to noise ratio, are presented in Fig. 3.3. Of the 15421 traces recorded on the chosen 42 shot gathers, 11020 were considered clear enough (pick uncertainty < 50 ms) to be used in the forward modelling. A total of 22410 rays derived through ray tracing from the picked travel times were used to obtain the final velocity model (see Table 2 for number of rays per shot). The number of rays per shot is contingent to the signal to noise ratio and varied due to the different number of travel times that were picked and used in the modelling.

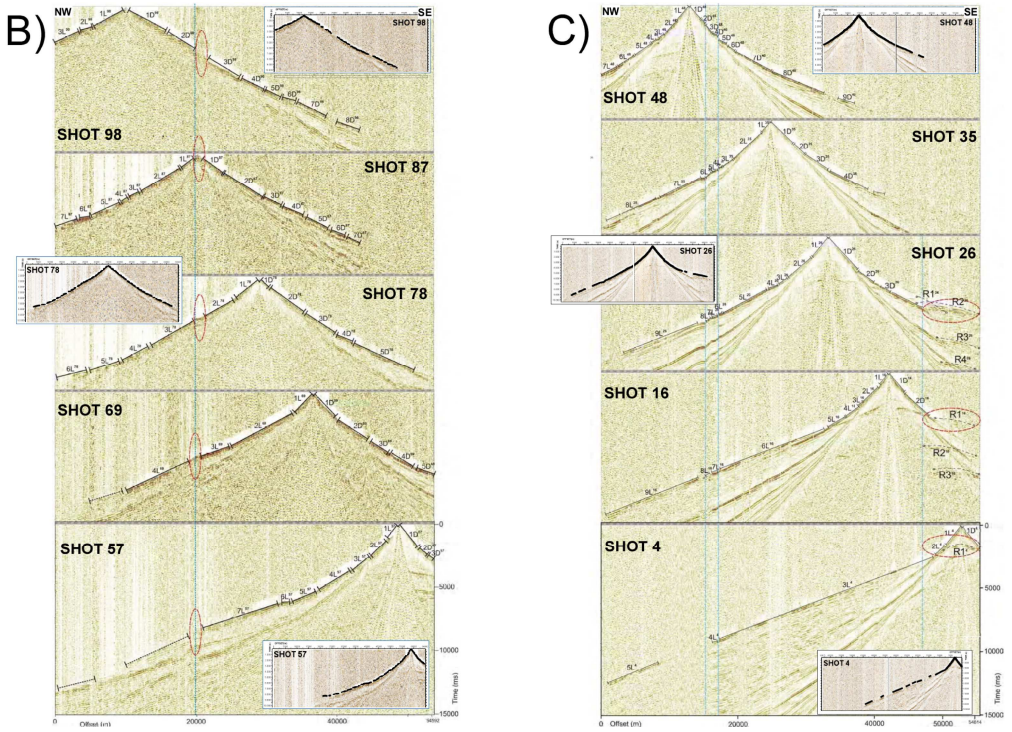

Fig.3.3. (*Continued*) Identification of refracted phases from shot gathers and recurrent variations of seismic attributes due to velocity perturbations or seismic ray illumination (see text for extended explanations): a) deployment I shot gathers 116 and 104; b) deployment II shot gathers 98, 87, 78, 69 and 57;c) deployment III shot gathers 48, 35, 26, 16, and 4. Shot locations are shown in Fig. 3.2. Insets represent average quality shot gathers displaying first arrival picks (picks uncertainty ~ 50 ms): 2 shots from deployment I (entirely acquired within the nappe complex) and, respectively, 3 shots for each of deployments II and III (westernmost shots also within the nappe complex and the rest within the foreland basin). The signal to noise ratio increased from deployment I to III with maximum quality in the Focsani Basin area. Refracted phases are labelled, for example, as **1L**^{116} being the first segment (layer) to the left on shot gather 116 and **4D**^{116} being the fourth segment (layer) to the right on shot gather 116. This terminology is used when referring to specific phases in the text though not all labelled segments are discussed individually.

3.4. Modelling approach

Ray tracing was done using RayInvr (Zelt and Smith, 1992). A graphical user interface and other portable RayInvr-based algorithms (RayGUI and SeisWide; Loss et al., 1998a and 1998b; Deping, 2003) were also used.

The seismic survey acquisition geometry was translated into a 2D synthetic orthogonal coordinate system. In order to account for the inherent crooked line geometry (Fig. 3.2), travel time misfits were calculated using real offsets instead of just projecting the crooked line onto a 2D straight line. Some misfits due to lateral

effects are introduced because the strike of emerging rays is set to a dominant azimuth that is perpendicular (sometimes not the case in reality) to geological structures. The maximum offset was 120 km while the depth lower limit was set to 20 km. Smoothing was applied to layer boundaries when two-point ray tracing was performed. The source and receiver locations were treated as offsets belonging to a full profile and not to a number of different deployments (three as in the seismic acquisition). The number of rays traced for each ray group (a group of seismic rays belonging to the same phase which is refracting or reflecting from the same layer) was set to 50. A minimum of 2 degrees for the take off angle for the refracted ray group in the first layer was chosen.

The main modelling steps adopted were: A) selecting specific model parameterizations; B) phase correlations and the choice of phases to model; C) assigning layers inferred from the apparent phase velocities and travel times; D) obtaining a ***preliminary model*** (referred to as "seismological velocity model" **SVM** – obtained by studying velocities, Fig. 3.3); E) incorporating known structural features (from geological, tectonic and geophysical studies) specifically required by the data into the preliminary model; and F) obtaining a ***final ray tracing velocity model*** (referred to as **FVM**).

These steps and the implied continuous interplay between preliminary and final velocity models effectively strengthened the model constraints and diminished its non-uniqueness. The choice of the number of shots used in the ray tracing was not governed by statistical principles but rather was inherited from the data. Too few shots led to a too smooth model and high data misfits while using too many made the ray tracing inappropriate given the limitations of the ray tracing algorithm.

The **SVM** (Fig. 3.4 and 3.5a) was obtained using 7459 rays, which were forward modelled simultaneously for all shots (10 shots). A global data fit of 0.241 s and a chi-squared value of 21.939was determined. An initial interpretation of the velocity model was performed and certain key elements of the seismological model were defined in order to be thoroughly tested for their robustness.

The more complex velocity model **FVM** was developed (Fig. 3.5b) using the velocity contrasts, the layering, the amplitude of velocity structures derived through the preliminary model. Simultaneously, information was incorporated from previous seismic observations (for example, industry reflection profiles) and velocity modelling results, geological mapping constraints and their lithological expressions (Bocin et al., 2005; VR99 and VR01 seismic surveys, for localisation and velocity models consult Hauser et al., 2001 and Hauser et al., 2007; Leever et al., 2006; see discussion section for details). Rays were traced through the model (Fig. 3.5c, d, e, f, g), either by grouping 5 shots and fitting the travel times for each consecutive layer (downwards) simultaneously or by individually modelling all boundaries corresponding to each shot. During ray tracing the velocity structures were

interpreted and classified into two main categories, primarily differentiated by their horizontal extents (calculated in terms of the covered number of shots) and by the velocity perturbation induced (of regional or local character). An average data fit of 0.156s was achieved (see Table 2 for detailed data fit along the seismic line). The

normalised chi-squared value was 9.194. The overall data fit decreased compared to the (2.5D) tomographic model (Bocin et al., 2005; 0.068s) partly because of the 2D discretisation of the crooked line but also because of the "geological" structure subjectively incorporated from independent data. The final number of layers is 9; velocity inversions were incorporated and layers were allowed to pinch-out. This led to a significant improvement compared to the initial **SVM**, satisfying the seismic data as well as the introduced independent geological constraints.

The data analysis (Fig. 3.3a, b and c) was done graphically for each shot gather from each of the three deployments. The gradients of refracted phases on each shot gather were translated to layers with nodal velocity values shaping the eventual velocity model "skeleton". Velocity perturbations related to fractures, major faults and complex structures (near isoclinal folds, fault zones, etc.) were considered to be the cause of time-offset graph disarrays and blurred alignments of seismic phases (such as sudden drops in amplitude).

3.5. Velocity model

3.5.1. SVM (preliminary model; Fig.*3. 4*)

Fig. 3.4 presents the preliminary velocity model (**SVM**) as well as the ray paths for all layers and shots used for modelling and the data fit between observed and calculated travel times. The **SVM** describes a velocity low depression (long red dashed line) almost 10 km deep to the east while, to the west, an assemblage (yellow dotted oval) of a higher (relative to those in the east) velocities is disturbed by two elevated high velocity zones (5.8-6.5 km/s basement domain velocities). The data analysis step (Fig. 3.3a, b and c) suggested that an average number of 6 distinctive velocity gradient-defined layers are present. Thus, the **SVM** consists of 6 layers of gradually increasing velocity with depth separated by five different velocity boundaries. It was observed during modelling that, even from the first layer, the velocity structure splits into two separate domains: from 0 to km 50 high velocities at shallow depths (see Fig. 3.4a., Nappe System, **NS**); from 50 to km 120 low velocities at deeper levels (see Fig. 3.4a., Foreland Basin, **FB**).

At the smaller offsets, similar to the tomographic velocity model (Bocin et al., 2005), the near surface layer has a moderately high velocity (2.9-3.2 km/s) with the exception of two "synclines" of low velocity (see Fig. 3.4a, **LV1** and **LV2**; 2.2-2.5 km/s) of ~7 and respectively ~10 km between km 28-32 and km 40-46. At km 45-50 strong narrow vertical variations of velocities (the short blue dashed prism) are

observed. At km 110 a high velocity unit (Major Fault, **MF**) vertically cuts the nicely layered 60 km long (km 50 to km 110) and 8 km thick depression of gradually increasing velocity. At deeper levels, a 4 km thick layer of 3.4-4.8 km/s is present along the whole seismic line.

Other striking features that are observed are the anomalous high velocity structures (5.5-6.8 km/s; basement domain velocities) at km 10-30 (basement unit 1, **B1**) and km 35-55 (basement unit 2, **B2**), which appear to displace the overlying layers upwards. Another interesting velocity structure present in the higher velocity domain is located at km 90 and suggests an abrupt change in velocity over a very short distance. Ray paths are presented in Fig. 3.4b. Fig. 3.4c gives the comparison between calculated and observed travel times. All the velocities structures were noted and preserved in subsequent steps during which the final velocity model was derived.

3.5.2. FVM (final model; Fig.*3.5*)

The interplay between the preliminary velocity model based purely on seismic interpretation of velocities (**SVM**) and the final velocity model (**FVM**) incorporating strong constraints derived from geological mapping driven by hydrocarbon explorations (Radulescu et al., 1976, Stefanescu et al., 1988, Stanica and Stanica, 1998, Matenco and Bertotti, 2000, Tarapoanca et al., 2003, Leever et al., 2006), their structural (Matenco et al. 2007, Schmid et al., 2008) and lithological expressions (Sandulescu and Visarion, 1988; Matenco and Bertotti, 2000) and previous geophysical velocity models (see Fig. 3.7a for ray tracing and tomographic inversion comparison, Bocin et al., 2005) has allowed a robust final model (**FVM**) with a reduced degree of non-uniqueness to be developed. The **FVM** is compared with the **SVM** in Fig. 3.5, which also shows ray paths for the **FVM** and the data fit for each shot used in forward modelling.

The number of layers in the **FVM** was increased to allow forward modelling of almost all of the observed travel time patterns. Thus, the **FVM** consists of 9 layers. The velocity model extends to a depth of about 15 km. As already seen during the interpretation of the **SVM**, velocity features lie between clearly defined (sub)vertical and (sub)horizontal boundaries. Integrating the previous "experience" (the **SVM** velocity patterns) with modelling the increased number of data led to two scales in which the velocity model could be perturbed. The terms "long wavelength" and "short wavelength" are used to refer to these, in order to facilitate further description and interpretation of the models. These terms are intended to express something of the amplitude as well as spatial scales of the constraints on various velocity features of the **FVM**. The "long wavelength" features have a regional character at the scale of the **FVM**, involving rays traced from 5 up to 15 shots. The "short wavelength" features, in contrast, are constrained by only 2 to 3 shots. As discussed in more detail below,

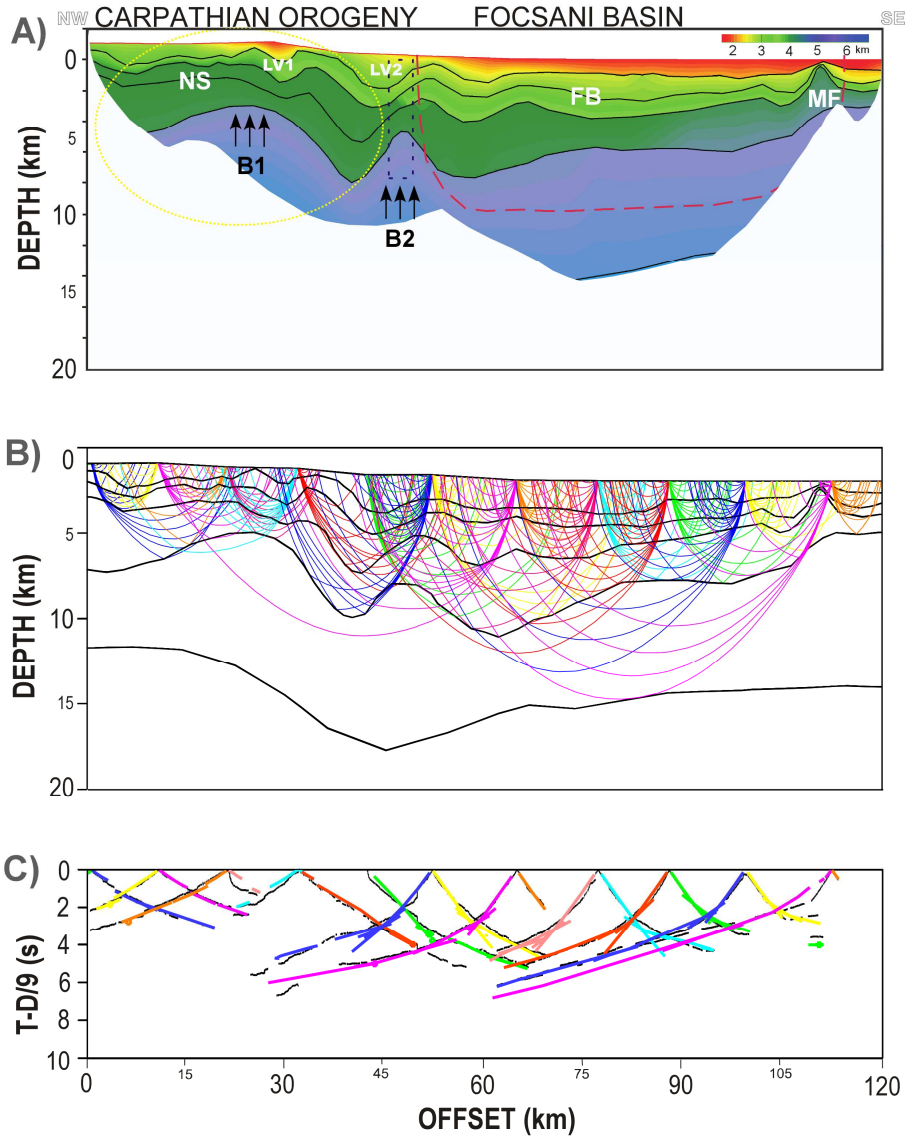

Fig.3.4. The "seismological" velocity model (**SVM**) obtained using only 10 shots from a total of 127: a) interpreted **SVM**; b) colour coded ray paths for the **SVM**; c) data fit between observed and calculated time for the **SVM** model; velocity reduction for the calculated vs. observed travel times graph is 6.5 km/s. See text (section 5.1) for velocity model analysis and labelling. The coloured envelope of the seismic velocity model also represents the ray path coverage. Labels: NS – nappe system; FB – foreland basin; MF – major fault; LV1, LV2 – syncline of low velocity; B1, B2 – basement material.

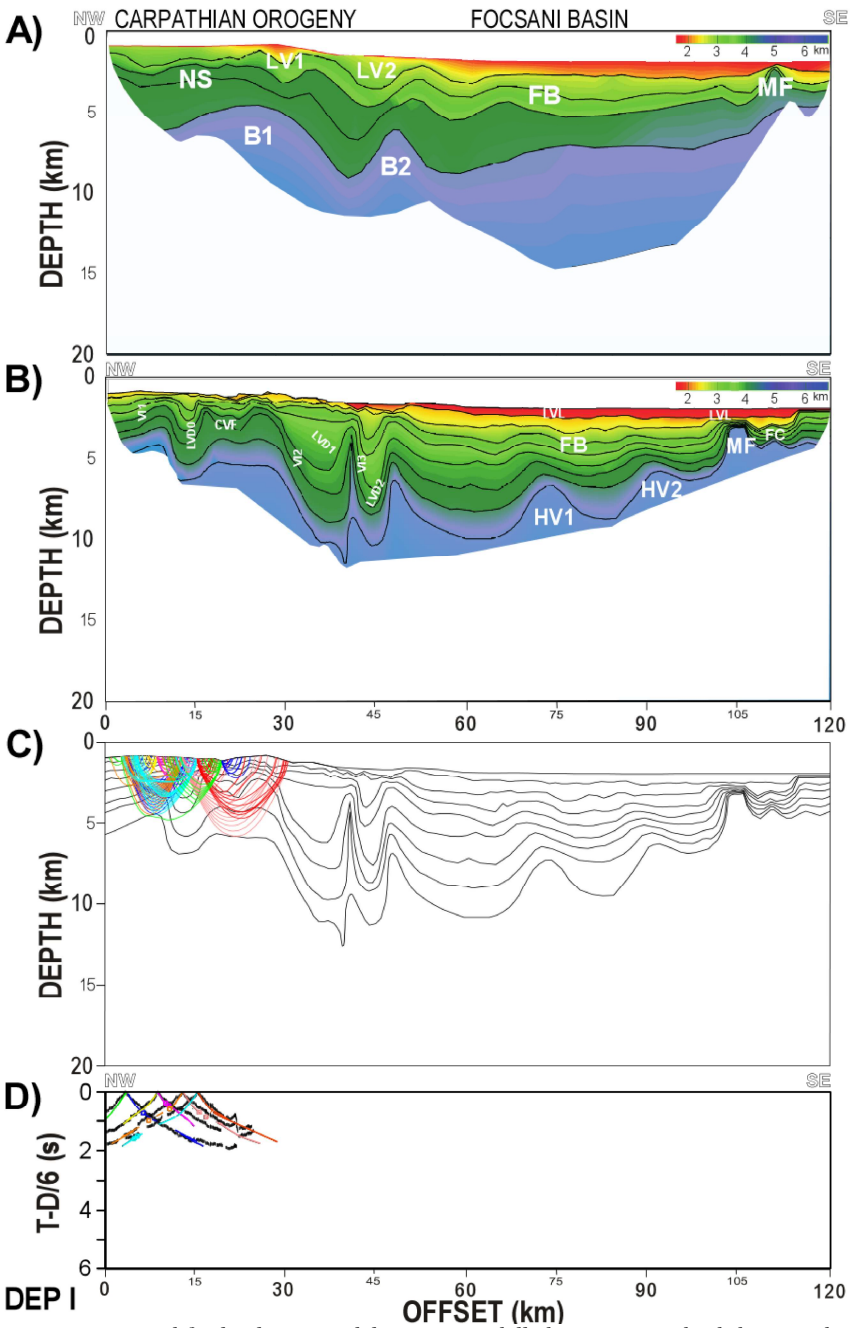

Fig.3.5. Uninterrupted final velocity model (**FVM**) modelled using every third shot (42 shots in total) and graphs of data fit between observed and calculated time for corresponding velocity key patterns and features (note change of horizontal scale, done to enhance clarity). a) **SVM** velocity model - the velocity structures from this model were noted and preserved and used as initial inputs; b) final velocity model (**FVM**). Graphs of velocity key patterns and features with data fit between calculated and observed travel times and colour coded ray paths: c) km 0 to 30; d) km 15 to 45. Velocity reduction is 6.5 km/s. Labels: VI1, VI2, VI3 – velocity inversions; CVF - complex of vertical faults; LVD0, LVD1, LVD2 – low velocity depression; B1, B2 – basement material; LVL low velocity layer; FB – foreland basin; HV1, HV2 – high velocity anomalies; MF – major faul; FC – fault complex.

the former will be interpreted as major faults, low or high velocity bodies, basement uplifts and major vertical velocity contacts (that disturb the velocity model regionally) while the latter will be associated to small faults, velocity inversions, small low velocity bodies and velocity discontinuities (that disturb the velocity model locally). Fig. 3.5 (c, d, e, f and g) presents, in increasing offset order, ray path coverage of the key features of the velocity model (robust "long wavelength" velocity anomalies) and their correspondent data fit. Fig 3.6 shows the distribution of ray coverage in the model. Specific features of the **FVM** discussed below are named with letter codes that appear as labels in Fig. 3.7.

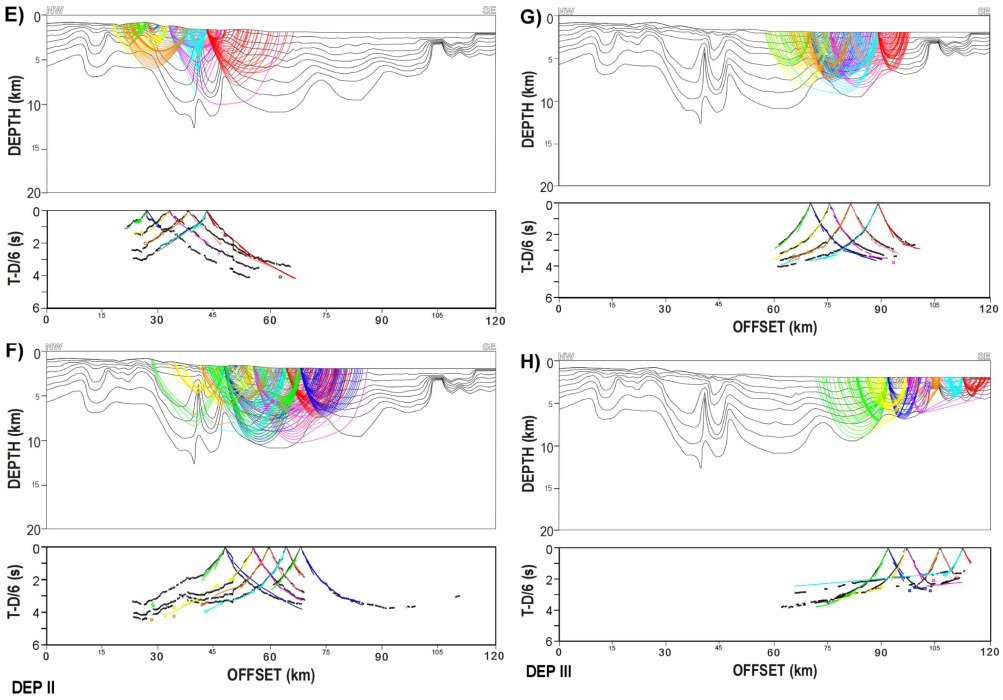

Fig.3.5. (Continued) Graphs of velocity key patterns and features with data fit between calculated and observed travel times and colour coded ray paths: e) km 30 to 60; f) km 45 to 80; g) km 65 to 100 and h) km 80 to 120.

3.5.2.1. "Long Wavelength" features of the FVM

Between km 0 and 12, inferred from 5 shots, a shallow high velocity (5.8-6 km/s) body at 3.5-4 km depth is present (**B1;** Fig. 3.7b**)**, indicated, for example, by phases 1L-4L^{116} and 3L-5DL^{104} on the shot gathers (Fig. 3.3a). Between segments 4D^{116} and 5D^{116} on the same shot gather a low velocity boundary appears in the oval (**LVD0**; Fig. 3.7b). Associated with the blurred zones present on both shot gathers (red dashed ovals) are velocity perturbations and poor ray path illumination in zones with low velocity concealed by higher velocities (in this case an almost vertical contact).

Located by more than 5 modelled shots from km 15 to km 30, another shallow high velocity body **B2** at a constant 4 km depth (Fig. 3.7b) is inferred. Analysing the travel times and imposed by high velocities (phase segments $4D^{116}$, $5D^{116}$, $6D^{116}$ and $1D^{104}$, $2D^{104}$, $3D^{104}$), a number of high velocity nodes are necessarily introduced for 4-5 consecutive shots used in the modelling. The ray coverage and data fit of the first 30 km of the profile are shown in Fig. 3.5c.

Between km 30 and 40 a thick succession of low velocity layers forms a depression (**LVD1;** Fig. 3.7b) that is covered by 4-5 shot gathers. The observed travel times require a sudden reduction of velocity (to the range 3.5-4.5 km/s) and the boundary nodes to root at deeper levels within this depression. Ray paths and observed and modelled travel times are presented in Fig. 3.5d. A pronounced vertical velocity discordance with the shape of a narrow prism (see also **SVM**) cuts through the covering layers at km 40. The structure is well constrained (rays from 5-6 modelled shots; Fig. 3.5d and 3.5e). On shot gathers from deployment II at km 38 to 42 offset (red dashed ovals Fig. 3.3b) blurred zones (due to velocity perturbations or poor ray path illumination) and increasing relatively high velocities ($2L^{78}$, $3L^{69}$, $6L^{57}$ and $7L^{57}$) repeat with almost identical shapes and attributes (deployment I from km 0 to 12). Between km 40 and km 52 another low velocity zone (**LVD2;** Fig. 3.7b) is modelled. Shot gathers show complexities in the area and segments of the picked refracted phases (3D-$5D^{98}$, $2D^{87}$, $1L^{78}$, $1L^{78}$,$1L^{69}$,$2L^{69}$, 3L-$4L^{57}$; Fig. 3.3b) exhibit low velocities. The migration of the low velocities in offset to the right on the shot gathers is possibly related to the different strike of the profile with respect to the structure. The low velocity layer **LVL** (1.6-2.4km/s) is pinching-out to the west around km 40.

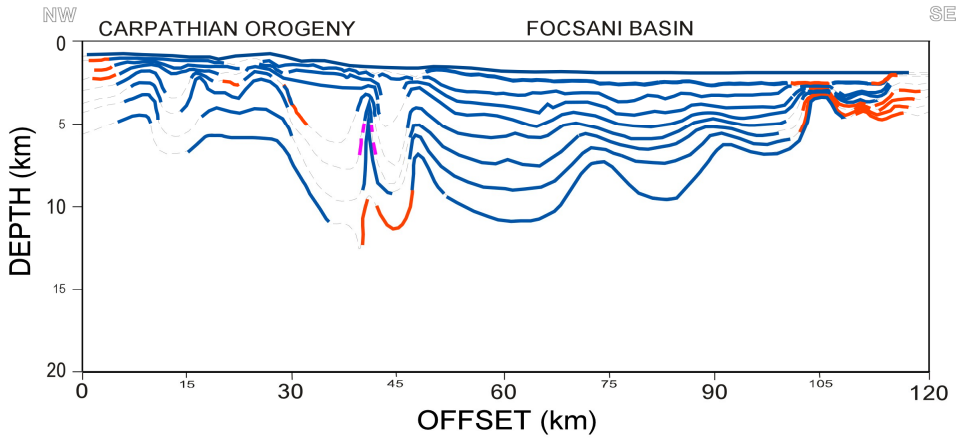

Fig.3.6. The refracted phase ray coverage: magenta segments represent unreversed coverage for the related layer; red segments represent those with single phase reversed coverage; dark blue represents those with multiple phase reversed coverage.

Starting at km 50 the velocity nodes along boundaries are redefined. There is a fairly sudden change from a domain with high velocities at relatively shallow depths to one with low velocities at greater depths (~ 7-8 km). A more gradual increase of velocity with depth was required by the data, leading to a change of nodal velocities and a new set of boundaries. Overall, the velocity structure of the last 70 km (20 shots; Fig. 3.5f and g) of the seismic profile delineates a thick succession (8 km) of relatively low velocity layers (labelled **FB** in Fig. 3.7b) thinning eastward that is punctuated at its base by three sub-vertical high velocity anomalies.

The first of these (**HV1**), located between km 70 and 80, is relatively wide, being covered by 4-5 shots and it exhibits a high velocity structure vertically displacing a set of horizontal layers. The velocity structure was recognised in small segments of the refracted phases ($2D^{48}$, $3D^{48}$, $4D^{48}$, $4L^{35}$, $5L^{35}$, $6L^{35}$, $6L^{26}$, $7L^{26}$, $8L^{26}$, $7L^{16}$, $8L^{16}$ and $4L^{4}$; Fig. 3.3c) from numerous shot gathers from Deployment III. The second (**HV2**) is located at km 90. It was observed on fewer shot gathers but is well correlated as the $3L^{26}$ and $4L^{26}$ segments in Fig. 3.3c. The third (**MF**; inferred also in the **SVM**, Fig. 3.4a), perhaps the most evident during modelling, is located around 100-105 km and occurs at a shallower depth (2 km). The anomaly was ray traced using travel times identified on almost all deployment III shot gathers. Strong reflected phases (R1, R2, R3 and R4 corresponding to shots 26, 16 and 4) are also visible on the presented shot gathers and, although they weren't modelled, they added valuable information to the ray tracing (information about depth, velocity boundaries nodes, etc).

3.5.2.2. "Short Wavelength" features of the FVM

Between km 0 and 12 a shallow velocity inversion (VI1) is present. Developed on several velocity boundary nodes, especially on the boundary between layers 4 and 5 (3.3 to 4 km/s velocity layers) this anomaly was incorporated in the velocity model in order to improve the fit. Another velocity inversion (VI2) is present (km 35-40) this time much stronger and thicker than the previous one, but having similar velocity ranges (3.3 to 4 km/s). It can also be identified on shot gather 87 (Fig. 3.3b) as a segment of low velocities ($4L^{87}$) between higher velocity segments ($3L^{87}$ and $5L^{87}$). Similarly, a velocity inversion (Fig. 3.7b) but with reverse expression within phase segments ($6D^{98}$ and $6L^{57}$) within the 3.3 to 4 km/s velocity interval appears to the east at km 43-45 (VI3). At km 110-120 small scale velocity perturbations (fault complex related; FC) are observed. They affect velocity boundaries with nodal velocities greater than 2.5 km/s.

3.5.2.3. The FVM versus the published tomography model

The long wavelength features of the **FVM** and the previously published tomography model (Bocin et al., 2005) outlined in Fig. 3.7a are similar, which suggests that they are somewhat robust, but the former clearly has provided greater structural resolution as was intended. These features include (1) the shallow high velocity body in the western most part of the model (**B1**); (2) the second shallow velocity body (**B2**) situated in the ray tracing model between km 15-30 and in the tomography model at 25-30 km (see Fig. 3.4b in Bocin et al., 2005); (3) the low velocity body (**LVD1**) at km 38 and km 3 depth; (4) the low "depression" (**LVD2**) associated to Subcarpathian nappe; (5) the **FB** basement backthrust; (6) the strike slip fault associated to **HV2** velocity anomaly and visible also in the tomography model (see Fig. 3.7a and b, Bocin et al., 2005) and (7) the major system of faults (**MF**).

3.6. Geological interpretation and discussion

The interpretation focuses on zones of anomalous velocity rather than, but not neglecting, an examination of the velocity layers themselves. The velocity model aligns conformably with previous observations about the south-eastern Carpathians and its foreland: a relatively high velocity domain corresponding to a highly deformed thin-skinned nappe complex (the western 50 km of the profile) but with abrupt changes of basement topography (uplift on crustal faults); and a relatively low velocity (increasing with depth) thick sedimentary basin (the rest of the profile) deposited on metamorphic basement and offset by faulting on new or reactivated faults. What previous geological studies failed to supply was an accurate estimate of the basement topography because of the complicated overlying structures (nappes and thrusting faults) and thick sedimentary overburden. This has been achieved here by complementing the earlier published tomographic model with a geologically focused and constrained forward modelling procedure that not only provides robust information about the basement topography but also inferences about ongoing uplift processes beneath the south-eastern Carpathians and at their contact with the Focsani Basin.

Between km 0 and 12 a shallow high velocity body (5.8-6km/s velocity and 3.5-4 km depth), seen also on previous velocity models (Bocin et al., 2005; Fig. 3.7a.), suggests basement thrusting associated with a reverse fault with a ~2 km offset. The shallow high velocity body **B1** at 3.5-4 km depth is interpreted as basement material because the velocity values correspond to those of crystalline rocks (5.8-6 km/s). A previous 3D tomographic study (Landes et al., 2004) also inferred high velocity material in this area but was not able to resolve its depth.

The previously unrecognized interpreted fault (Fig. 3.7b, "Proposed crustal fault 1") is based on an inferred step-like velocity structure. It appears to offset much

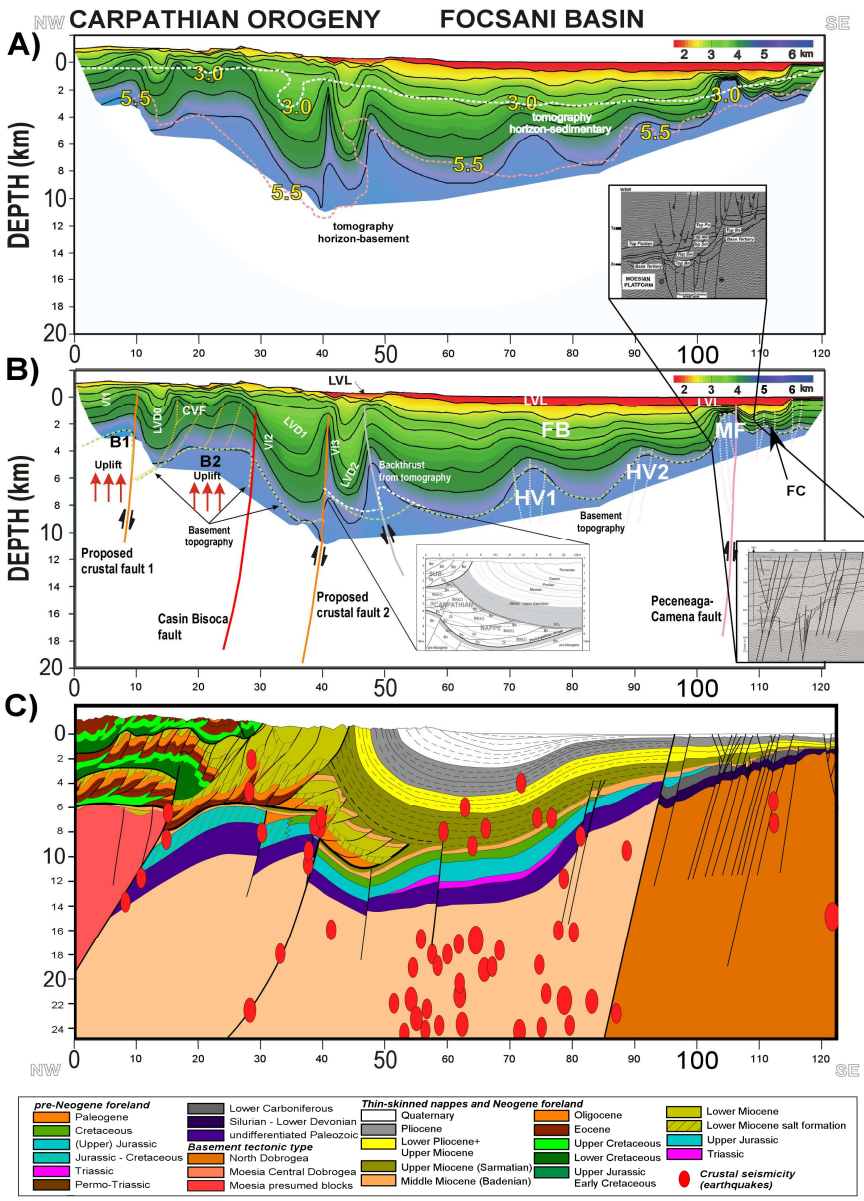

Fig.3.7.a) Comparison of tomography (Bocin et al., 2005) and ray tracing velocity models (this study): white dashed line represents the sedimentary cover boundary of velocities lower than 3 km/s; pink dashed line (5.5 km/s) represents the basement topography obtained from tomography. b) Interpreted final velocity model (see text). The insets shows: ; upper and lower right – Peceneaga Camena major fault system seen on two different seismic sections (Tarapoanca et al, 2003, Leever et al., 2006); lower centre - the interpretation of a shallow seismic section (Leever et al., 2006) where an alternative interpreted structure has been identified (see text). c) Geological cross section across the thin skinned nappes of the south-eastern Carpathians and the foreland basin (modified after Matenco et al., 2007); the vertical exaggeration is 2 to 1. The earthquakes (red ellipses) were projected along strike of Tertiary structures into the cross section; relative magnitudes are indicated by the size of the ellipse. Note that the original geological cross-section is located ~20 km north of the DACIA-PLAN profile and was projected along orogenic strike. Structures that have a direction oblique to this strike might not be located in the same place along the sections.

of the sediments, ending near the surface just beneath the low velocity layer of 1.6-2.8 km/s. At the same offset, but shallower, the short wavelength velocity inversion (**VI1**) correlates well with an intercalated succession of Eocene-Oligocene and Upper-Lower Cretaceous sedimentary layers within the Tarcau nappe. Located from km 28 to km 35, another shallow high velocity body (**B2**; seen also in the **SVM** model, Fig. 3.4a) suggests an uplifted crystalline basement in which the Casin Bisoca fault would play an important kinematic role (Fig. 3.7b). A complex of vertical faults (**CVF**), interpreted on the basis of (near) vertical boundaries within the velocity model, slice through the low velocity cover. They can be considered as structural "anomalies" associated with the nappe structure or as features inherited from salt movement phenomena. **B1** and **B2** are fairly robust features of the velocity model as explained earlier.

Between km 30 and 40 a wide "depression" of low velocity material (**LVD1**) is inferred that can be associated with the Neogene Subcarpathian nappe. Another velocity inversion zone (**VI2**) is present, thicker than the previous one, perhaps related to the inter-bedding of Lower Miocene salt with other sediments (velocities of 4-4.5 km/s are within the range for salt).

At km 40 a pronounced narrow body characterised by high velocities (the prism of velocity with upper boundary from 5 to 5.5 km/s, lower boundary from 6 to 6.8 km/s) cuts through the overriding layers and, if interpreted as a structural feature, it could represent the prolongation of a previously mapped crustal fault (Fig 3.7b, "Proposed crustal fault 2"; Leever et al., 2006, Matenco et al., 2007). Due to its vertical extent and disturbance of almost all other layers in the model it is interpreted to be an active (Pliocene-Pleistocene; Leever et al., 2006) fault. The vertical displacement is approximately 2.5 km. This feature is quite robust, seen in almost 40% of the data (shot gathers, travel times graphs, ray tracing, etc) and incorporated in the **SVM** as well (dashed body Fig. 3.4a). It is also associated with recent seismic activity, as is the Casin Bisoca fault (Matenco et al., 2007, see Fig. 3.7c).

Another low velocity body (**LVD2**) between km 40 and km 50 can be interpreted in two ways. 1) It is the western flank of the Focsani syncline affected by a backthrust, in agreement with the previous tomography model (see Bocin et al., 2005; their Fig. 3.7a) but impossible to model in that direction as the modelling technique accepts only unique velocity values for velocity boundaries at the same offsets; in this case, the frontal part of the Subcarpathian nappe structurally defines a triangle zone (see Matenco and Bertotti, 2000). 2) More recent seismic and structural data have demonstrated the incompatibility of a backthrust in the near-surface. The Focsani Basin sediments unconformably overlie the frontal thin-skinned units, being subsequently truncated by a more internal Subcarpathian thrust (Fig. 3.7b, see Leever et al., 2006). The low velocity layer (1.6-2.4 km/s), which pinches out to the west around km 45, mimics the contact between the Subcarpathian nappe and Focsani

Basin, the latter underthrusting locally the former (Tarapoanca et al., 2003). A velocity inversion (Fig. 3.7b) with the same velocity layer configuration as in the previous low velocity depression **LVD1,** suggests similar origins; thus, the **LVD2** velocity body is considered also to represent a component of the Subcarpathian nappe. All the previous velocity structures (between km 0-50) are part of the south-eastern Carpathians nappes system.

The widespread low velocity body (**FB**) which runs approximately from km 45 for 60 km eastwards and goes as deep as 9 km depth is interpreted as the deep foreland Focsani Basin.

The wide high velocity structure (**HV1**) between km 70 and 80 displaces the deeper horizontal layering of the **FB** and is associated with a fault zone roughly perpendicular to the seismic profile. With a similar geometry as the **HV2** velocity anomaly located at km 90, these type of structures are well known in this area of the Moesian Platform from petroleum exploration, the basement being uplifted and subsequently eroded in pre-Miocene times (i.e. pre-Focsani Basin evolution), the latest erosion being interpreted as Paleogene (Paraschiv, 1983; see also Stefanescu et al., 1988). The velocity contrast is the one between uplifted basement and adjacent Mesozoic strata and/or the morphology of the erosional surface.

The velocity highs (**HV1**, **HV2**, **MF**, etc.) in the model are interpreted as fault zones suggesting that there is some degree of basement uplift involvement, such as in a transpressional flower structure. Some previous studies (Chiarabba and Amato, 1997; Honda and Yomogida, 2003) interpret similar kinds of high velocity anomalies as transpressional (or transtensional) fault zones or segments of faults where, due to anisotropic effects, high velocity is preferentially observed in the direction of rupture propagation.

The third (**MF**; Fig. 3.7b insets and present also in the **SVM**, Fig. 3.4a) located around km 100-105 is interpreted as representing the Peceneaga-Camena crustal fault (zone) that separates the Moesian Platform from the uplifted North Dobrogean block. This fault, while it has a rather complex Mesozoic evolution (see Hippolyte, 2002), has more than 1 km normal offset at the level of the Middle Miocene strata, and can be associated with syn-tectonic patterns until Quaternary times (Leever et al., 2006). At km 110-120 some small velocity anomalies are observed, in agreement with the Middle Miocene of graben and horst geometry defined by Tarapoanca et al. (2003) in the same area. The "short wavelength" velocity anomalies (**FC**) are interpreted as being a fault complex that cuts through the sedimentary cover locally influencing the basement topography. Although the reflections were never modelled, some of them, the stronger ones, were observed on several records (outlined R1s, R2s, R3s and R4s in Fig. 3.3c). These strong reflections are derived from the relatively shallow basement at the eastern end of the profile (cf. Panea et al., 2005).

3.7. Summary and conclusions

A forward ray tracing velocity model derived from more than 10000 travel times picked from 42 shot gathers along a 140 km line crossing the south-eastern Carpathian bending zone and the deep (foreland) Focsani Basin. Given the acquired degree of redundant and reversed ray coverage in the final velocity model, these data allow an upper crustal domain geological interpretation to be proposed that illuminates the spatially and temporally coupled complex contact between the south-eastern Carpathian nappe complex and its foreland basin.

Two different scales of velocity anomalies were defined in the course of the modelling process: "long wavelength" anomalies observed by 5 to 15 shots, which are robust features of the model and constituted the focus of the modelling approach, and "short wavelength" anomalies observed by 2 to 3 shots, which perturb the velocity model locally.

In particular, the model results refine basement structure beneath the south-eastern Carpathian nappe stack and Focsani Basin and allow the following conclusions to be made.

1) Structural anomalies at the base of the supra-basement layers in the velocity model are interpreted as faults or fault systems affecting basement and, in some cases, overlying sedimentary layers in the area of south-eastern Carpathians nappe complex and foreland basin.

2) Reverse faults, including at least one that was previously unrecognised, on which crystalline rocks or highly metamorphosed Mesozoic sedimentary cover of the crystalline basement have been elevated to depths as shallow as 3.5-4 km (with a vertical displacement of at least 2-2.5 km) are identified beneath the Vrancea Zone in the external south-eastern Carpathians.

3) The inferred (reverse or not) faults in the Vrancea Zone appear to affect strata almost to the present-day surface and may therefore remain active. Two, the Casin Bisoca Fault and the "Proposed Crustal fault 2" can be associated with recent upper crustal seismicity.

4) The velocity model is compatible with models in which pronounced uplift in the Carpathian Vrancea Zone is coupled with contemporaneous adjacent foreland subsidence post-dating the main Miocene orogenic nappe emplacement.

5) Normal faults and flower structures, the presence of which is supported by previous geological and industrial seismic profiling, are associated with the tectonic subsidence of the foreland Focsani Basin.

6) Intracrustal earthquakes recorded on the projected paths of the inferred faults suggests that the topographic evolution along the DACIA-PLAN profile

area, from the Vrancea Zone to its foreland basin, is coupled with synchronous uplift-subsidence movements within the larger regional Pannonian-Carpathian system affected by Pliocene-Quaternary contraction and inversion.

The ray tracing of the DACIA-PLAN refraction data constrained a velocity model that provides a valuable upper crustal "boundary condition" for future studies of the structure and processes which are evolving in the Vrancea Zone area of the south-eastern Carpathians.

Acknowledgments

The DACIA-PLAN 2001 seismic survey was part of the larger Pannonian-Carpathians Netherlands Research Centre for Integrated Solid Earth Science (ISES) multi-disciplinary framework. The modelling research was held during research fellowship visits, part of the joint PhD of AB at the VU University, Amsterdam, Netherlands and University of Bucharest, Romania. Ionelia Panea is thanked for her continuous support to process the data at Delft University using ProMax and afterwards creating the initial inputs for the modelling procedure. We wish to thank to Ari Tryggvason and the anonymous reviewer for their constructive and professional reviews that lead to improved balance and focus in the paper.

References

Bocin, A., Stephenson, R., Tryggvason, A., Panea, I., Mocanu, V., Hauser, F., Matenco, L., 2005. 2.5 D seismic velocity modelling in the south-eastern Romainan Carpathians Orogen and its foreland, Tectonophysics, Volume 410, 273-291.

Burchfield, B.C., 1976. Geology of Romania. Geol. Soc. Am., Spec. Pap., Volume 158, 82.

Chiarabba, C., Amato, A. 1997. Upper-crustal structure of the Benevento area (southern Italy): fault heterogeneities and potential for large earthquakes Geophysical Journal International, Volume 130, 229–239.

Cloetingh, S. A. P. L., Burov, E., Matenco, L., Toussaint, G., Bertotti, G., Andriessen, P. A. M., Wortel M. J. R., Spakman, W., 2004. Thermo-mechanical controls on the mode of continental collision in the SE Carpathians (Romania). Earth and Planetary Science Letters, Volume 218, 57-76.

Deping, C, 2003. SeisWide (http://seismic.ocean.dal.ca/sortware.php).

Dicea, O., 1995. The structure and hydrocarbon geology of the Romanian East Carpathians border from seismic data, Pet. Geosci., Volume 1, 135-143.

Ellouz, N., Roure, F., Sandulescu, M., Badescu, D., 1994. Balanced cross-sections in the Eastern Carpathians (Romania): a tool to quantify Neogene dynamics. In: Roure, F., Ellouz, N., Shein, V.S., Skvortsov, I. (Eds.), Geodynamic Evolution of Sedimentary Basins, Technip, Paris, pp. 305–325.

Hauser, F., Raileanu, V., Fielitz, W., Bala, A., Prodehl, C., Polonic, G., Schulze, A., 2001. VRANCEA'99 – the crustal structure beneath the southeastern Carpathians and the Moesian Platform from a seismic refraction profile in Romania. Tectonophysics, 340, 233-256.

Hauser, F., Raileanu, V., Fielitz, W., Dinu, C., Landes, M., Bala A., Prodehl, C., 2007. Seismic crustal structure between the Transylvanian Basin and the Black Sea, Romania. Tectonophysics.Volume 430, 1-25.

Heidbach, O., Ledermann, P., Kurfeß, D., Peters, G., Buchmann, T., Matenco, L., Negut, M., Sperner, B., Müller, B., Nuckelt, A. and Schmitt, G., 2007. Attached or not attached: slab dynamics beneath Vrancea, Romania, International Symposium on Strong Vrancea Earthquakes and Risk Mitigation. Oct. 4-6, 2007, Bucharest, Romania, pp. 4-20.

Honda, R., Yomogida, K., 2003. Effect of complex fault geometry and slip style on near-fault strong motions and static displacement. Earth Planets Space, Volume 55, 515-530.

Hippolyte, J.C., Sandulescu, M., 1996. Paleostress characterization of the "Wallachian" phase in its type area, southeastern Carpathians, Romania. Tectonophysics 263, 235–249.

Hippolyte, J.C., 2002: Geodynamics of Dobrogea (Romania): new constraints on the evolution of the Tornquist–Teisseyre Line, the Black Sea and the Carpathians. Tectonophysics, 357, 33-53.

Landes, M., Fielitz, W., Hauser, F., Popa, M., CALIXTO Group, 2004. 3-D upper crustal tomographic structure across the Vrancea Seismic Zone, Romania. Tectonophysics, Volume 382, 85-102.

Leever, K.A., Matenco, L., Bertotti, G., Cloetingh, S.A.P.L., and Drijkoningen, G.G., 2006, Late orogenic vertical movements in the Carpathian Bend Zone - seismic constraints on the transition zone from orogen to foredeep: Basin Research, Volume 18, 521-545.

Loss, J., ten Brink, U., Pecher, I., 1998a, RayGUI - a graphical 2-D ray-tracing interface for UNIX: EOS, Volume 79, 334.

Loss, J., Pecher, I., ten Brink, U., 1998b, RayGUI - a graphical 2-D ray-tracing package for UNIX: U.S. Geological Survey Open-File Report 98-203.

Martin, M., F. Wenzel, and CALIXTO Working Group (2006), High-resolution teleseismic body wave tomography beneath SE Romania: II. Imaging of a slab detachment scenario, Geophys. J. Int., 164, 579 – 595, doi:10.1111/j.1365-246X.2006.02884.x

Matenco, L., Bertotti, G., 2000. Tertiary tectonic evolution of the external East Carpathians (Romania). Tectonophysics 316, 255– 286.

Matenco, L., Bertotti, G., Cloetingh, S., Dinu, C., 2003. Subsidence analysis and tectonic evolution of the external Carpathian-Moesian platform region during Tertiary times. Sediment. Geol., Volume 156, 71-94.

Matenco, L., G. Bertotti, K. Leever, S. Cloetingh, S. Schmid, M. Tărăpoancă, and C. Dinu (2007), Large-scale deformation in a locked collisional boundary: Interplay between subsidence and uplift, intraplate stress, and inherited lithospheric structure in the late stage of the SE Carpathians evolution, Tectonics, 26, TC4011, doi: 4010.1029/2006TC001951.

Morley, C.K., 1996. Models for relative motion of crustal blocks within the Carpathian region, based on restorations of the outer Carpathian thrust sheets. Tectonics 15, 885–904.

Panea, I., Stephenson, R., Knapp, C., Mocanu, V., Drijkoningen, G., Matenco, L., Knapp, J., Prodehl, K. 2005. Near-vertical seismic reflection image using a novel acquisition technique across the Vrancea Zone and Foscani Basin, south eastern Carpathians. Tectonophysics, Volume 410, 293-309.

Paraschiv, D., 1983. Sur les facteurs structogenetiques du secteur Roumain de la plate-forme Moesienne. Ann Inst Geol Geofiz, LX: 189-198.

Radulescu, D.P., Cornea, I., Sandulescu, M., Constantinescu, P., Radulescu, F., Pompilian, A., 1976. Structure de la croute terrestre en Roumanie, Essai d'interpretation des etudes sismiques profondes. Ann. Inst. Geol. Geofiz., L 50, 5– 36.

Roure, F., Roca, E., Sassi, W., 1993. The Neogene evolution of the outer Carpathian flysch units (Poland, Ukraine and Romania)" kinematics of a foreland/fold-and-thrust belt system. Sedimentary Geology, 86: 177-201.

Royden, L.H., 1993a. The tectonic expression slab pull at continental convergent boundaries. Tectonics, Volume 12, 303-325.

Royden, L.H., 1993b. Evolution of retreating subduction boundaries formed during continental collision. Tectonics, Volume 12, 629-638.

Saintot, A., Stephenson, R. A., Stovba, S., Brunet, M.-F., Yegorova, T., Starostenko, V. 2006. The evolution of the southern margin of Eastern Europe (Eastern European and Scythian platforms) from the earliest Precambrian–Early Palaeozoic to the Early Cretaceous. In: Gee, D. G. and Stephenson, R. A. (ed.) European Lithosphere Dynamics. Geological Society, London, Memoirs, 32, 481–505.

Sandulescu, M., 1984. In: Geotectonica Romaniei, Ed. Tehnica, Bucharest, 336.

Sandulescu, M., Visarion, M., 1988. La structure des plate-formes situees dans l′avant-pays et au-dessous des nappes du flysch des Carpathes orientales. St. Tehn. Econ., Geofiz., Volume 15, 62–67.

Schmid, S., Bernoulli, D., Fügenschuh, B., Matenco, L., Schefer, S., Schuster, R., Tischler, M. and Ustaszewski, K., 2008. The Alpine-Carpathian-Dinaridic orogenic system: correlation and evolution of tectonic units. Swiss Journal of Geosciences, 101(1): 139-183.

Stanica, D., Stanica, M., 1998. 2D modelling of the geoelectric structure in the area of the deep-focus Vrancea earthquakes. CERGOP ''South Carpathians'' Monogr. 7 (37), 193–203, Warszawa.

Stefanescu, M., and Working Group, 1988. Geological cross sections at scale 1:200,000, Map A9-14, Inst. Geol. Geofiz., Bucharest.

Stefanescu, M, 2006. Subcarpathian Nappe - Analysis of Hydrocarbon Prospectivity in the Gresu and Nereju Blocks. Rompetrol E&P Report, Bucharest.

Tarapoanca, M., Bertotti, G., Matenco, L., Dinu, C., Cloetingh, S., 2003. Architecture of the Focsani Depression: a 13 km deep basin in the Carpathians Bend Zone (Romania). Tectonics, Volume 22, 1074.

Tarapoanca, M., 2004. Architecture, 3D geometry and tectonic evolution of the Carpathians foreland basin. PhD Thesys, Vrije Universiteit, Amsterdam, The Netherlands.

Visarion, M., Sandulescu, M., Stanica, D., Veliciu, S., 1988. Contributions a la connaissance de la structure profonde de la plateforme Moesienne en Roumanie. St. Tehn. Econ., Geofiz., Volume 15, 68– 92.

Zelt, C. A., R. B. Smith, 1992. Seismic traveltime inversion for 2-D crustal velocity structure. Geophysical Journal International, Volume 108, 16-34.

CHAPTER IV

DACIA PLAN GRAV MAN'S. FROM ACQUISITION TO PROCESSING

"Refining is inevitable in science when you have made measurements of a phenomenon for a long period of time."

Charles Francis Richter

"An experiment is a question which science poses to Nature, and a measurement is the recording of Nature's answer."

Max Planck

4.1. Introduction

The south-eastern Carpathians, Vrancea Zone and Focsani Basin constitute an area that was investigated by numerous geoscientific studies that sum dozens of years of field observations and countless hours (maybe enough to travel to a remote galaxy) of personal/team work. The "*Wild Eastern Carpathians*" blossomed geosciences as it represents a zone strongly prone to earthquakes where the efforts to understand active dynamic processes met the genuine curiosity of different working groups.

This chapter presents a localized effort to supplement, with densely spaced high accuracy gravity and magnetic data, the previously existing geophysical data. The continuous progress of geological imaging requires regular acquisition of new data to support their increasing resolution requirements. Otherwise, the interpretations, due to "sufficiency", will reach a "*Status Quo*". The ISES funded potential field project

responded to this and provided a set of new data that, integrated with seismic information, would lead to new interpretations.

4.1.1. Previous information

High (densely spaced) resolution gravity and magnetic data are scarcely available over the Romanian territory and where they are present the access to them is partly restricted. What was considered to be useful though, the larger spacing and ready to use data, is mentioned below. The Romanian Gravity Map was constructed on the basis of 78026 gravity stations, giving a mean coverage of 0.33 stations/km^2. The network has a 5'x7'.5 density. The gravity meters used for measurements were: Norgaard 33%, GAK 24%, Sharpe 36%, Askania 5%, and Worden 2%. The geomagnetic map of Romania was obtained from regional, airborne geomagnetic surveys over the Romanian territory between years 1962 and 1968 (Cristescu et al., 1962-1968). The measurements were conducted for seven years in a row by Prospectiuni S.A.

A number of independent studies that aimed to map the particularities of the Romanian lithosphere are also available for use. Various geophysical experiments, using different methods, inferred information about the architecture (the depth and lateral distributions) of the basement platform. Detailed interpretations of (electro)magnetic anomalies connected with geological structures (foreland, hinterland, nappe system, internal or external mountainous depressions) were made by several authors (Gavat el al., 1965; Constantinescu et al., 1972; Airinei, 1985; Visarion et al., 1988, 1998; Stanica et al., 1999; Besutiu, 2001, Wonik et al., 2001; Sprinceana and Besutiu, 2005; etc). Similarly, gravity surveys and their modelling and interpretation were focused on specific geological areas and proposed a number of interpretations about various anomalies on the Romanian territory (Socolescu et al., 1964; Atanasiu et al., 1996; Matenco et al., 1997; Besutiu et al., 2001; Hackney et al., 2002; Sperner et al., 2004; Szafian et al., 2006; Ioane et al., 2005a; Ioane et al., 2005b; Raileanu et al., 2005; Zadeh et al., 2005; etc).

4.1.2. Instrumentation

The DACIA PLAN GRAV MAN'S survey represented a gravity and magnetic data field acquisition project that combined traditional and modern technologies with proficient long-established (more than 50 years of history) measuring methods. The instrumentation used for the acquisition came from different partners of the ISES framework. The relative gravity meters were borrowed from Department of Earth Sciences, Utrecht University, the GPS instruments came from TU Delft Faculty of

Aerospace Engineering and the magnetometers were the property of the Geophysics Department of the University of Bucharest.

The gravity survey was completed using two different Worden compact temperature-compensated quartz gravity meters. These gravity meters can measure with an approximate accuracy of 0.01 mgal. For detailed photo close-ups and illustrative representations of the system concept and interior consult the Annex 1. Both Worden gravity meters were Pioneer type with a range of 2100 dial divisions and each having a different dial constant: one equal to 0.0955 mgal/division used in the 2005 campaign; and, the other equivalent to 0.104 mgal/division used in the 2006 campaign. In the 2005 campaign a Sharpe gravity meter from the University of Bucharest was taken in the field but after two failed (too large closing drift errors) drift tests and due to a limited range of dial division (only 1000) it was not used for measurements. Both Worden gravity meters were first verified in the field and the drift was considered to be resolute and coeval under the upper limit of error necessary to conduct a gravity survey.

Three Proton Precession Magnetometers (PPMs - made at the Institute of Atomic Physics, Bucharest) were used for the magnetic survey that was completed during the 2005 campaign. The principals of use and a scheme of the magnetometers along with a picture from the field campaign are presented in Annex 2. All three magnetometers were verified/repaired (as necessary) at Prospectiuni S.A. for electronic malfunction before departing in the field and they were calibrated and tested on two calibration points, one just outside Bucharest and one in Brasov. The PPMs sensors were filled with kerosene.

The GPS survey was complementary and in support of the gravity and magnetic survey in order to provide exact horizontal positioning and accurate elevations in millimetric scale order of the measurement points (stations). It is commonly known that gravity varies with height (for each third metre one milligal), and, therefore, it was necessary to use GPS measurements for rapid and accurate determination of station coordinates. The field deployment involved 5 Leica 500 systems with SR530 receivers and AT502 antennas (see Annex 3). The same GPS systems were used previously in yearly GPS campaigns as part of the larger ISES framework project (van der Hoeven et al., 2005).

4.2 Data acquisition

The DACIA PLAN GRAV MAN'S (Danube and Carpathian Integrated Action on Processes in the Lithosphere and Neotectonics Gravity and Magnetic Survey) gravity and magnetic survey was accomplished in two campaigns: first, in July-August 2005 (23rd of July to 6th of August), when 80% of the gravity data were acquired and all the magnetic stations and GPS positions were measured; second, in June (21st to 25th of

June) 2006, when an extra number of gravity stations were measured with airlifted (IAR-316B *Alouette* III helicopter) support from the Romanian Air Force in order to close a small gap in the central part of the profile.

As previously stated the present survey overlaps the deep reflection seismic profile DACIA PLAN but not entirely, ending near Dumitresti (see Figure 4.1). The profile was extended to the west with an extra stretch of 5 km as intuitively it was desired to cover and discover the prolongation (to the West) of a robust and geophysically evident transition concealed by surrounding structural complexities. The 2005 campaign was split into two main stretches mainly because of the time duration of gravity cycles, GPS accuracy and logistical issues: in July measurements were made in a sector near Comandau-Secuiu-Vintileasca and the logistical and scientific base was set at Comandau; in August measurements were made in the Vintileasca-Jitia-Chiojdeni-Dumitresti area (on the other side of the Carpathian crest) with the logistics base station moved to Focsani and the scientific base station to Chiojdeni. Details regarding the scientific reasons for choosing these locations are explained later in this chapter, in the subsection corresponding to each method. The data acquisition represented at that time a novel combination of methodologies that summed differential high quality GPS and densely spaced resolute gravity and magnetic measurements.

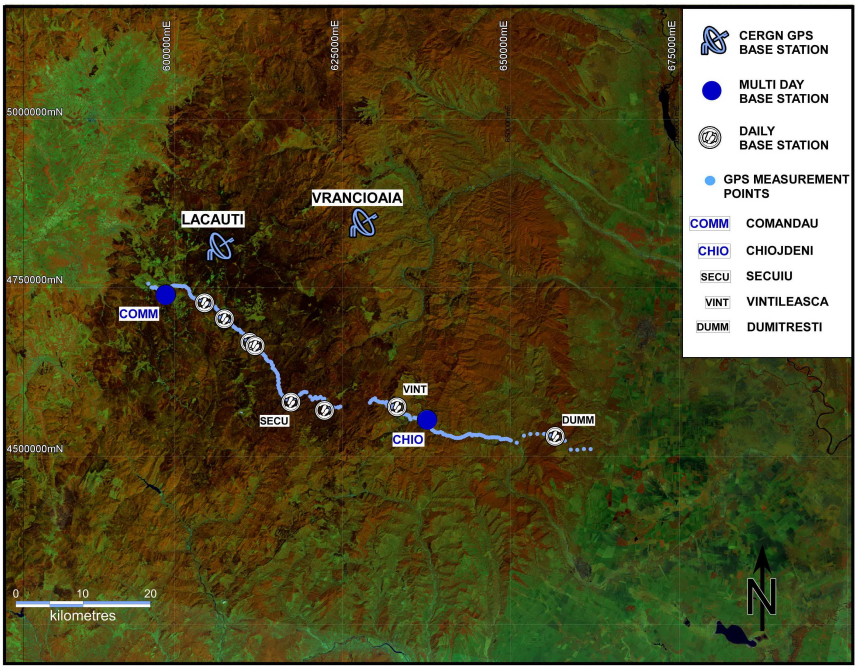

Fig.4.1. DACIA PLAN GRAV MAN'S GPS survey. CERGN base stations, multi day base stations, daily base stations and GPS measurement points. The image behind is a high resolution LANDSAT image.

4.2.1. GPS data acquisition

The GPS survey was conducted to provide high accuracy positioning support for the gravity and magnetic profile. Specifically, determination of gravity station elevation was the main requirement for conducting the complementary GPS survey. In the field the GPS measurements preceded the rest of the survey. The GPS teams (two rover teams), after a reconnaissance and staking visit in the field, measured several hours or a day ahead of the other teams. The pace of measuring was in step with the other geophysical surveys and, in so doing, any problems with localisation could be addressed directly in the field without affecting the overall schedule.

The observation time required for an accurate measurement depends on the following factors: baseline length, number of satellites, satellite geometry (GDOP - ***G****eometric* ***D****ilution* ***o****f* ***P****recision*) and ionosphere. Therefore, in order to have shorter baseline distances between permanent stations and control stations of the profile the GPS survey was split into two main stretches when the scientific base stations were set at Comandau and later at Chiojdeni. Table 1 presents an approximate guide for baseline lengths and resulting observation times.

Obs. Method	**No. satellites GDOP ≤ 8**	**Baseline Length**	**Approximate time observation**	
			By day	By night
Rapid Static	4 or more	Up to 5 km	5 to 10 mins	5 mins
	4 or more	5 to 10 km	10 to 20 mins	5 to 10 mins
	5 or more	10 to 15 km	Over 20 mins	5 to 20 mins
Static	4 or more	15 to 30 km	1 to 2 hours	1 hour
	4 or more	Over 30 km	2 to 3 hours	2 hours

Table1. Approximate guide for baseline lengths and resulting observation times

The methods of measuring in the field with differential GPS were a combination of *Static Relative Positioning* and *Rapid Static Relative Positioning* procedures (see Ghilani and Wolf, 2008 for details). The *Static Relative Positioning* method was used to transfer the coordinates from two *permanent stations*, part of the ISES/CRC-461 network, located at Lacauti and Vrancioaia (see Figure 4.1), to two *multi day base stations* located at Comandau and Chiojdeni (see Figure 4.1). Finally, to complete the surveying procedure framework (control points spread/network) there were established *daily base stations* located less than 10 km distance from the area that was supposed to be surveyed. Consequently, using the *Static Relative Positioning* method, the *daily base stations* coordinates were determined using as the *"permanent stations"* the *multi day base stations* (Comandau or Chiojdeni, depending on the localisation). To determine the measurement points coordinates (gravity or magnetic) of the profile

there were used one or two *rover stations*/teams applying the *Rapid Static Relative Positioning* method.

The relative accuracy with both (static and rapid static) relative positioning methods are in the range of ± 3 to 5 mm + 1 ppm (GPS Accuracy = error + [ppm error x distance to base]; for this survey ≤ 20 mm) with the observation that rapid static method is suitable to measure base lines up to 20 km. Nevertheless, in order to achieve this kind of resolution optimum satellite configuration (GDOP) and appropriate ionospheric conditions must prevail (see Figure 4.2 for overall GDOP and satellite visibility).

Two log sheets used for surveying stations are shown in Annex 4: one used for notes regarding daily base stations details and one for rover stations that contains operator notes while measuring in the field. The information noted on the log sheets (antenna height, time, antenna serial number, etc.) were used in the processing stage.

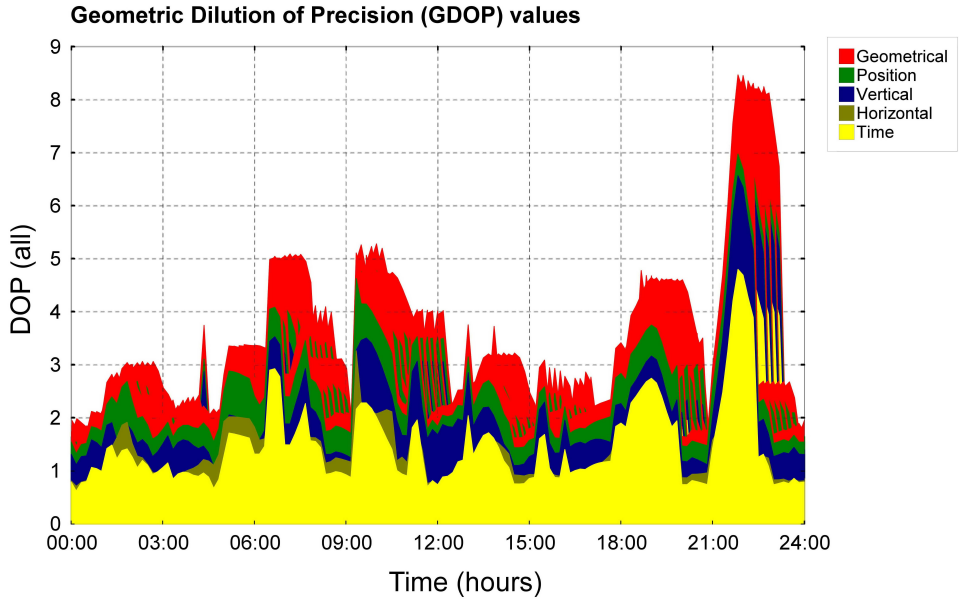

Fig.4.2. The Geometric Dilution of Precision (GDOP) and satellite visibility during the DACIA PLAN GRAV MAN'S survey (for the July 23rd to August 6th 2005 period).

More than 95% of the station coordinates were determined using the differential GPSs. For the rest of the stations the horizontal positions were obtained using both handheld GPS and less accurate differential GPS measurements whilst for the elevation a Leica leveller was used, tied to nearby differential GPS sites. The accuracy of the levelled stations was good enough (< 10 cm; < 0.03 mGals error - below gravity meter resolution) for making them available for further geophysical investigations.

4.2.2. Gravity data acquisition

The gravity survey was performed initially to complement the previous deep reflection seismic survey DACIA PLAN but developed to be a relevant experiment and a useful study when integrated with the magnetic survey and other geophysical investigations. The gravity survey was designed to produce an accurate and detailed profile of gravity anomalies of the south-eastern Carpathians and its foreland. The profile was projected to overlap the former DACIA PLAN seismic profile but only for the westerly orogenic and foreland-orogeny transition segment of it.

To link the gravity data to the Romanian National Gravity Network and to make them comparable to previous surveys an extensive number of ties between absolute gravity (control) points (Targu Secuiesc and Dumitresti) and points from the profile (see Figure 4.3) were performed. The exact number and date of acquisition of ties are presented in Table 2. It is important to acknowledge that after setting two main transferred absolute gravity (scientific) base stations at Comandau and Dumitresti in 2005 a third one was established/placed at Secuiu (tied to Nereju) in 2006. Therefore, base stations at Comandau, Secuiu and Dumitresti are considered as "*first order*". "*Second order*" ties (Figure 4.3) between points of the profile and "*first order*" base stations were established in order to increase the accuracy and repeatedly verify the "*absolute*" state of our own gravity network.

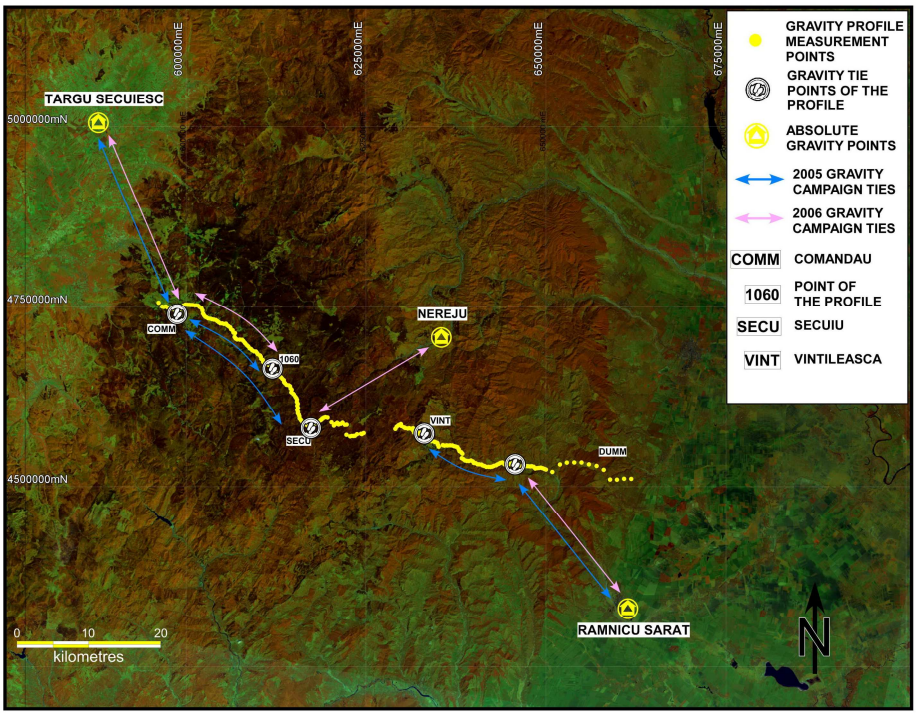

Fig.4.3. DACIA PLAN GRAV MAN'S gravity survey. Absolute gravity points, gravity tie points, and gravity measurement points. Behind: high resolution LANDSAT image.

Absolute Gravity @Targu Secuiesc = 980544.52							
K= 0.0955 mgal/div							
23.07.2005							
station	*time*	*reading*	*time elapsed*	*drift rate*	*corrected reading*	*readings anomaly*	*absolute gravity*
TS	11:00	2109.9	0.00	-2.75	2109.9		
COMM	12:10	973.6	-0.05	-2.75	973.733758	108.5038761	**980436.0161**
TS	13:37	2109.6	-0.11	-2.75	2109.9		
31.07.2005							
station	*time*	*reading*	*time elapsed*	*drift rate*	*corrected reading*	*readings anomaly*	*absolute gravity*
COMM	5:35	985	0.00	0.00	985		
1060	6:35	631.8	-0.04	0.00	631.8	33.7306	**980402.12**
SECU	7:10	981	-0.07	0.00	981	0.382	**980435.47**
1060	7:49	631.1	-0.09	0.00	631.1	33.79745	**980402.05**
COMM	8:40	985	-0.13	0.00	985		
station	*time*	*reading*	*time elapsed*	*drift rate*	*corrected reading*	*readings anomaly*	*absolute gravity*
COMM	8:40	985	0.00	15.16	985		
1060	9:40	632.5	-0.04	15.16	631.8684211	33.72406579	**980402.13**
SECU	10:21	980.5	-0.07	15.16	979.4368421	0.531281579	**980435.32**
1060	11:00	633.2	-0.10	15.16	631.7263158	33.73763684	**980402.11**
COMM	11:50	987	-0.13	15.16	985		
01.07.2007							
station	*time*	*reading*	*time elapsed*	*drift rate*	*corrected reading*	*readings anomaly*	*absolute gravity*
TS	6:21	2121.9	0.00	-8.58	2121.9		
COMM	7:27	985	-0.05	-8.58	985.3933775	108.5363825	**980435.98**
TS	8:52	2121	-0.10	-8.58	2121.9		
K= 0.104 mgal/div							
21.06.2006							
station	*time*	*reading*	*time elapsed*	*drift rate*	*corrected reading*	*readings anomaly*	*absolute gravity*
TS	10:52	1893.9	0.00	14.95	1893.90		
COMM	12:22	848.5	-0.06	14.95	847.57	108.8187803	**980435.70**
TS	13:55	1895.8	-0.13	14.95	1893.90		
TS	13:55	1895.8	0.00	-18.37	1895.80		
COMM	15:48	848	-0.08	-18.37	849.44	108.821302	**980435.70**
TS	17:11	1893.3	-0.14	-18.37	1895.80		
station	time	*reading*	*time elapsed*	*drift rate*	*corrected reading*	*readings anomaly*	*absolute gravity*
COMM	18:02	846.9	0.00	0.00	846.9		
1060	18:55	521	-0.04	0.00	521	33.8936	**980401.96**
COMM	20:18	846.9	-0.09	0.00	846.9		

Table2a. Gravity ties in area Comandau-Secuiu-Vintileasca

Taking into account different "*depths to significant structures*" the gravity profile was designed to comprise representative short and long wavelengths attributively co-genetic to structures. Therefore, a spacing of 250 m between gravity stations was chosen. The former shot locations of the DACIA PLAN seismic survey were used for guidance. The gravity stations were measured in the field using (as mentioned before) two Worden gravity meters and, for better handling the levelling process, an adjustable metal tripod of approximate 20 cm height. Covering long distances was possible by using cars as taxiing vehicles. A special case represents the 2006 campaign when, in order to complete the tie between Nereju and Secuiu (a double measured tie) and to measure the previously (2005 campaign) remote and inaccessible points

Absolute Gravity @Ramnicu Sarat= 980546.92							
K= 0.0955 mgal/div							
02.08.2005							
station	*time*	*reading*	*time elapsed*	*drift rate*	*corrected reading*	*readings anomaly*	*absolute gravity*
RS	10:51	2088.1	0.00	18.67	2088.1		
DUMM	11:50	1833.6	-0.04	18.67	1832.835185	24.37778981	**980522.54**
RS	12:39	2089.5	-0.08	18.67	2088.1		
03.08.2005							
station	*time*	*reading*	*time elapsed*	*drift rate*	*corrected reading*	*readings anomaly*	*absolute gravity*
DUMM	6:38	1835	0.00	0.00	1835		
VINT	7:55	906.9	-0.05	0.00	906.9	88.63355	**980433.79**
VINT	9:09	906	-0.10	0.00	906	88.7195	**980433.71**
DUMM	10:03	1835	-0.14	0.00	1835		
DUMM	10:03	1835	0.00	3.56	1835		
VINT	11:23	907.6	-0.06	3.56	907.4019802	88.58561089	**980433.84**
VINT	12:36	907.9	-0.11	3.56	907.5212871	88.57421708	**980433.85**
VINT	15:30	909.8	-0.23	3.56	908.9905941	88.43389827	**980433.99**
DUMM	16:47	1836	-0.28	3.56	1835		
04.08.2005							
station	*time*	*reading*	*time elapsed*	*drift rate*	*corrected reading*	*readings anomaly*	*absolute gravity*
DUMM	7:05	1836.3	0.00	-0.83	1836.3		
VINT	8:41	907	-0.07	-0.83	907.0556522	88.74283522	**980433.68**
VINT	11:27	907.6	-0.18	-0.83	907.7518841	88.67634507	**980433.75**
DUMM	12:50	1836.1	-0.24	-0.83	1836.3		
DUMM	5:55	1843.2	0.00	-7.85	1843.2		
VINT	7:01	915.4	-0.05	-7.85	915.76	88.57052	**980433.86**
VINT	9:40	915	-0.16	-7.85	916.2272727	88.52589545	**980433.90**
DUMM	11:25	1841.4	-0.23	-7.85	1843.2		
K= 0.104 mgal/div							
22.06.2006							
station	*time*	*reading*	*time elapsed*	*drift rate*	*corrected reading*	*readings anomaly*	*absolute gravity*
RS	18:14	1923.3	0.00	-25.87	1923.3		
DUMM	19:12	1686	-0.04	-25.87	1687.042188	24.5708125	**980522.35**
RS	20:22	1921	-0.09	-25.87	1923.3		
23.06.2006							
station	*time*	*reading*	*time elapsed*	*drift rate*	*corrected reading*	*readings anomaly*	*absolute gravity*
RS	9:56	1911.7	0.00	-13.31	1911.7		
DUMM	10:55	1675.3	-0.04	-13.31	1675.845378	24.52888067	**980522.39**
RS	11:55	1910.6	-0.08	-13.31	1911.7		
Absolute Gravity @Nereju= 980501.37							
24.06.2006							
station	*time*	*reading*	*time elapsed*	*drift rate*	*corrected reading*	*readings anomaly*	*absolute gravity*
SECU	15:01	1437.1					
NEREJU	16:28	1831.5	0.00	-56.00	1831.5		
SEC	16:59	1195.9	-0.02	-56.00	1197.105556	65.97702222	**980435.39**
NEREJU	17:22	1829.4	-0.04	-56.00	1831.5		

Table2b. Gravity ties in area Vintileasca-Jitia-Chiojdeni-Dumitresti

along the roughest topography segment of the profile, a helicopter provided airlifted support.

The gravity stations were deployed only at some distance from abrupt changes of local topography or any pertinent noise (to be considered in the field) in

order to simplify reductions. Along the profile the measurements were done in traverses (loops) less than three hours long. Stations were reoccupied in order to control directly in the field the drift and eventually cut-off the gravity tidal effects.

4.2.3. Magnetic data acquisition

The magnetic survey was acquired in conjunction with the gravity survey; integration of the two methods is no longer unusual but rather a common scenario. It was proposed to supplement the gravity profile with magnetic data in order to constrain better the lithology of sub-surface structures and complement the expected new interpretations. The "*magnetic tool*" has over the years been an efficient way of determining physical contacts between or within different/same geological units or structures. The magnetic profile was entirely acquired during the 2005 campaign and followed closely in the field and spatially the gravity survey (Figure 4.4).For reduction purposes, several daily base stations were established in the field that measured diurnal variations. Therefore, while surveying there were at least two Proton Precession magnetometers used: one as a base station instrument that measured at 5 minute intervals the magnetic field intensity (Figure 4.4); and the other instrument for measuring stations (rover; Figure 4.4). Magnetometer producers recommend 60 km or so as the largest distance to be of practical use in a survey. Whellams (1996) suggests that for correcting a geomagnetic survey, the base

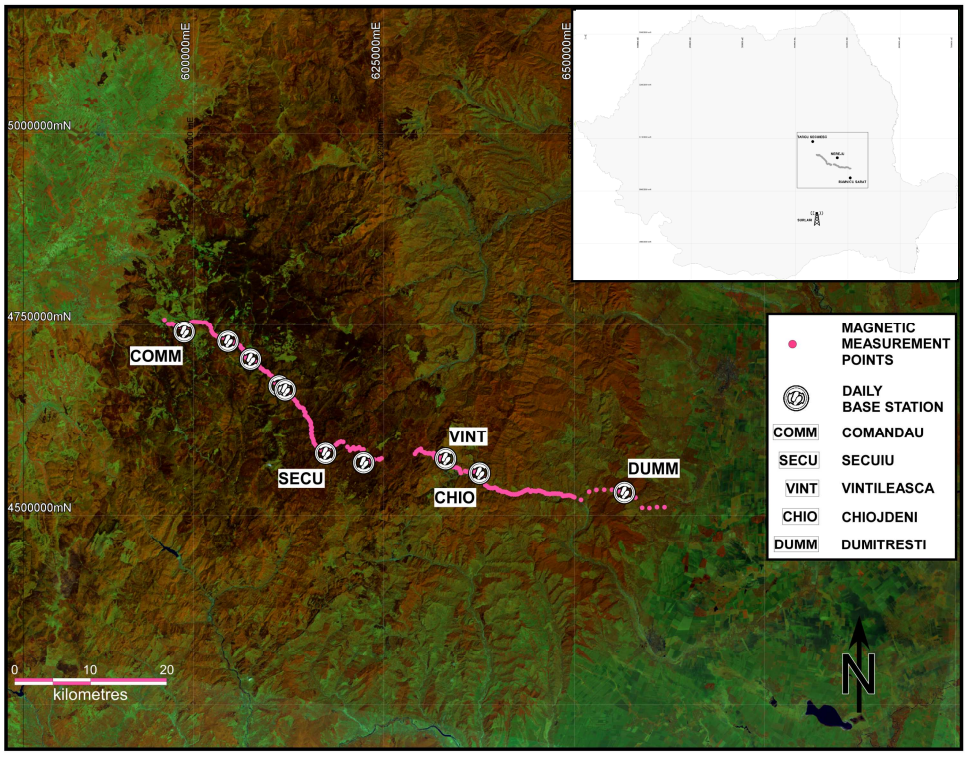

Fig.4.4. DACIA PLAN GRAV MAN'S magnetic survey. Daily base stations and magnetic measurement points localisation. Behind: high resolution LANDSAT image. Upper right corner: Map of Romania with the position of the DACIA PLAN GRAV MAN'S survey in relation with the Surlari Romanian Magnetic Observatory.

stations should be located at a short distance (15 km) from the survey area. The distance between magnetic stations kept the same 250 m spacing. Three successive instrument readings were taken in order to check the readings grouping or eventual malfunctions and the principle was applied objectively, either in the case of a base station or a rover station. When the presence of obvious sources of noise (iron fences, cars, ferrous garbage, pipes, etc.) on the path of the profile and because the method permitted, the magnetic measurements were deployed to "*safer environments*" not far from the profile.

4.3. Data processing

Data processing was performed separately for each survey by implementing specific algorithms and procedures. As was specified in the previous section some *in the field* decisions were made to help the processing flow. Software developed for commercial use, free downloaded sources or self developed algorithms were used to process the data. The processing flow did not follow a well known recipe but rather it was developed by applying various reduction methods successively. This experiment became a novel method for processing gravity and magnetic data when handled similarly.

4.3.1. GPS data processing

The GPS data were processed using two different software packages: (1) SkiPro, a complete GPS office software package that accompanies Leica GPS System 500 Series Hardware; (2) Gipsy-Oasis II (GPS-Inferred Positioning SYstem and Orbit Analysis SImulation Software) developed by the Jet Propulsion Laboratory from California Institute of Technology.

The data were processed separately/independently in Amsterdam/Bucharest (SkiPro) and Delft (Gipsy). After a thorough analysis it was concluded that SkiPro was the most appropriate software to use in this particular investigation and, thereafter, the processing of data with Gipsy was dropped. Gipsy Oasis II failed to handle ambiguities inherent to how the data were acquired and provided large errors due to the less than sufficient epoch overlapping characteristics adopted for the specific rapid static measurement requirements of the survey.

The "*General Guide to Static and Rapid-Static*", "*Getting Started with SKI-Pro*" and some other manuals for Leica 500 System can be downloaded from this location:

http://www.leica-geosystems.com/corporate/en/downloads/lgs_page_catalog.htm?cid=227.

The processing steps are presented within these manuals so will not be presented here in great detail; some basic notions and specific steps that were necessary are, however, described. Between each base station (see GPS acquisition section; permanent station, multi day base station or daily base station; Figure 4.1) and a rover station there were computed a number of baselines, but not before the WGS84 exact coordinates for the base station were known; the baseline computations were resolved with a specific logical value for the "Ambiguity Status" (an essential indicator if centimetre level accuracy with short observation times is desired): **Yes** - indicates that the determination of the integer number of cycles between the satellites and the GPS receiver was successful, i.e. the baseline calculation is correct; **Yes*** - indicates that the result should be treated with caution; **No** - indicates that the ambiguities could not be resolved; **?** - indicates that no attempt was made to resolve the ambiguities. When **No** and **?** are present than the baseline should be computed manually but taking into account that baselines longer than 20 km cannot be resolved. Another cause for the unresolved ambiguity was that the overlap between rover and base station was too short (too few epochs); this issue can be resolved matching the rover station with a different better overlapping base station. These kinds of situations were met within the present sets of data and they were resolved by applying the above mentioned solutions. From a total of 255 positions, for only 3% of them the ambiguity status could not be resolved (**No** and **?**) and the computation dropped. Finally, after the coordinates were determined with a satisfactory accuracy the data were exported in an ASCII file format that was later used to concatenate/link the gravity and magnetic measurement points with real coordinates (whatever the system of coordinates).

4.3.2. Gravity data processing

Standard gravity data corrections were performed in order to obtain the Bouguer anomaly values for each point of the profile. The data were corrected also for surrounding terrain (gravity) effects. The numerical/computed solutions for gravity reductions were developed through information published in the literature or by adopting/implementing simple documented algorithms. The computation of the Free Air Anomaly, the Simple Bouguer Anomaly and inner zones (Hammer) terrain corrections was realised using Microsoft Excel spreadsheets. A simple DOS program and a higher resolution Digital Elevation Model (DEM) were used for outer zones (Hammer) terrain corrections and consequently the determination of the Complete Bouguer Anomaly. The gravity processing steps included the calculation of the theoretical gravity, the Free Air Anomaly and the Bouguer Anomaly in its simple form and, consequently, in its terrain corrected form. Beforehand, the gravity data

were corrected for drift and gravity tides. This correction was performed using the advantage of acquisition procedure. A diagram for theoretical gravity field reductions and correction techniques is presented in Figure 4.5.

Fig.4.5. Diagram/flow chart for gravity field corrections.

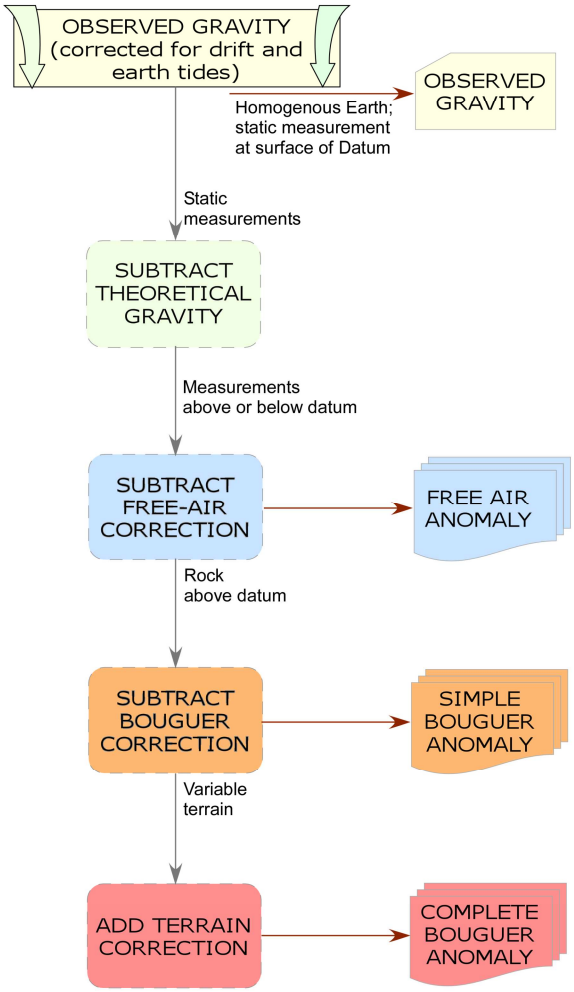

The theoretical gravity was calculated in order to isolate the effect of lateral variations in density within the Earth; therefore the bulk gravity effects of the Earth due to latitude are to be removed. The theoretical gravity expression conformably to International Gravity Formula 1980 (Helmert's equation - the 1980 Geodetic Reference System Formula that has been adopted at the XVIII General Assembly of IUGG in Canberra, December 1979) is:

$$g_t = 978032.7(1.0+0.0053024 \sin^2(\theta) - 0.0000058 \sin^2(2\theta)) \text{ miligal } (10^{-5} \text{ m*s}^{-2})$$

where θ is the gravity measurement point latitude in degrees based on the 1980 Geodetic Reference System. The gravity effect of the latitude is removed by subtracting the theoretical value from the observed values. The measured gravity (observed value) is obtained after the gravity meter reading was multiplied with the gravity meter constant and the absolute value of gravity was transferred from the Romanian National Gravity Network to the measuring point. The absolute value is transferred by comparing the two relative readings, one at the absolute base station and one at the measuring point.

The Free Air correction is applied to correct for variations in elevation (above or below the reference ellipsoid). Therefore the vertical gradient of gravity (vertical rate of change of the force of gravity – 0.3086 mGal* m^{-1}) is multiplied by the elevation of the measurement station and the result is added in order to obtain the Free Air Anomaly. Its expression is given by the following formula:

$$FAA = g_o - g_t + 0.3086*h$$

where g_o represents the observed gravity (measured gravity in mGal), g_t represents theoretical gravity (mGal), h represents the elevation above mean sea level (m) and 0.3086 represent the vertical gradient of gravity ($\delta g/\delta z$).

The Simple Bouguer Anomaly is obtained after the correction for the gravitational attraction of the slab of material between the observation point and the mean sea level is applied (slab correction). The Simple Bouguer Anomaly expression for static land measurements is given by the formula:

$$BA = g_o - g_t + (0.3086 - 2\pi G\rho_c)*h$$

where g_o represents the observed gravity (measured gravity in mGal), g_t represents theoretical gravity (mGal), 0.3086 represent the vertical gradient of gravity ($\delta g/\delta z$), G represents gravitational constant ($6.672*10^{-11}$ $m^3*kg^{-1}s^{-2}$ or $6.672*10^{-6}$ $m^2*kg^{-1}*mGal$), ρ_c represent the density of crustal rock (2670 kg/m^3) and h represents the elevation above mean sea level (m).

The complete (or refined) Bouguer anomaly is obtained after Terrain Corrections are applied. Its expression is:

$$CBA = g_o - g_t + (0.3086 - 2\pi G\rho_c)*h \text{ or } BA + TC$$

where TC represent the terrain correction. The differential gravitational effect of the unevenness of the terrain or the effect of nearby masses above (mountains) or mass deficiencies below (valleys) is called the terrain effect. Terrain corrections can be performed in different ways (Banerjee, 1998; Nahavandchi, 1999; Nowell, 1999; Hwang et al., 2003; etc) but the Hammer (Hammer, 1939) charts method was chosen to be used. The method was updated to modern techniques and benefited from the computer aided calculations. The inner zone corrections (Hammer chart

zone A) were done using observations made by line of sight noted in the field regarding the slopes/elevations nearby the gravity measurement points. Thereby, for each gravity station an approximation of the slope was done for distances of 3, 20 and 100 m. As mentioned earlier the gravity stations were kept away from abrupt changes in elevation so that the gravity effect of a valley or a step versant could be avoided. The expression used for terrain correction calculus came from Hammer (1939):

$$B_{TC} = 2 \pi \sigma \gamma (H - H_0)$$

where σ is the density of the surface soil or rock, γ is the gravitational constant and $H-H_0$ represents the elevation of the gravity station above the level (sea) datum. The density used while calculating was 2300 kg/m^3. It was preferred this value of density as an approximation of the average density of rocks (the volume of sedimentary rocks is prevalent to other types) that resides within the first 100 m of the Hammer inner zones.

For the rest of the Hammer zones (out to ~ 22 km), instead of using topographical maps or notes in the field, the *HamXYZ* DOS program was used that calculates automatically for all stations the gravity effect of terrain using a Digital Elevation Model. The high resolution elevation grid was obtained from the 90 m DEM available for the Romanian territory. Annex 5 presents the control file used for applying the gravity terrain corrections; it should be noted that a constant density approximated to the mean value of density for the crust was used (2670 kg/m^3).

Annex 6 presents the Microsoft Excel spreadsheets used for calculating the gravity corrections. It includes those for the drift and tide correction, the theoretical gravity (latitude) correction, the Free Air correction, the simple Bouguer correction and the Hammer inner zones terrain corrections. In Figure 4.6a the DACIA PLAN GRAV MAN'S final reduced Bouguer gravity anomaly profile is shown.

4.3.3. Magnetic data processing

The magnetic data processing was performed in order to obtain the complementary (to gravity) magnetic anomaly profile (Figure 4.4). It was performed using free specialized software. The process itself is not complicated; the magnetic data reductions included only two operations: correct the data for diurnal variations and the IGRF (International Geomagnetic Reference Field) correction.

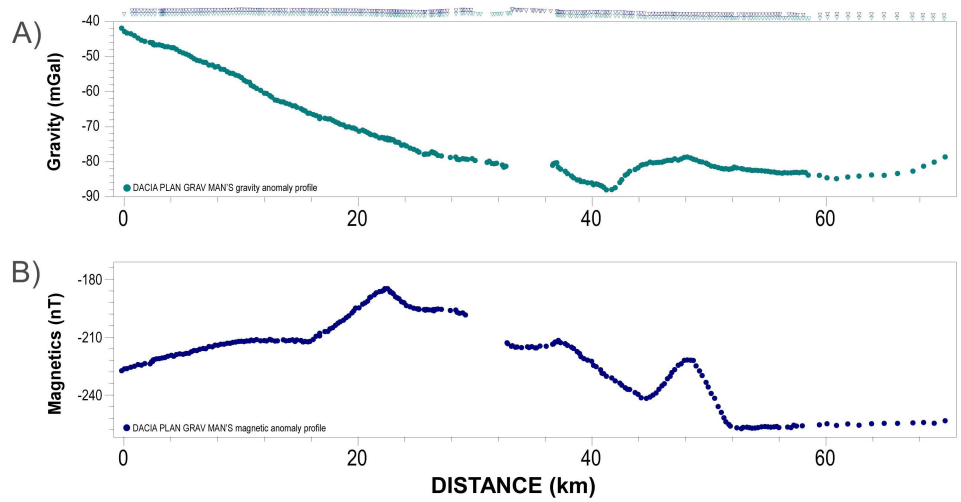

Fig.4.6. DACIA PLAN GRAV MAN'S potential field profiles after all reductions were applied. a) the complete Bouguer gravity anomaly profile after correcting for instrumental drift and tides, latitude, free air, Bouguer and terrain corrections; b) the magnetic anomaly profile after correcting for the IGRF and diurnal variations.

As mentioned in the acquisition subsection the diurnal variations were measured using a daily base station where the magnetic field intensity was measured at 5 minute intervals. The data were edited and introduced into an ASCII file. Also an ASCII file with the rover station measurements were edited and then imported into *GEMLinkW* specialized magnetic processing software. The *GEMLinkW VERSION 4.0* software, developed by the Canadian Company GEMSYS (http://www.gemsys.ca/). Using the two imported ASCII files the data were corrected for diurnal variations in two ways:

Corrected Value = Rover Field - Base Field + Datum

when the observation time of the rover and base stations matched (same reading time); the *rover field* represents the observed rover magnetic field intensity, the *base field* represents the observed base station intensity, the *datum* represents the average magnetic field area intensity (in our case was $4.8250*10^{-5}$ T) and consequently:

Corrected Value = Rover Field - Interpolated Base Field + Datum

when the observation time of the rover and base stations are different (different reading time); the *rover field* represents the observed rover magnetic field intensity, the *interpolated field* is obtained by interpolating the closest in time two base readings, the *datum* represents the average magnetic field area intensity. For comparison 1 minute observations using from the Surlari Romanian Geomagnetic Observatory were also used to compute for diurnal geomagnetic variations, but since this observatory is more than 200 km from the area of the investigation, data reduced with the local, temporary magnetic base station were considered to be superior.

The International Association of Geomagnetism and Aeronomy (IAGA) released the 10th Generation International Geomagnetic Reference Field, the latest version of a standard mathematical description of the Earth's main magnetic field, in December 2004. The IGRF is a series of mathematical models of the Earth's main field and its annual rate of change (secular variation). It expression is:

$$V(r,\theta,\lambda,t) = R\sum_{n=1}^{n}\left(\frac{R}{r}\right)^{n+1}\sum_{m=0}^{n}(g_n^m(t)\cos m\lambda + h_n^m(t)\sin m\lambda)P_n^m(\theta)$$

where r, θ, λ are geocentric coordinates (r is the distance from the centre of the Earth, θ is the colatitude, i.e. 90° - latitude, and λ is the longitude), R is a reference radius (6371.2 km); $g_n^m(t)$ and $h_n^m(t)$ are the coefficients at time t and $P_n^m(t)$ are the Schmidt semi-normalised associated Legendre functions of degree *n* and order *m*. The main field coefficients are functions of time and for the IGRF the change is assumed to be linear over five-year intervals. The IGRF computation was done using the QCTool software (http://www.qc-tool.com/en/index.php). The software allows calculating the IGRF as a function of Latitude, Longitude, height and time.

The magnetic anomaly expression is:

$$\Delta T = T_{obs} - T_{IGRF} - T_{diurnal\ variation}$$

Annex 7 presents the Microsoft Excel Spreadsheet that was used to compute the magnetic anomaly. Figure 4.6b shows the DACIA PLAN GRAV MAN'S magnetic anomaly profile after the IGRF and diurnal variation corrections were applied.

4.4. Comparison with previous data

Both DACIA PLAN GRAV MAN'S gravity and magnetic profiles were tied, as mentioned in the acquisition subsection, to a national network. The DACIA-PLAN gravity profile was tied to the Romanian National Gravity Network (5x7 km network) and by comparison (Figure 4.7a) it can be seen that it mimics the shape of the compiled national network Bouguer anomaly. Differences are, however, present and represent the consequences of normal drift of the theoretical field or due to

different reduction techniques. The most significant difference is located in the middle of the profile and is mainly due to the poor spatial resolution in this area (station spacing too great) of the national network data.

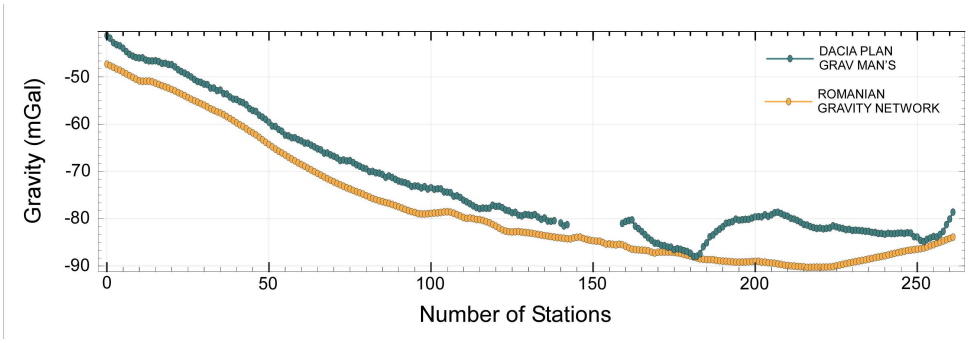

Fig.4.7. Comparison with previous data. a) Comparison between IInd order National Gravity Network and DACIA PLAN GRAV MAN'S gravity profiles.

The magnetic profile was linked to the Romanian Aeromagnetic Total Field Anomaly Map. Comparison between this and the DACIA-PLAN profile (Figure 4.7b) was possible by using the specific IGRF value for the epoch when the measurements where performed. The profiles correlate well in the western part but important differences arise elsewhere although some features are similar. The explanation for the differences resides partly in the instrumentation, different method of acquisition (land vs. airborne) or different reduction procedures but the higher resolution of the new, more densely spaced land magnetic measurements (250 m vs. 5x7.5 km) is probably paramount.

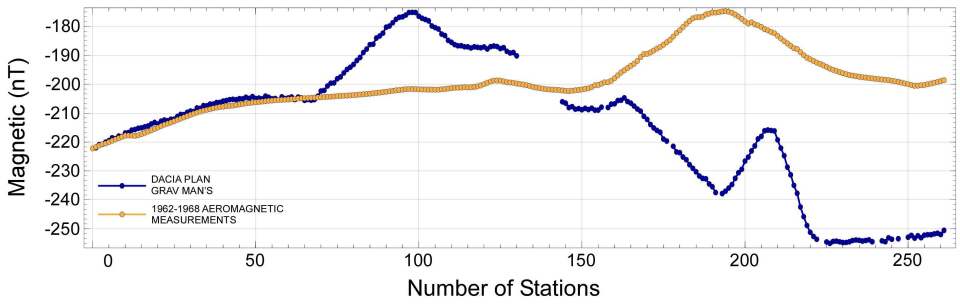

Fig.4.7. (*Continued*) Comparison with previous data. b) Romanian ΔT anomaly map profile vs DACIA PLAN GRAV MAN'S ΔT profile.

4.5. Conclusions

The acquisition procedure combined fast and accurate GPS measurements with densely spaced gravity and magnetic data and may represent a precedent for further

surveys. In 10 days with a small but efficient team of only eight people with relatively low costs (instruments lent by various partners) a 70 km long gravity and magnetic survey, with measurements every 250 m, was accomplished. The survey results represent a state of the art potential field dataset (profiles) for the Vrancea Zone – south-eastern Carpathian area. Surveying also provided valuable information for future development of the methods themselves: limitation of obsolete instruments – sensitive to temperature and short cycles of measurements (Worden gravity meter); GPS base stations and baselines establishment; etc.

The processing technique presented here constitutes a *"blueprint"* for further processing flows. With almost no costs but equivalently endless documentation hours the gravity and magnetic data reduction produced a highly resolved set of data. The manipulation of the data within the processing flow is attributed to their size but further optimization can be developed.

Acknowledgments

We wish to thank to the students who were with us in the field and gave a great deal of help acquiring the DACIA PLAN GRAV MAN'S data: Cristina Marin, Marian Iancu, Ioan Munteanu, Gabi Paal, Iulian Voinescu. We present our best appreciation to Andre van der Hoeven that, despite losing precious possessions at the beginning of the campaign, helped us to design and perform the GPS and leveller measurements. Taco Broerse and Boudewijn Ambrosius are thanked for giving a try processing the GPS data with Gipsy Oasis II at Delft. We are thankful to the Faculty of Aerospace Engineering from Delft for lending the GPSs (Leica 500 System) and the leveller. Henk van der Meer from Utrecht Universiteit is thanked for providing us for both campaigns the Worden gravity meters. We acknowledge the Romanian Air Force and the pilot Capt. Paul Cristea for supporting the airlifted operations during the 2005 campaign. Finally we wish to offer our thanks to the anonymous people that helped us to accomplish a successful campaign.

References

Airinei, St., Stoenescu, S., Velcescu, G., Romanescu, D., Visarion, M., Radan, S., Roth, M., Besutiu, L., Besutiu, G., 1985. Distribuţia anomaliei magnetice Za pe teritoriul României. St. cerc. geol., geofiz., geogr., Geofizică, 23, p. 12–19.

Atanasiu, L., Rosca V., Rogobete, M., 1996, A three-dimensional modelling of the East

Carpathian Bend: 1st Congress of Balkan Geophysical Society, Abstr. Book, Athens, 266-267.

Banerjee, P., December 1998. Gravity measurements and terrain corrections using a digital terrain model in the NW Himalaya. Computers & Geosciences, Volume 24, Issue 10, 1009-1020

Besutiu, L., 2001. Vrancea active seismic area: a continental unstable triple junction? Rev. Roum. Géophys., 45, 59–72.

Besutiu, L., Zlăgnean, L., Horomnea, M., 2005. Non-tidal gravity changes across major lithosphere boundaries on the Romanian territory: Suppl. Journ. Balkan Geophysical Society, 8, 237-240.

Constantinecu, L., Cornea, I., Enescu, D., 1972. Structure de la croûte terrestre en Roumanie d'après les données géophysiques. Rev. Roum. Géophys., 16 (1), 3–20.

Cristescu Tr., Stefanciuc Al., 1962 - 1968. Prospectiuni aeromagnetice pentru diverse substante în regiunile: Depresiunea Panonica, Banat, Crisana, Muntii Apuseni, Carpatii Orientali, Campia Romana, Dobrogea, Carpatii Meridionali, Depresiunea Transilvaniei, Platforma Moldoveneasca, Arhiva Agentiei Nationale pentru Resurse Minerale A.N.R.M. – Prospectiuni S.A..

Gavat, I., Airinei, St., Botezatu, R., Socolescu, M., Stoenescu, S., Vencov, I., 1965. Contribution de la gravimétrie et de la magnétométrie à l'étude de la structure profonde du territoire de la R.P. Roumaine. Rev. Roum. Géophys. (Géologie), 9 (1), 81–107.

Ghilani, C. D. and Wolf, P. R., 2008. Elementary Surveying: An Introduction to Geomatics. 12th Ed. Pearson Prentice Hall, Upper Saddle River, NJ.

Hackney R., Martin M., Ismail-Zadeh A., Sperner B., Ioane D. and the CALIXTO Working Group. 2002. The gravity effect of the subducted slab beneath the Vrancea region, Romania, Geologica Carpathica 53, 119-121, Bratislava.

Hammer, S., 1939. Terrain corrections for gravimeter stations, Geophysics, 4, 184-194.

van der Hoeven, A.G.A., Mocanu, V., Spakman, W., Nutto, M., Nuckelt, A., Matenco, L., Munteanu, L., Marcu, C., Ambrosius, B.A.C., 2005. Observation of present-day tectonic motions in the Southeastern Carpathians: Results of the ISES/CRC-461 GPS measurements: Earth and Planetary Science Letters, v. 239, n. 3-4, p. 177-184.

Hwang, C., Wang, C., Hsiao, Y., December 2003. Terrain correction computation using Gaussian quadrature. Computers & Geosciences, Volume 29, Issue 10, 1259-1268.

Ioane, D., Ion, D., 2005a. A 3D crustal gravity modelling of the Romanian territory. Journal of Balkan Geophysical Society, 8, 189-198.

Ioane, D., Calota, C., Ion, D., 2005b. Deep geological structures as revealed by 3D gravity stripping: western part of the Moesian Platform, Romania. Journal of Balkan Geophysical Society, 8, 129-138.

Matenco, L., Zoetemeijer, R., Cloetingh, S. and Dinu, C., 1997. Lateral variations in mechanical properties of the Romanian external Carpathians: inferences of flexure and gravity modelling. Tectonophysics, 282, 147-166.

Nahavandchi, H., 1999. Terrain correction computations by spherical harmonics and integral formulas. Physics and Chemistry of the Earth, Part A: Solid Earth and Geodesy Volume 24, Issue 1, 73-78.

Nowell, D. A. G., October 1999. Gravity terrain corrections - an overview. Journal of Applied Geophysics, Volume 42, Issue 2, 117-134

Socolescu, M., Bisir, D., Popovici, D., Visarion, M., Rosca, V., 1964. Structure of the Earth's crust in Romania based on the gravimetric data. Rev.Roum.Geophysique, 8.

Sprinceana, V., Besutiu, L., 2005. The airborne geomagnetic map of Romania: A new look: Suppl. Journ. Balkan Geophysical Society, 8, 163-166.

Stanica, M., Stanica D., Furnica, C. (1999), The placement of the Trans-European Suture Zone on the Romanian territory by electromagnetic arguments. Earth Planet Space, 51, 1073–1078.

Szafian P., Horvath F., 2006. Crustal structure in the Carpatho-Pannonian region: insights from three-dimensional gravity modelling and their geodynamic significance. Int. J. Earth Sci (Geol Rundsch) 95: 50–67.

Visarion, M. (1998), Gravity anomalies on the Romanian territory. In: Sledzinski, J. (ed.), Reports on the Geodesy CEI CERGOP "South Carpathians" Monograph, 7 (37), Politechnika, Warszawska, 133–138.

Visarion, M., Sandulescu, M., Stanica, D., Atanasiu, L., 1988. An improved model of the East Carpathians. Rev. Roum. Géophys., 32, 43–52.

Whellams, J.W., 1996. Spatial inhomogeneity of geomagnetic fluctuation fields and their influence on high resolution aeromagnetic surveys, Ph.D. Thesis, Flinders University.

Annexes

Annex 1 Worden gravity meter. A conceptual section through Worden gravity meter. Photos with actual gravity measurements during 2005 and 2006 campaigns.

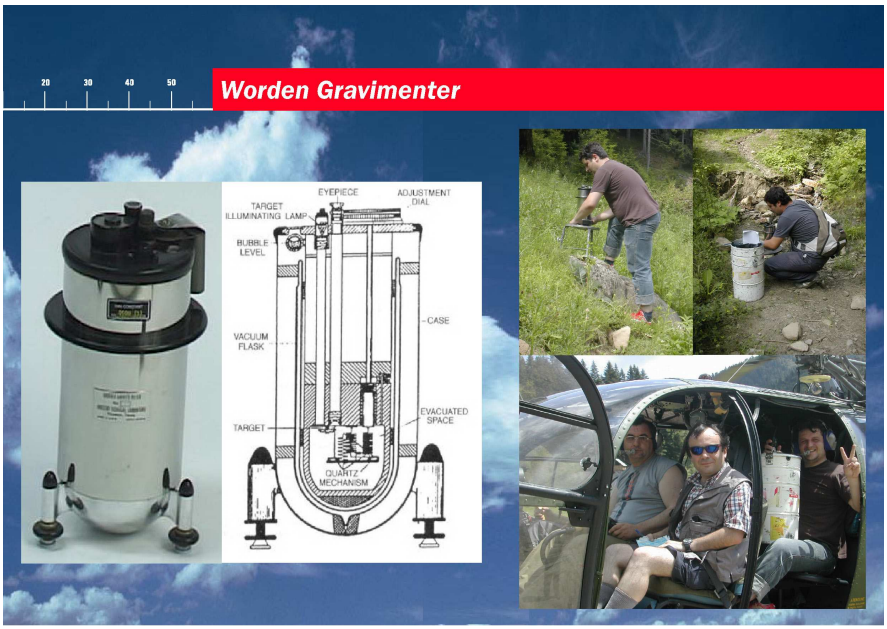

Annex 2 Proton Precession Magnetometer. A conceptual scheme of the PPM. Photo taken in the field in 2006 campaign with the magnetic operator surveying.

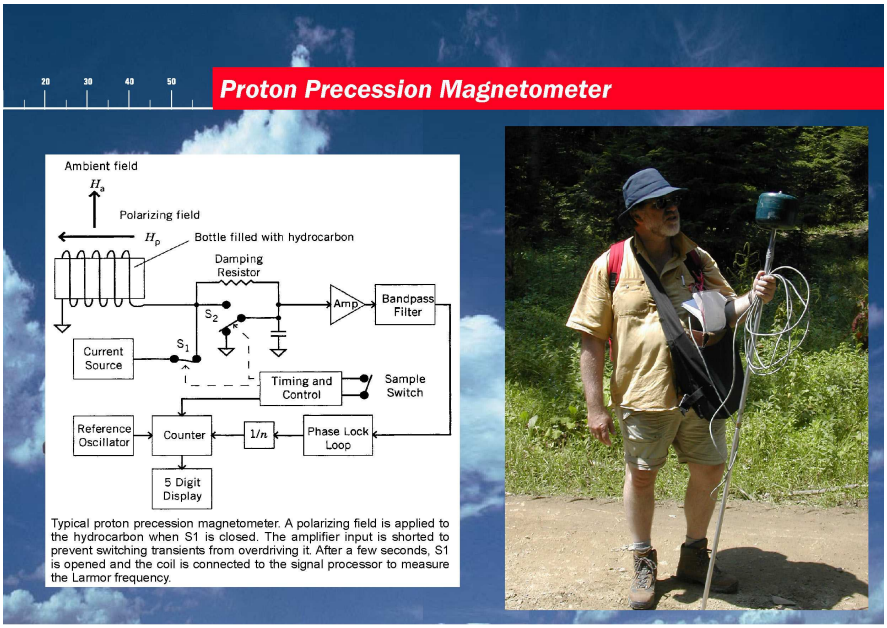

Annex 3 Leica 500 GPS system. Photo taken in the field during 2005 campaign with the GPS operator surveying (levelling operation).

Annex 4 Scanned images with GPS daily base station and GPS measurement log sheet notes.

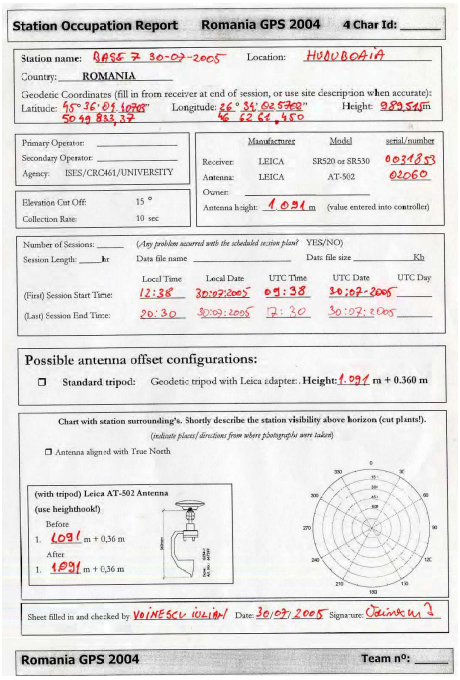
Station Occupation Report Romania GPS 2004 4 Char Id: _____

Station name: BASE 7 30-07-2005 Location: HUNUBOAIA

Country: ROMANIA

Geodetic Coordinates (fill in from receiver at end of session, or use site description when accurate):

Latitude: 45° 36' 01,10788" 50 49 833,37 Longitude: 26° 31' 02,57492" 46 62 62,450 Height: 989,551m

Primary Operator: _____

Secondary Operator: _____

Agency: ISES/CRC461/UNIVERSITY

	Manufacturer	Model	serial/number
Receiver:	LEICA	SR520 or SR530	0031853
Antenna:	LEICA	AT-502	02060
Owner:			

Antenna height: 1.091 m (value entered into controller)

Elevation Cut Off: 15 °

Collection Rate: 10 sec

Number of Sessions: _____ (Any problem occurred with the scheduled session plan? YES/NO)

Session Length: ____hr Data file name _____ Data file size _____Kb

	Local Time	Local Date	UTC Time	UTC Date	UTC Day
(First) Session Start Time:	12:38	30:07:2005	09:38	30:07:2005	
(Last) Session End Time:	20:30	30:09:2005	17:30	30:07:2005	

Possible antenna offset configurations:

❐ Standard tripod: Geodetic tripod with Leica adapter. Height: 1.091 m + 0.360 m

Chart with station surrounding's. Shortly describe the station visibility above horizon (cut plants!).

(indicate places/directions from where photographs were taken)

❐ Antenna aligned with True North

(with tripod) Leica AT-502 Antenna

(use heighthook!)

Before

1. 1.091 m + 0,36 m

After

1. 1.091 m + 0,36 m

Sheet filled in and checked by VOINESCU IULIAN Date: 30/07/2005 Signature: _____

Romania GPS 2004 Team nº: _____

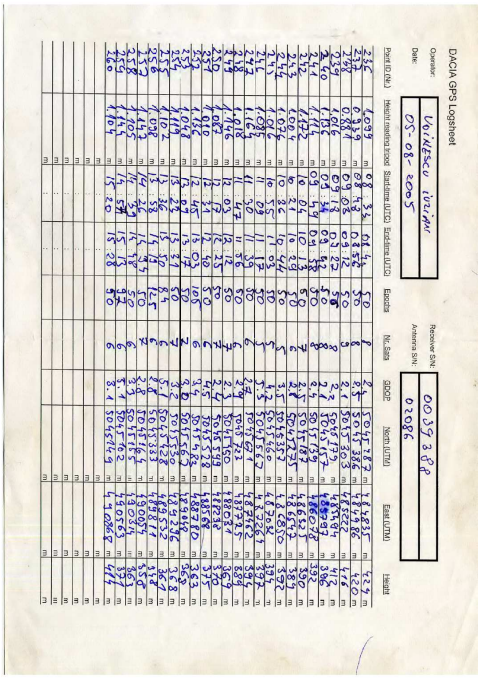
DACIA GPS Logsheet

Operator: VOINESCU IULIAN

Date: 30 - 08 - 2005

Receiver S/N: 0031853

Antenna S/N: 02060

Point ID (No.) | Height meters to mark | Start time UTC h | End time UTC h | Epochs | No. Sats | GDOP | North (UTM) | East (UTM) | Height

D:\...\romania_utm35.dat	path - filename (e.g.,) for the topo data
M M M	units for x, y, z; M is meters, F, feet
2.67	density of the terrain
M	unit of the zones and sectors
10	number of zones
6 100 180	sectors/zone, inner radius of zone, outer radius of zone
8 390	sectors/zone, outer radius of zone
8 895	sectors/zone, outer radius of zone
12 1529	
12 2614	
12 4469	
16 6652	
16 9902	
16 14741	
16 21943	

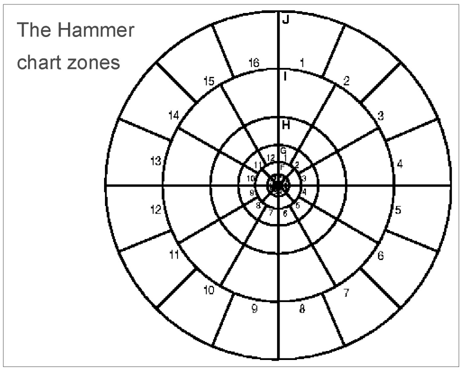

Annex 5 Content of the *HamXYZ* control file and Hammer zones chart.

column A	column B	column C	column D	column E	column F	column G	column H	column I	column J	column K	column L
Station	**rone**	**rtwo**			**Height**	**zSector I**	**zSector II**	**zSector III**	**zSector IV**	**z_realSector I**	**z_realSector II**
ID	inner radii	outer radii	ang. ap. of sector	density	h	elevation	elevation	elevation	elevation	h	h
9001	0	3	1.570796327	2.3	1047.9					1062.2	1062.2
1001	0	3	1.570796327	2.3	1062.2	0	0	0	-2	1062.2	1062.2
1002	0	3	1.570796327	2.3	1063.2	0	0	0	0	1063.2	1063.2
1003	0	3	1.570796327	2.3	1066.4	0	0	0	0	1066.4	1066.4
1004	0	3	1.570796327	2.3	1070.2	0	0	0	0	1070.2	1070.2
1005	0	3	1.570796327	2.3	1075.4	0	0	0	0	1075.4	1075.4
1006	0	3	1.570796327	2.3	1077.3	0	0	0	0	1077.3	1077.3
1007	0	3	1.570796327	2.3	1086.4	0	0	0	0	1086.4	1086.4
1008	0	3	1.570796327	2.3	1087.3	0	0	0	0	1087.3	1087.3
1009	0	3	1.570796327	2.3	1095.5	0	0	-1	-1	1095.5	1095.5
1010	0	3	1.570796327	2.3	1107.6	0	0	0	0	1107.6	1107.6
1011	0	3	1.570796327	2.3	1105.4	0	0	0	0	1105.4	1105.4
1012	0	3	1.570796327	2.3	1110.3	0	0	0	0	1110.3	1110.3
9001	0	3	1.570796327	2.3	1047.9	0	0	0	0	1047.9	1047.9

column M	column N	column O	column P	column Q	column R	column S
z_realSector III	**z_realSector IV**	**Terrain Correction Sect. I**	**Terrain Correction Sect. II**	**Terrain Correction Sect. III**	**Terrain Correction Sect. IV**	**TC Total**
hh						
1062.2	1060.2	0.0010617549	0.0010617549	0.0010617549	0.0010617521	**0.004247017**
1062.2	1060.2	0.0010617549	0.0010617549	0.0010617549	0.0010617521	**0.004247017**
1063.2	1063.2	0.0010617563	0.0010617563	0.0010617563	0.0010617563	**0.004247025**
1066.4	1066.4	0.0010617607	0.0010617607	0.0010617607	0.0010617607	**0.004247043**
1070.2	1070.2	0.0010617661	0.0010617661	0.0010617661	0.0010617661	**0.004247064**
1075.4	1075.4	0.0010617733	0.0010617733	0.0010617733	0.0010617733	**0.004247093**
1077.3	1077.3	0.0010617759	0.0010617759	0.0010617759	0.0010617759	**0.004247103**
1086.4	1086.4	0.0010617883	0.0010617883	0.0010617883	0.0010617883	**0.004247153**
1087.3	1087.3	0.0010617895	0.0010617895	0.0010617895	0.0010617895	**0.004247158**
1094.5	1094.5	0.0010618004	0.0010618004	0.0010617991	0.0010617991	**0.004247199**
1107.6	1107.6	0.0010618163	0.0010618163	0.0010618163	0.0010618163	**0.004247265**
1105.4	1105.4	0.0010618135	0.0010618135	0.0010618135	0.0010618135	**0.004247254**
1110.3	1110.3	0.0010618199	0.0010618199	0.0010618199	0.0010618199	**0.004247279**
1047.9	1047.9	0.0010617343	0.0010617343	0.0010617343	0.0010617343	**0.004246937**

Microsoft Excel Spreadsheet - Terrain Corrections using Hammer method for the inner zones

column A	column B	column C	column D	column E	column F	column G	column H	column I	column J	column K	column L	column M
Gb1 @ COMM=		**980435.85**	**973.6**		**T1 curv corr=**	**1.46**	**T4curv corr=**	**0.00**				
K 2005 =	**0.0955**	**div/mgal**	**92.9788**		**T2 curv corr=**	**0.00**						
K 2006 =	**0.104**	**div/mgal**	**h instr =**	**0.25**	**T3 curv corr=**	**0.00**						
Station ID	**Date**	**Time**	**Latitude**	**Longitude**	**Radian**	**Hs**	**Reading Meter**	**Readin Meter DC**	**Drift_rate**	**Rc**	**g_tide**	**Rt**
						height (m)	dial	drift corr		corr read mgal	tide corr	tide corr read
9001	7/24/2005	13:40	45.7596	26.2688	0.7987	1047.873	974.1	974.10	0.00	93.03	0.09	93.12

column N	column O	column P	column Q	column R	column S	column T	column U	column V	column W	column X
Rh	**Ga**	**Gl**	**Gfa**	**Gba**	**Gcc**	**Gba+TC**	**TC Inner 0-3**	**TC Inner 3-20**	**TC Inner 20-100**	**TC Outer 100-22000**
Rt+0.308596*hi	Gb1+(Rh-Rb1)-(T-Tb1)d	lat corr	Ga-Gl+0.308596*Hs	Bouguer	Curvature cor	Bouguer + terr corr	terr corr	terr corr	terr corr	terr corr
93.19	980436.06	980688.74	70.69	-46.56	1.15	**-46.71**	0.00	0.00	0.00	0.98

Microsoft Excel Spreadsheet used to calculate Free Air Anomaly Simple and Complete Bouguer Anomaly

column A	column B	column C	column D	column E	column F
Rb1 (base read 1)	974.1	***d (drift)***	**9.3913**		
Rb2 (base read 2)	975.0				
Gb1 (abs G base 1 mgal)	980435.85				
Gb2 (abs G base 2 mgal)	980435.85				
Tb1 (base time 1)	13:40				
Tb2 (base time 2)	15:58				
Station ID	**Date**	**Time**	**Reading Meter**	**Drift**	**Drift_rate**
			dial		
9001	7/24/2005	13:40	974.1	974.10	0.00
1001	7/24/2005	14:00	954.6	954.47	0.13
1002	7/24/2005	14:19	945.4	945.15	0.25
1003	7/24/2005	14:28	939.4	939.09	0.31
1004	7/24/2005	14:36	928.7	928.33	0.37
1005	7/24/2005	14:42	918.8	918.40	0.40
1006	7/24/2005	14:48	911.6	911.16	0.44
1007	7/24/2005	14:53	901.4	900.92	0.48
1008	7/24/2005	15:03	880.1	879.56	0.54
1009	7/24/2005	15:10	860.1	859.51	0.59
1010	7/24/2005	15:18	840.0	839.36	0.64
1011	7/24/2005	15:27	820.4	819.70	0.70
1012	7/24/2005	15:34	799.9	799.16	0.74
9001	7/24/2005	15:58	975.0	974.10	0.90

Microsoft Excel Spreadsheet used to calculate the drift and gravity tides corrections

Annex 6 Microsoft Excel Spreadsheets used for gravity corrections calculus: the theoretical gravity (latitude) correction, the Free Air correction, the simple Bouguer correction, drift and tide correction and the Hammer inner zones terrain corrections.

column A	column B	column C	column D	column E	column F	column G	column H	column I
ID	**Day**	**Latitude**	**Longitude**	**Elevation**	**Average**	**Diurnal Corr**	**IGRF**	**Anomaly nT**
1001	**7/24/2005**	45.7706	26.2867	1061.617	48230.25	48226.95	48364.68	**-137.73**
1002	**7/24/2005**	45.7704	26.2901	1064.726	48257.75	48253.25	48364.85	**-111.60**
1003	**7/24/2005**	45.7702	26.2932	1065.588	48260.75	48255.65	48365.04	**-109.39**
1004	**7/24/2005**	45.7700	26.2964	1070.704	48256.50	48251.1	48365.14	**-114.04**
1005	**7/24/2005**	45.7697	26.3005	1074.035	48256.50	48250.3	48365.34	**-115.04**
1006	**7/24/2005**	45.7697	26.3031	1077.140	48258.25	48250.75	48365.49	**-114.74**
1007	**7/24/2005**	45.7692	26.3060	1079.739	48258.25	48246.75	48365.54	**-118.79**
1008	**7/24/2005**	45.7675	26.3089	1086.254	48264.75	48251.15	48365.14	**-113.99**
1009	**7/24/2005**	45.7659	26.3119	1092.845	48269.25	48255.05	48364.79	**-109.74**
1010	**7/24/2005**	45.7631	26.3138	1100.513	48267.75	48253.15	48363.95	**-110.80**
1011	**7/24/2005**	45.7589	26.3148	1107.223	48264.25	48250.15	48362.65	**-112.50**
1012	**7/24/2005**	45.7568	26.3164	1114.109	48261.00	48246.9	48362.02	**-115.12**

Annex 7 Microsoft Excel Spreadsheets used for magnetic corrections

CHAPTER V

LOCAL GRAVITY AND MAGNETIC MODELLING IN THE VRANCEA ZONE SOUTH-EASTERN CARPATHIANS. INFERENCES ON BASEMENT AFFINITY AT THE EDGE OF THE EAST EUROPEAN CRATON*

"To raise new questions, new possibilities, to regard old problems from a new angle, requires creative imagination and marks real advance in science."

Albert Einstein

ABSTRACT

Integrated 2D gravity and magnetic modelling has been carried out along a 71 km long profile, called DACIA PLAN GRAV MAN'S that crosses the seismically active Vrancea zone in the south-eastern Carpathian bend. The densely spaced potential field survey that complements the previously acquired DACIA PLAN 2001 deep reflection seismic survey represents a methodical approach to broader scale tectonics and regional geodynamics. The model is tightly constrained by the previously inferred (in this

---

* *This study is based on Bocin, A., Stephenson, R., Matenco, L., Mocanu, V., 2009. Local gravity and magnetic modelling in the Vrancea Zone south-eastern Carpathians: Inferences about basement affinity and the edge of the East European Craton. to be submitted to an ISI journal.*

thesis) seismic velocity models that were in their turn synchronously/comprehensively constrained by geology and seismic industry lines. The integrated gravity and magnetic model supports the existence of structures such as shallow uplifted basement blocks, active crustal faults or uncovers structural features like noticeable basement topography and crustal thickness. After potential field modelling, interpretation and integration with seismic inferred information, a set of novel information has been obtained, which is a key element enabling the discrimination of various regional crustal/basement blocks. Previously defined crustal affinities generally rely on widely spaced, regional datasets, which have less predictability for the upper crustal geometries and geophysical characterisation of basement units in the area of the south-eastern Carpathians and Focsani Basin. The physical continuity of properties that defines one crustal block and its bounding fault structures, corroborated with physical properties contrasts between neighbouring blocks supports a more reliable geological interpretation of the geophysical model. Subsequently, plate boundaries are subject to redefinition/refinement in the study area. The geological interpretation allows further conclusions on the origins of the pre-orogenic structures (rifted basin) and the presence of a coeval supra-basement layer, which are correlated with the inferred crustal boundary in the south-eastern Carpathians. The boundary zone, along with the general increase of the crustal thickness from west to east, possibly correlates with the presence of the Teisseyre Tornquist Zone that separates Precambrian terranes from areas characterized by younger metamorphism to the west, which were accreted during Phanerozoic times.

Keywords: DACIA PLAN GRAV MAN'S, potential field modelling, crustal differentiation, basement uplift.

5.1. Introduction

DACIA PLAN GRAV MAN'S (Danube and Carpathian Integrated Action on Processes in the Lithosphere and Neotectonics Gravity and Magnetic Survey) is a 71 km densely spaced (250 m between stations) gravity and magnetic survey acquired in conjunction with the previously executed seismic survey DACIA PLAN 2001 (Bocin et al., 2005; Panea et al., 2005; Bocin et al., 2009). The potential fields profile is coincident over approximately 90% of its length with the deep reflection seismic profile, the rest representing a small prolongation from the western extremity of the seismic profile. It crosses, from WNW to ESE, the Targu Secuiesc basin with a mean altitude of ~1000m, starting near the locality of Comandau, subsequently crossing rough topography of the nappe complex of the south-eastern Carpathians and the western flank of the foreland Focsani Basin, ending near Dumitresti (Figure 5.1).

The thin-skinned thrust belt of the south-eastern Carpathians (Figure 5.2) contains sediments of Lower Cretaceous to Upper Miocene in age (e.g. Sandulescu et al., 1981) and was emplaced during the Miocene, when a 140-160 km shortening took place (Ellouz et al., 1994; Morley, 1996). In the frontal part the south-eastern Carpathians, the deep Focsani Basin contains Middle-Miocene - Quaternary sediments, which partly overlie the Carpathians foreland units (Tarapoanca et al., 2003; Figure 5.2).

The deep structure of the south-eastern Carpathians and its foreland is well studied in terms of geological (e.g., Stefanescu et al., 1988; Dicea et al., 1996; Morley, 1996; Schmid et al., 2008 and references therein) and seismic interpretation,

including deep reflection profiles such as the DACIA PLAN or shallower petroleum exploration seismic lines (e.g., Tarapoanca et al., 2003; Bocin et al., 2005; Panea et al., 2005; Leever et al., 2006 and references therein).

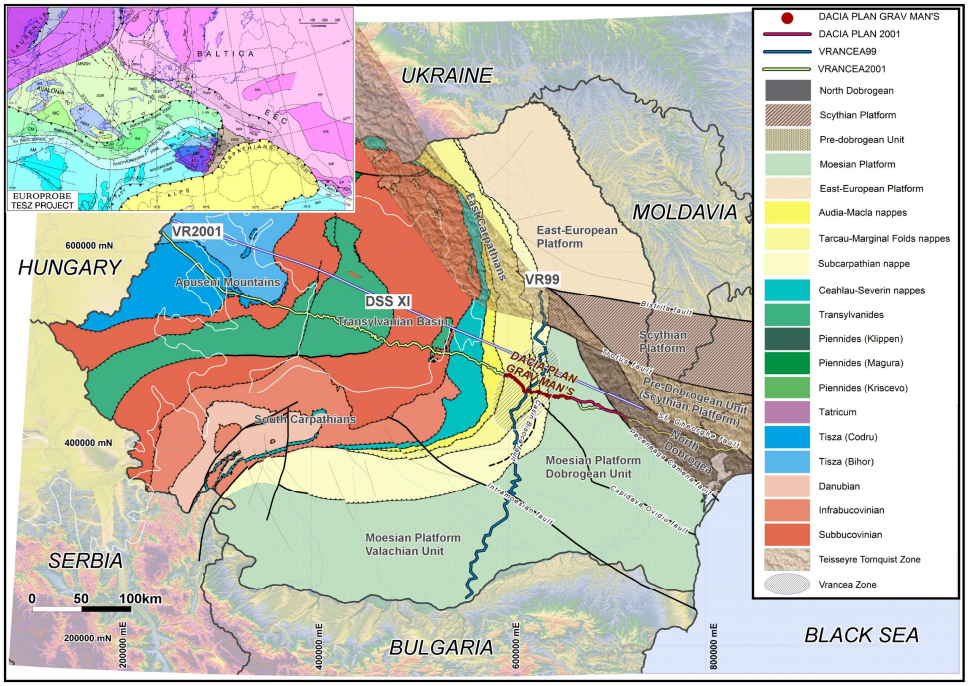

Fig.5.1. Tectonic map of the Romania (zoom in from Schmid et al., 2008). The topography in the background is derived from the 90 metres resolution Shuttle Radar Topography Mission data sets (National Geospatial-Intelligence Agency - NGA and the National Aeronautics and Space Administration - NASA) and projected to the Pulkovo 1942 Romania Stereo70 system.

Beneath the well-studied shallow system of thin-skinned nappes, the structural geometries and the crustal affinities of various blocks are much less known. A large number of geophysical studies has been dedicated to the study of the crustal structure of the south-eastern Carpathians, using in particular geothermal and magnetotelluric methods (e.g., Visarion et al., 1978; Stanica and Stanica, 1993; Stanica et al., 1999; Andreescu and Demetrescu, 2001; Demetrescu et al., 2007) but also gravity (e.g., Visarion et al., 1988b and references therein), crustal seismology (e.g., Bala et al., 2003), lower resolution DSS (Radulescu et al., 1976) and seismic reflection (e.g., Raileanu et al., 1994; Mocanu et al., 1996; Bocin et al., 2005; Panea et al., 2005, Mucuta et al., 2006). Nevertheless, a detailed geometry of the crustal blocks and direct constraints on their affinities are poorly known, in particular as it might constrain the evolution of the Carpathians during Miocene collision and processes related to the deep Vrancea seismicity.

The DACIA PLAN GRAV MAN'S combined gravity and magnetic profile crosses over the seismically active Vrancea zone, where strong intermediate-mantle

earthquakes (6.5-7.2Mw) are geographically confined in a narrow 100x150 km area at depths between 70 to 210 km (Oncescu and Bonjer, 1997; Wenzel et al., 1999 and references therein). In a shallow position, smaller magnitudes earthquakes are recorded over a larger area in the south-eastern Carpathians and its foreland (Bala et al., 2003; Knapp et al, 2005). The intense intermediate-mantle seismicity in the area is thought to be related to a number of mechanisms such as slab detachment, oceanic or continental lithosphere delamination, thermal re-equilibration, lithospheric instability or combinations of these (e.g. Girbacea, 1998; Chalot-Prat and Girbacea, 2000; Wortel and Spakman, 2000; Sperner et al., 2001; Wenzel et al., 1998a,b, 2002; Cloetingh et al., 2004; Sperner et al., 2004; Knapp et al., 2005; Panea et al., 2005; Houseman and Gemmer, 2007).

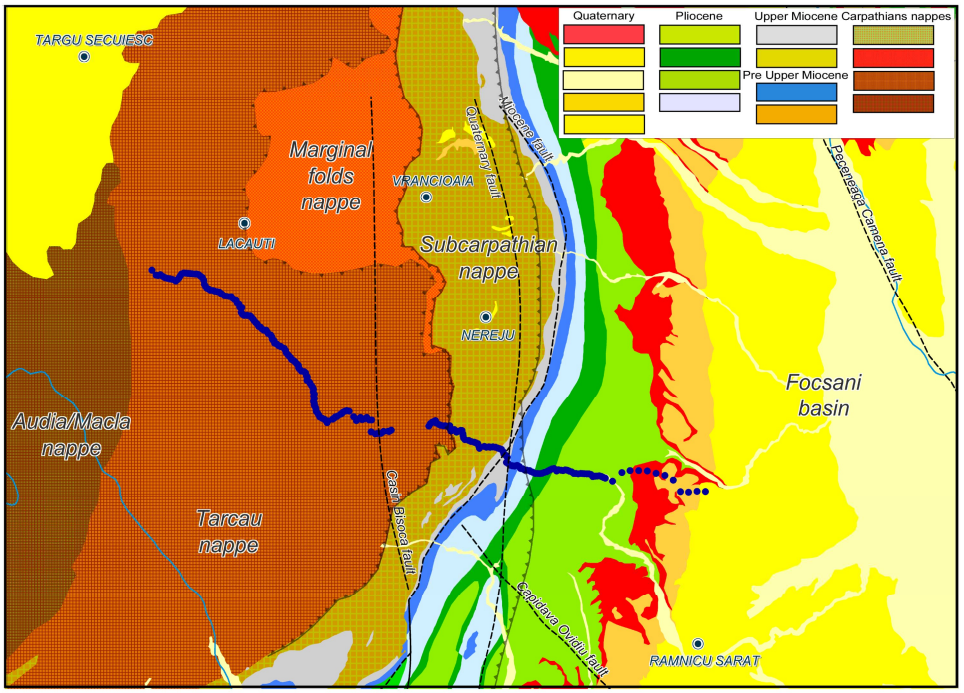

Fig.5.2. Geologic map with basement details (compiled and simplified by Leever et al. (2006) and Matenco et al. (2007) from the 1:200.000 geological maps published by the Geological Institute of Romania).

One interesting and hence debated issue is the correlation between the Palaeozoic Europe and East-European Craton along the Tornquist-Teissere Lineament in the foreland of the Carpathians. While most of existing studies seem to converge towards a prolongation into Romania situated near or inside the Scythian - North-Dobrogea geological province (e.g., Cantini et al., 1991 – see Figure 5.1), significant deformations recorded in the Moesian Platform during the Upper Proterozoic - Mesozoic and its local Gondwanan affinities (e.g., Tari et al., 1997; Seghedi et al.,

2005; Vaida et al., 2005) suggest the need for a higher-resolution study of the geophysical characteristics of this rather unique feature (Figure 5.1).

This chapter presents a 2D local high resolution potential field model of the south-eastern Carpathians integrated with previous geophysical observations and its correlation with regional gravity and magnetic datasets. The objective of this chapter is to infer information about basement composition, crustal affinity and crustal boundaries in the area of the south-eastern Carpathians and its foreland basin.

5.2. Constraints on the deep structure of the south-eastern Carpathians

According to Sandulescu (1988), the orogenic structure of the south-eastern Carpathians formed during two overall shortening episodes, a Cretaceous period involving the "Dacides" (or Tisza-Dacia block, e.g., Csontos and Voros, 2004) and a Miocene period in which the "Moldavides" (or the external thin-skinned units) were deformed. In this model these events took place in response to the subduction of the supposed Ceahlau-Severin Ocean, which was connected in more proximal parts to more stable, European-derived units (the so called "Carpathians embayment", Balla, 1987), beneath the Tisza-Dacia continental block (e.g., Schmid et al., 2008 and references therein). The Ceahlau/Severin Ocean would have opened during the Late Jurassic and evolved as a passive margin during Early Cretaceous times, its oceanic relicts or associated sediments being preserved at present within the Ceahlau Nappe (Stefanescu, 1976, Figure 5.1). Further to the east the outer Carpathians nappes contain mainly turbidites of uppermost Jurassic - Miocene age, found at present in the Moldavides system (e.g., Sandulescu et al., 1981). Its deformation is mainly characterized by east to east-south-eastward directed thrusting with local transpression (e.g., Zweigel et al., 1998; Morley, 1996; Hippolyte and Sandulescu, 1996). The Moldavides sediments were thrusted over the Moesian Platform during the Miocene (Sandulescu, 1988).

A younger phase of compressional deformation is documented by thrusts and high angle transpressional structures, defined as the "Valachian" phase of deformation (Sandulescu et al., 1988; Hippolyte and Sandulescu, 1996). This event started near the beginning of the Quaternary and was oblique to the general curvature of the south-eastern Carpathians bend; it is generally interpreted as out-of-sequence and late-orogenic (Leever et al., 2006; Matenco et al., 2007). The western flank of the Focsani Basin was uplifted and tilted eastwards during this tectonic event, as observed by numerous seismic industry lines and boreholes (Tarapoanca et al., 2003). This kinematics is in agreement with the geometry of the Palaeozoic-Mesozoic sedimentary cover beneath the Carpathians thin-skinned nappes, herewith defined as combination between two geophysical units, a ***supra-basement*** overlying a thick

Palaeozoic -Mesozoic sequence, which was detailed/mapped by deep seismic studies (Bocin et al., 2005, Landes et al., 2004; Panea et al, 2005, Bocin et al., 2009) and inferred from seismic interpretation, magnetotelluric and geothermal studies, tomographic and ray tracing velocity models (Figure 5.4, Chapter II and III see also Radulescu et al., 1979; Radulescu, 1981; Stanica and Stanica, 1993; Raileanu et al., 1994, Demetrescu et al., 2005). The geological significance of these two sequences are yet to be solved, but most probably their separation is related to the widespread Permo-Triassic rifting event recorded in the Moesian Platform, its late Triassic-Jurassic inversion and the subsequent post-tectonic cover (Tari et al., 1997; Georgiev, 2001; Panea et al., 2005).

The nappe complex and the foreland basin (Figure 5.2) have been studied and constrained by geological information (e.g., Sandulescu, 1988), seismic industry lines (e.g., Stefanescu et al., 1998, Tarapoanca et al, 2003) and by deep reflection or refraction surveys (DACIA PLAN 2001 - Bocin, et al., 2005, Panea et al, 2005; VRANCEA99 Hauser et al, 2001; VRANCEA2001 - Hauser et al., 2007).

5.2.1. Crustal blocks defined at the local scale in the foreland or beneath the south-eastern Carpathians

In the foreland of the south-eastern Carpathians a number of blocks have been defined traditionally by a combination of geological observation in boreholes and geophysical interpretations (e.g., Visarion et al., 1988; Sandulescu and Visarion, 1988a; Raileanu et al., 1994). The East European and Scythian platforms represent two crustal blocks delimited to the south by the Trotus Fault and presumably continuing westwards beneath the Carpathian nappes with their former passive margin involved in the nappe pile thrusting during the Miocene shortening events (Visarion et al., 1988b). The main characteristic of the East European Platform is an Archaean – Mid-Proterozoic metamorphosed basement and a Vendian-Early Palaeozoic to Mesozoic sedimentary cover interrupted by a large number of unconformities (Ionesi, 1989; Sliaupa et al., 2006). The affinities of its basement indicate always European fauna similar to the overall East-European domain. The overall crust indicates larger thicknesses, reaching locally 50 km (e.g., Enescu et al., 1992). At the S and SW edge of the East European Platform and related to its latest Precambrian–Early Palaeozoic (pre- Variscan) tectonic evolution, the Scythian Platform (Figure 5.1) is an area that has been considered as the passive margin of the East European Craton reworked by Late Proterozoic and younger tectonic events (Stephenson et al., 2004; Saintot et al., 2006).

The Pre-Mesozoic basement of areas located south of the Trotus fault (Figure 5.1) consists of an array of essentially Gondwana-derived terranes that were accreted to the margin of the East European Craton during the Caledonian and Variscan

orogenies (Ziegler 1981, 1990; Pharaoh et al. 2006). The metamorphic basement of the Moesian Platform is essentially of latest Proterozoic in age (Visarion et al. 1988a), similar with the one of the East European Platform. However, in the area traversed by gravity-magnetic profile, existing interpretations suggest that the Moesian Platform underwent significant Variscan deformation and was accreted to the Scythian Platform during the Late Carboniferous (Seghedi 2001). In the process of this, the latter also became overprinted by Variscan deformation (e.g. Zonenshain et al. 1990). Following the Permo-Triassic rifting event, the Moesian block may have been separated from the Scythian Platform until its accretion during the Jurassic Cimmerian tectonic events with the North Dobrogean orogen along the present Peceneaga-Camena fault, a structure displaying repeated tectonic deformations through mid-Cretaceous times (e.g. Seghedi 2001; Hippolyte, 2002, see Figure 5.1).

The depth to Moho within the Moesian Platform is 34-40km, with the exception of the Focsani Basin, where larger values are recorded due to the exceptional 13km of Miocene basin fill (e.g., Radulescu, 1988; Enescu, 1992; Tarapoanca et al., 2003; Martin et al., 2005; Hauser et al., 2007). The sedimentary cover of the Moesian Platform reaches up to its maximum of 18 km in the Vrancea area and thins elsewhere to 8-10 km (Cornea et al., 1981; Panea et al., 2005; Bocin et al., 2009). A thick Upper Palaeozoic (Upper Cambrian-Westphalian) detritic and carbonatic succession of up to 6.5 km is subsequently unconformably overlain by up to 5 km of Permo-Triassic, mainly clastics and mafic volcanism with layers of Permian evaporites and tuffs, ultimately covered by up to 3 km of Triassic carbonatic and Jurassic-Cretaceous detritic-carbonatic sequences (e.g., Ionesi, 1989). Following a major period of Paleogene erosion (Paraschiv, 1997), the Paleozoic-Mesozoic succession, which contains a fauna with strong Gondwanian affinities (Vaida et al., 2005), is overlain by the Carpathian foredeep clastics starting with the Middle Miocene.

The Moesian Platform is conventionally separated into three main units (Figure 5.1), a "Dobrogean" domain between Trotus and Intramoesian faults, a "Valachian" domain west of the Intramoesian fault, while the third unit is represented by the Danubian nappes of the South Carpathians (Visarion et al., 1988). These Danubian nappes represent a piece of Moesia that was accreted to the South Carpathians upper plate during the Late Cretaceous collision recorded during the closure of the Ceahlau-Severin ocean (e.g., Berza et al., 1994; Iancu et al., 2005) and that moved north- and eastwards from its original southward position during the Paleogene-Lower Miocene rotation of the upper Carpathians units (e.g., Csontos et al., 1995). Besides the late Proterozoic metamorphism, the Danubian nappes of the South Carpathians were significantly deformed and metamorphosed during Variscan times (Seghedi et al. 2005; Iancu et al. 2005), a situation which implies a more Paleozoic Europe- type of affinity (senso Pharaoh, 1999; Winchester et al., 2002) to this tectonic unit. This is an interesting observation because the Danubian unit is

interpreted to be prolongated eastwards, in the area crossed by the DACIA PLAN GRAV MAN'S profile in the south-eastern Carpathians subsurface, beneath the thin-skinned nappe pile (Visarion, 1978; Stefanescu, 1988; Schmid et al., 2008).

5.2.2. Geophysical properties of foreland crustal blocks in the larger context of Paleozoic Europe and East European Platform

The SW boundary of the East European Platform is the NW–SE striking Teisseyre-Tornquist Zone (TTZ), which separates the East European Platform, with its uppermost Precambrian metamorphism, from the Paleozoic-deformed Europe, repeatedly reactivated during Late Paleozoic, Mesozoic and early Cenozoic times (Ziegler, 1990). In local Romanian studies, the TTZ is traditionally interpreted to overlap across the Scythian Platform and North Dobrogean orogen (Cantini et al., 1991; Stanica et al., 1999, Figure 5.1). In general the TTZ is associated to a prominent Moho step in Central Europe (from a Paleozoic Europe-type of thin crust (32–34 km) to the cratonic crust with thickness of 42–44 km). In Romania, a westward crustal thinning of 5 - 10 km is inferred across the TTZ (e.g., Botezatu and Calota, 1983; Sandulescu, 1984; Guterch et al., 1986; Stanica and Stanica, 1993, Krolikowski and Petecki, 1997; Stanica et al., 1999, Andreescu and Demetrescu, 2001).

At a larger scale, the Trans-European Suture Zone (TESZ) is the most significant lithospheric boundary zone in Europe. It is a broad and complex/accretion zone between the Archaean–Proterozoic south-western margin of the East European Craton and the younger Neoproterozoic–Palaeozoic mobile belts (polyphase Caledonian, Variscan and Alpine orogenic cycles) of western Europe (e.g. Gee and Zeyen, 1996; Pharaoh et al, 1997; Pharaoh, 1999; Winchester et al., 2002). At a larger scale than the TTZ, Moesian Platform is generally interpreted to be also a part of TESZ (Pharaoh et al., 2006).

The fundamental contrast between the strongly magnetic crust of the East European Craton and the less magnetic crust of Phanerozoic-accreted Europe has been recorded on various regional magnetic maps (land, aero or satellite data, e.g., Figures 5.7). Most of the area of the East European Craton is characterised by high frequency and amplitude magnetic anomalies, reflecting the strongly magnetic nature of the upper and middle crust (Williamson et al., 2002). A strong gravity gradient zone running NW–SE across this important boundary (TTZ), in the Central Europe (and presumably similarly in its southern prolongation) is one of the most important features of geophysical fields of central Europe (Krolikowski and Petecki, 1997). It is either associated with crustal thinning or to a deep fracture outlined by the horizontal gradient that marks the lateral heterogeneity within or at the edge of the TTZ (Grosse et al. 1990).

Previous geothermal modelling in the south-eastern Carpathian area integrated with deep seismic sounding and gravity data indicated an interesting crustal differentiation between three distinct blocks beneath the thrusted nappe pile (Visarion et al., 1978): a Danubian unit is separated form the Dobrogean block of the Moesian Platform by a unit with "intermediate" characteristics, possibly the eastern distal continental passive margin of Moesia. The study suggested that the area is tectonically active due to the large horizontal gradient of 200-300°C/100km between the inner and outer part of the south-eastern Carpathians and the heat flow values that increase westward from 45 to 88 mW/m2, which correlates well with inferences from gravity studies about crustal thinning in the area (from 45 to 37 km).

An electrical conductivity anomaly at mid-crustal depth, detected by magnetotelluric studies, that is spatially associated with the previous recorded high values of heat flow (73-126 mWm), interpreted as the limit between the TESZ with the East-European domain beneath the Carpathian nappes (Veliciu and Visarion, 1984; Stanica and Stanica, 1993; Stanica et al., 1999). This contact is also marked by a high geoelectrical anomaly, interpreted as a former subduction zone (e.g., Stanica and Stanica, 1993).

The presence of such types of highly differentiated crustal blocks beneath the south-eastern Carpathians nappe pile is also suggested by other more recent geothermal measurements and their modelling (Andreescu and Demetrescu, 2001; Demetrescu et al., 2005), gravity modelling (Visarion et al., 1988b), crustal seismology (Bala et al., 2003) and (deep) seismic studies (Radulescu et al., 1976; Mocanu et al., 1996).

5.3. DACIA PLAN GRAV MAN'S profile

A set of densely spaced data acquired during two consecutive years of field campaigns were processed and an integrated gravity and magnetic model has been obtained. An initial gravity and magnetic structural model was constructed using as a priori information data derived from the mapped and depth-extrapolated geology and previous seismic investigations (Vrancea99, VRANCEA2001, DACIA PLAN 2001; Hauser et al., 2001, Hauser et al., 2007, Bocin et al., 2005, Panea et al., 2005, Bocin et al., 2009).

5.3.1. Data acquisition

A 71 km long **DACIA PLAN GRAV MAN'S PROFILE** gravity and magnetic profile traverses the major tectonic units of the south-eastern Carpathians and its foreland (Figure 5.3a). The profile coincides with, for almost entirely its length, the previous deep reflection seismic survey DACIA PLAN 2001; the exception is a 4 km

stretch added to the west of the survey. At its eastern extremity the profile stops around Dumitresti (DUMM Figure 5.3a; seismic shot 64 in Bocin et al., 2005). Measurement points were placed, as a consequence of the proposed survey resolution (depths of investigation or wavelength vs. anomalous body or the spatial extent of the source of the anomaly), at 250 m intervals (azimuthal projection of the distance and not the actual road distances). As the chosen stations, elevation determination was in the range of centimetres (less than 10 centimetres) as all the measurement points were positioned using differential GPS instruments (for methodology see Chapter IV). From a total of 263 stations only 3 of them required separate levelling, caused by poor satellite configuration geometries (GDOP) or a too narrow azimuth clearance that made positioning impossible with GPS.

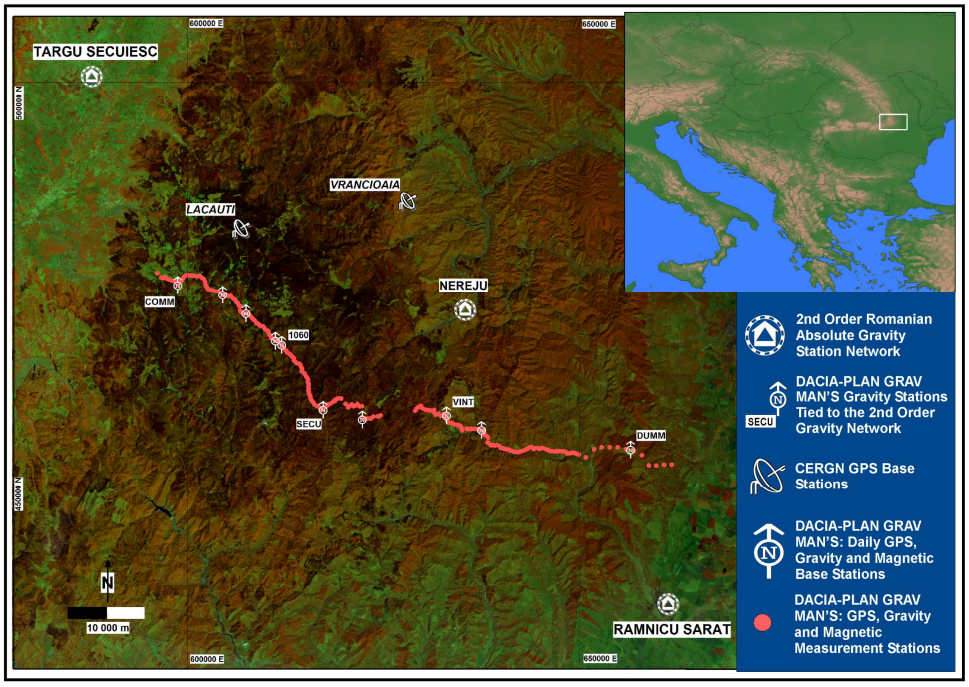

Fig.5.3.a) Data acquisition (background LANDSAT image). Profiles with GPS, gravity, magnetic and seismic stations;

The gravity data were acquired in two consecutive years' field campaigns due to difficult terrain conditions and to the complex methodology of acquisition (ties, levelling of the gravimeter, drift) and using two Pioneer Worden gravity meters (for instrument details consult Chapter IV). Almost 95% of the data were collected during the 2005 campaign when ties to absolute gravity points from the Romanian National Gravity Network (Targu Secuiesc and Ramnicu Sarat; Figure 5.3a) were performed.

A local gravity base station network (as part of the gravity and magnetic survey design) that incorporated 5 ("intermediary") base stations (Figure 5.3a; for

details see Chapter IV) was created to where the absolute gravity values were translated (transported) from the regional gravity network. Four of these also represent points of measurements within the profile. The following year, a helicopter was used to cover areas not surveyed during the first field campaign (inaccessible to be measured within a reasonable timespan and, hence, instrumental drift by using a car as transportation between points) allowing 12 additional stations to be measured in very rough terrain conditions. Ties with base stations established in the previous year were re-measured and a new tie between an intermediary point from the profile (SECU; Figure 5.3a) and the absolute gravity station at Nereju (part of the Romanian National Gravity Network; Figure 5.3a) was established. The magnetic data were measured entirely during the 2005 campaign using two proton magnetometers, one as a daily base station (measuring diurnal variations) and one of the two others as a rover station (see Chapter IV for details).

5.3.2. Data processing

The GPS data were collected in a differential GPS mode using Leica 530 instruments. The data were processed using SKIPro software. The less than a few centimetres error coordinates were transferred from two CEGRN points (Lacauti and Vrancioaia; Figure 5.3a) to two multi-day GPS base stations (COMM - Comandau and DUMM - Dumitresti; Figure 5.3a). Further, the coordinates were transferred to a set of daily base stations (same as the magnetic diurnal variation base station). Baselines between base stations and rover stations (usually two rovers were deployed in the field) were geometrically designed to not exceed 15 km in order to decrease the positioning errors and reduce the time needed in the field to measure (the longer the baselines, the longer the time for positioning and the bigger the error). For more than 80% of the data the automated processing stream ran smoothly and no ambiguities were encountered (see Chapter IV for details). Where, due to high ambiguity, the coordinates could not be resolved, the processing was done manually. Scenarios with different or multi baselines were tried and thereby all the coordinates were determined (see Table 1 for error estimation). The gravity data were processed using a composite methodology that included customized Microsoft Excel Spreadsheets and a DOS executable. The data were reduced to Bouguer Anomaly (for details see Chapter IV) and tied to the Romanian Gravity Network. Earth tides and topographical (terrain) corrections were applied in order to obtain the Complete Bouguer Anomaly. Earth tides and drift corrections were performed using drift curves (drift vs. time graphics) obtained by closing a measuring cycle at every 3rd hour (or, in the case of major elevation differences, less than this). Terrain corrections using Hammer charts (see Chapter IV) were applied to the gravity data. A 90 m resolution digital elevation model (DEM) was used for correcting the data for the slab

effect (21943 m radius of the outermost used ring of the terrain correction Hammer chart; see Figure 5.3b).

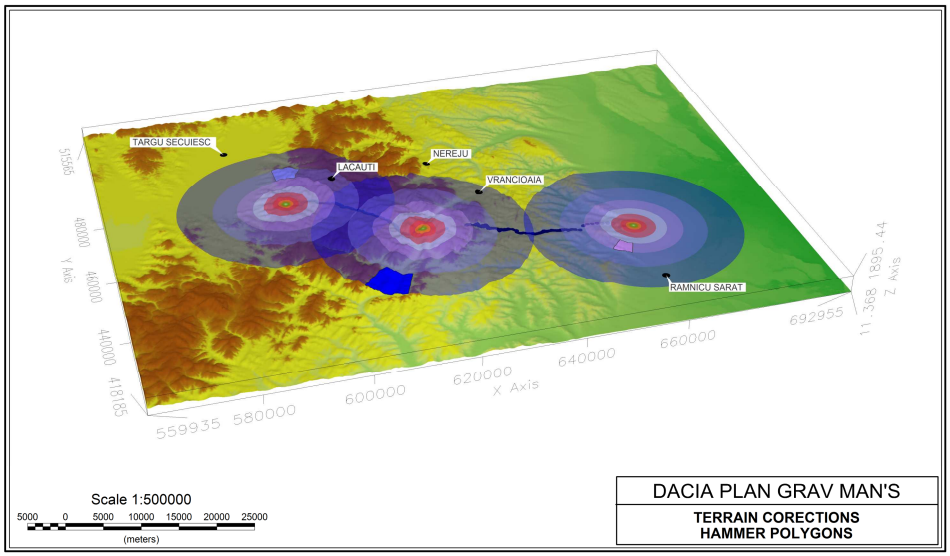

Fig.5.3. (*Continued*) b) 3D structure of the area and reduction issues. Hammer chart overlaid on the 3D structure. Commentaries about DEM and reduction procedure can be found within Chapter IV.

The magnetic data were reduced for diurnal variations and IGRF theoretical effects. The diurnal variations were applied using base station observations recorded daily at every 5 minutes. The local diurnal variations (daily 5 minutes observations) were considered robust and resolute as they conveyed local storms or any otherwise remotely local noise. The IGRF values for the measurement points were calculated using QC-Tools software whilst the diurnal variations were applied independently but synchronously to all points using GEMSYS software (see Chapter IV for further details).

5.3.3. Gravity and magnetic profiles

The gravity and magnetic data used in the modelling were entirely acquired from the DACIA PLAN GRAV MAN'S survey. As a consequence of positioning misfits due to a larger error than accepted in a gravity survey some gravity measurements were omitted whilst modelling. Therefore, the general overall quality of data was high. The short distances between stations was conformable to the desired resolution and led to a lower degree of uncertainty for the inferred structures shapes and depths. From a total of 266 proposed or measured gravity stations 246 were considered of sufficient quality for modelling. Stations number 998, 1099, 1121, 1085 and 1127 were removed from the modelling procedure due to poor positioning. A small stretch of 15 stations (between 1131 and 1146 ~ 3.5 km of data hiatus) were

impossible to be measured with the gravimeter due to rough terrain conditions and unacceptable drifts (the helicopter could not land due to high ascending air currents). In the case of magnetic data from a total of 266 proposed magnetic stations all were measured but only 239 were used for modelling. Some, sparsely distributed measurements were excluded due to high noise levels (probably caused by fences, underground object or the proximity to road traffic). Due to a base station magnetometer malfunction (the over-qualified operator turned it off early) a stretch of 14 stations were measured but they could not be corrected for diurnal variations.

5.4. Crustal model

5.4.1. Physical properties and a priori constraints

The density values that have been used in the modelling are listed in Table 1 and presented also in the accompanying gravity model figures. Values for the shallow sedimentary cover of the Focsani Basin were derived from seismic velocities using a compilation of formulas (Nafe-Drake curve published by Ludwig et al., 1970; Gardner et al., 1984; Christensen and Mooney., 1995) or by consulting previous gravity studies (Bielik et al. 1998; Yegorova and Starostenko, 2002; Bielik et al., 2005; Ioane and Ion, 2005; Raileanu et al., 2005). The same principle of deriving density values from seismic velocities was used to obtain densities in the shallower layers from south-eastern Carpathians area. Therefore data from boreholes velocity information (available in previous depth-converted models from seismic information; Leever, 2006) and published tomographic or ray tracing velocity models (Bocin et al., 2005; Bocin et al., 2009; Hauser et al., 2007) were used. In so applying objective principles or by direct measurements on the rocks the entire shallower layers densities were determined in the following way.

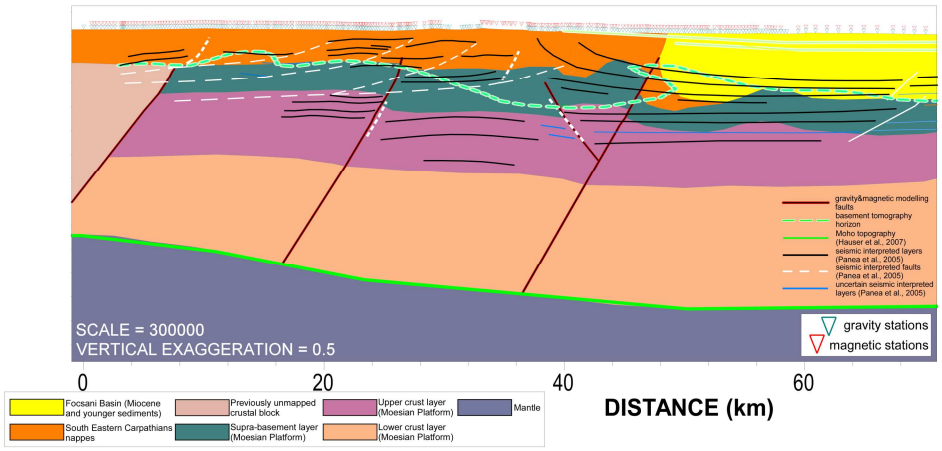

Fig.5.4. The a priori seismological constraints used to construct the model. Simplified potential field model overlaid by: DACIA PLAN 2001 seismic section interpretation (Panea et al., 2005) and tomography basement topography (Bocin et al., 2005); VRANCEA2001 seismic ray tracing model (Hauser et al., 2007) - the lower crust layers were a priori introduced in the gravity and magnetic modelling; DACIA PLAN 2001 seismic ray tracing model (Bocin et al., 2009) - the upper crust interpretation was used whilst modelling.

Densities of the ***supra-basement*** layers were inferred from previous interpretations of a Mesozoic or older sedimentary cover of basement (Bocin et al., 2005; Panea et al., 2005; Hauser et al., 2007; Bocin et al., 2009). The Moho topography determined in the previous ray tracing model (Hauser et al., 2007) was adopted as is as an *a priori* constraint. Figure 5.4 shows the correlation between the gravity and magnetic models as well as the inferred constraints from previous seismic velocity models (Bocin et al., 2005; Hauser et al., 2007; Bocin et al., 2009) and seismic interpretations (Panea et al., 2005). The crystalline basement densities were initially set conformably to the same rules but during modelling the densities were perturbed as necessary, within what were considered to be highly acceptable ranges

Foreland sedimentary domain		
S1	very light pink	1900
S2	light yellow	2020
S3	gray	2200
S4	yellow	2240
S5	Brown/put real color	2360
Orogenic sedimentary domain		
Σ	dashed grey	1770
O1+Σ	dashed light brown	1880-1900
O1	light brown	2210
O2	light green	2310
O3	red	2360
O4	lila	2380
O5	orange	2370-2380
O6	green	2420
Supra-basement		
SBAS1	dark green	2470
SBAS2	indigo	2490
SBAS3	blue	2520
SBAS4	brown	2680
SBAS5	violet	2720
Fundament Crystalline basement		
CB1	dark pink	2830
CB2	pink	2940

All values are given in SI units kg/m^3

(see discussion and interpretation section for details). The geometry and density of the lower crust was also defined from the seismic velocity models.

Table 1, Density values that have been used in the modelling

Table 2 presents the magnetic susceptibilities that have been used in the model. These values were inferred from studies concerning geophysically and tectonically similar areas and therefore using a novel interpretation of the regional tectonics (see discussion and interpretation section for susceptibilities correlations with other areas), different crystalline basement sectors and a number of layers with specific susceptibilities were introduced in the model.

Magnetic susceptibilities values used in model

SBA3	blue	0.015
SBA5	violet	0.007
CB1	dark pink	0.006
CB2	pink	0.025

All values are given in SI units.

Table.2 Magnetic susceptibilities used for modelling

5.4.2. Potential field modelling methodology

The high resolution acquisition of the DACIA PLAN GRAV MAN'S profiling combined with earlier results of ray tracing and tomographic modelling allow a well constrained geological interpretation of complex geophysical acquisition, which is, by methodology, a novel approach to a rigorous sequence of steps, which led to a final outcome that is considered to have a high level of robustness.

Gathering seismic information and correlating it with the potential field models is a commonly used procedure. For this case the gravity and magnetic methods were used to constrain some specific questions derived from the seismics (due to the very complex structures the seismic images are blurred) about the composition of some high velocity bodies (Bocin et al., 2005; Bocin et al., 2009) and, in so doing, novel information was obtained about the regional tectonic framework and possibly the timing of emplacement of the different crystalline and/or ***supra-basement*** units.

The gravity and magnetic data were modelled using a forward modelling approach. The GMSYS 2D potential field modelling software developed by NGA's (a Geosoft Oasis module) was used to derive the models. The potential field model's response is calculated using the Talwani et al. (1959) and Talwani and Heirtzler (1964) methods and incorporating the algorithms described in Won and Bevis (1987). The edge effects were reduced in two steps: a) by introducing to the left and right of the model an extra of 40 km long seismic derived structure (obtained from Panea et al., 2005 and Hauser et al., 2007) and b) by extending the model domain plus and minus 30,000 kilometres at each end of the profile. The modelling was performed by simulating a number of tabular prisms with their axes perpendicular to

the profile; the 2-D blocks and surfaces were presumed to extend to infinity in the strike direction.

5.4.3. Preferred model (Figure 5.5)

The geological model used as a primary input for the gravity and magnetic modelling is taken from the regional cross section 15 of Stefanescu et al (1988), recently improved by Matenco et al. (2007) and Schmid et al. (2008) with shallow and deep seismic reflection profiles in particular in the area of the Focsani Basin and the transition with the Carpathians nappes (Tarapoanca et al., 2003; Leever et al., 2006).

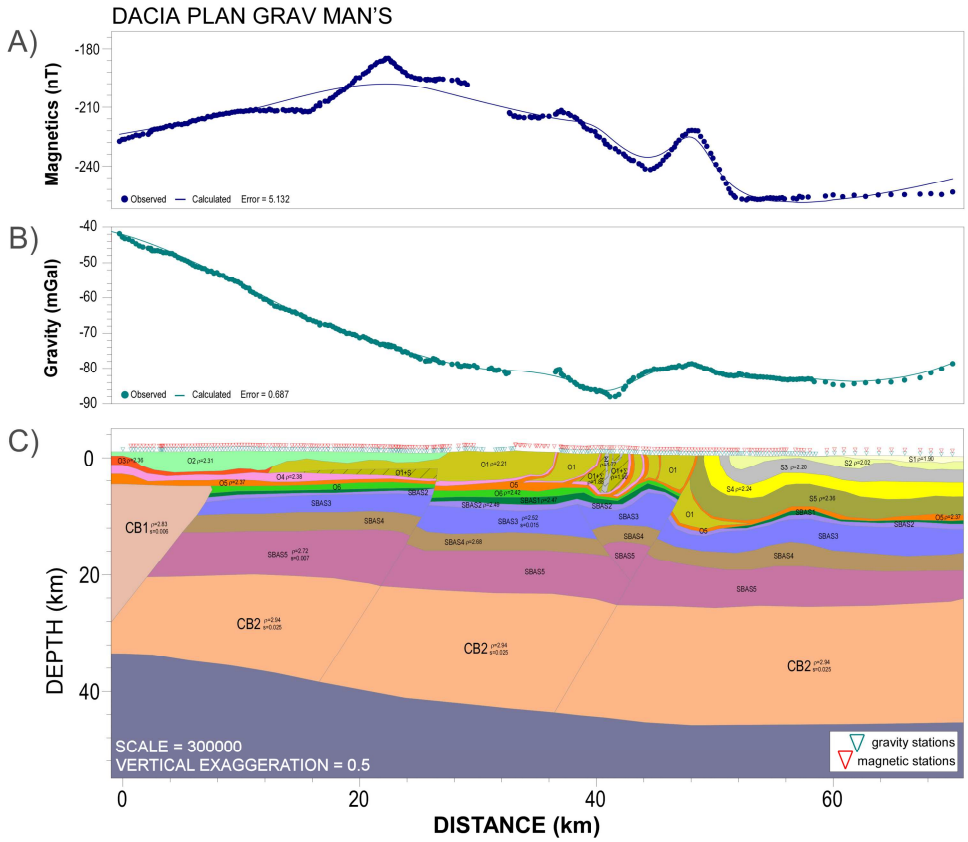

Fig.5.5. The final preferred crustal model and the fit between calculated and modelled gravity and magnetic profiles. The initial geological model used as a primary input for the gravity and magnetic model and then perturbed is derived from the cross section 15 of Stefanescu et al (1988) improved by Matenco et al. (2007) and Schmid et al. (2008).

This geological model has been modified for a best fit between calculated and modelled gravity and magnetic profiles, the result being displayed in Figures 5.5 and 5.6. The gravity model comprises a number blocks each with constant density. The minimum difference of density between blocks that was thought to be significant for

modelling was 20-30 kg/m^3, more than required to simulate a geological contact expressed in the short or long wavelength gravity field. The background density of the model was set as 2300 kg/m^3 although, in the sense of modelling local anomalies, as in the present case, this is not very important. The preferred gravity model for simplification reasons (and latter interpretation) is presented in terms of three main categories that share properties from a structural point of view and are thereafter split into domains with associated densities: the first category comprises the shallower structures (Carpathian nappes and the Miocene-Quaternary sediments of the Focsani Basin); the second category consists the ***supra-basement***, representing the lower part of the upper crust and a thick stack of deeper structures identified within the middle part of the crust; the third category includes the lowermost part of the model corresponding to lower crust.

The first category was split into two main domains mainly inferred from seismic ray tracing information (see Chapter 4). The densities were obtained after conversions from seismic velocities were performed using different formulas or constraints (see *Physical properties and a priori constraints* subsection and the references within). One domain corresponds to the blocks between km 0 and 50 and has relatively higher densities for sedimentary rocks (between 2310 and 2420 kg/m^3; hard consolidated sedimentary rocks domain, generic called "***orogenic sedimentary domain***" Os – see Table 1). The lithology consists of shales, stratified silicolites and sandstones with additional marls, limestones, tuffs and conglomerates, salt, etc (e.g. Sandulescu et al., 1981). The other domain consists of a thicker ensemble of blocks between km 50 and 70 and it contains low sedimentary densities (between 1900 and 2360 kg/m^3; unconsolidated and consolidated sedimentary rocks domain, "***foreland sedimentary domain***" Ss – see Table 1). The lithology includes alternations of sandstones, conglomerates, tuffs, marls, etc (e.g. Sandulescu et al., 1981). The density increased with depth for the first 10 km of the model, only a small degree density inversion was met between block O2 and O4 with a 10 kg/m^3 inversion for the O3 block. The density inversion was inferred from seismic ray tracing and lithological constraints though the extent and the shape of the blocks were not necessarily modelled to mimic them. In the "*orogenic sedimentary domain*" complexities in the model were simulated to accommodate shallow features that influence the gravity profile, such as salt structures and local geological heterogeneities. In the "***foreland sedimentary domain***" the layers (S1-S5) lie horizontally but small variations in thickness and depth are accommodated. At the contact between the orogenic and sedimentary domains a fault pierces O1 and tilts the S2-S4 layers into an almost vertical disposition.

The second category consist two distinct domains: the ***supra basement*** domain and the thick Paleozoic-Mesozoic sequence related to the Permo-Triassic rifting event ("***Paleozoic- Mesozoic sequence -rift-"***). The ***supra-basement*** (SBASs in Table 1) domain has densities in the range of 2470 to 2680 kg/m^3. The lithology is

inferred from previous studies (e.g., Stefanescu et al., 1988; Visarion, 1988; Tari et al., 1997), and contains carbonate successions, clastic sediments. It is present for the entire length of the profile except the westernmost 8 km of the profile. It is affected by a number of crustal faults. The "rift" sequence has a density of 2720 kg/m^3, a density that would correspond to limestones, variations of sandstones, pyroclastites, etc. (e.g., Stefanescu et al., 1988, Visarion 1988, Tari et al., 1997).

The third category is represented by the basement and it is mainly split in two sectors: at the westernmost part of the model, a block (basement sector 1) with a 2830 kg/m^3 density that lies at shallower depths (~ 5 km) and three more blocks that runs for the rest of the model with a common density of 2940 kg/m^3. A model that does not have this change in the basement affinity ***cannot*** satisfy the gravity gradient in the western part of the profile. The shallow elevated basement sector 1 is constrained by the seismic velocity models (mentioned in the physical constraints section) that indicate velocities of 6000–6200 m/s and conformable to densities of 2820-2840 kg/m^3 (based on the Nafe-Drake relationship). The crystalline sector 2 has a density of 2930 kg/m^3 and is constrained by the 6300-6400 m/s seismic velocities inferred from the ray tracing model of Hauser et al (2007). The crust is thinning westward significantly with more than 15 km (a priori constrain; see previous section). The lithology is mentioned below where the magnetic model is integrated with the gravity results.

The magnetic model has the same model space as the gravity model, with which it is integrated. In comparison with the gravity model only a few blocks have magnetic susceptibilities (see Table 2 for details). The ***supra-basement*** blocks SBAS3 and SBAS5 present fairly high magnetic susceptibilities of 0.015 SI and respectively 0.007 SI. They can be associated with sedimentary and low grade metamorphic rocks (limestones, sandstones, slate, etc). The basement sectors have different susceptibilities, sector 1 having 0.006 SI and can be interpreted as various types of metamorphic and igneous rocks (gneisses, amphibolites, granites, etc) while sector 2 blocks comprise rocks with 0.025 SI susceptibilities and they could be associated with gneisses, granulites, granitoids and mafic granulites.

5.5. Geological interpretation: discussion and implications

The DACIA PLAN GRAV MAN'S potential field anomalies (gravity and magnetic) represent a combination of long (first order) and short (second order) wavelength components. The interpretation is focused on the longer wavelengths (above local effects); therefore, deeper structures are investigated. During modelling the shallower (shorter wavelength) structures were used as control manoeuvres for decreasing the overall error. The shorter wavelengths are not subject to

reinterpretation (but not overlooked while modelling) as they were interpreted by previous geological or geophysical studies.

5.5.1. Basement affinities

Figure 5.6 shows the simplified geological interpretation version of the gravity and magnetic model with some key features of the geological model based on previously information inferred from seismic studies such as ray tracing and tomography. The supra-basement pre-orogenic unit can be geologically correlated with the Jurassic-Cretaceous cover of the Moesian Platform overlying sediments associated with the earlier rifting episode. This was also inferred by previous regional low resolution interpretations such as Visarion et al. (1988) and Matenco et al. (2007) and was identified as reflective upper crust structures in Panea et al. (2005) and Enciu et al. (2008). These studies have also identified the *Palaeozoic-Mesozoic "rift"* structure, which can be correlated with the Permo-Triassic rifting events described above.

The main part of the fault systems observed in the preferred models in the crust below the thin-skinned nappe pile were derived from ray tracing modelling (Bocin et al., 2009), but were fully confirmed by the gravimetric and magnetic preferred model.

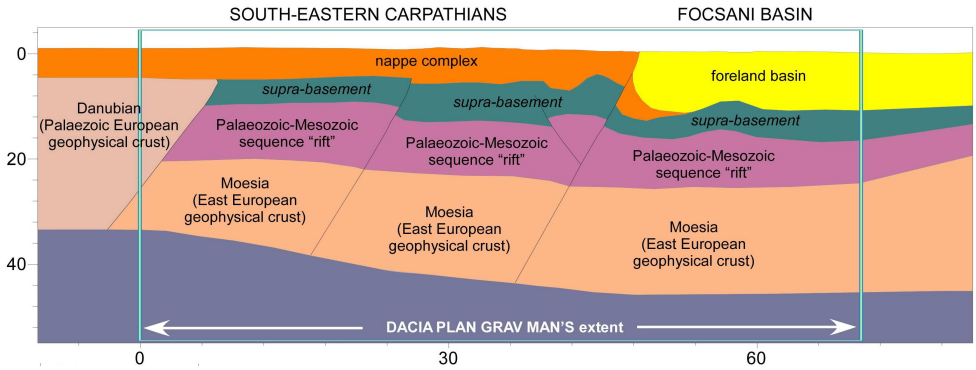

Fig.5.6. The simplified potential field model used for the geological interpretation and the structural key features of the profile. The bottom of the ***Palaeozoic- Mesozoic sequence "rift"*** that corresponds to the limit between middle and lower crust was modelled *a priori* after Hauser et al. (2007) tough does not geometrically mimics the Permo Triassic rift that was correlated/interpreted with/as.

Along the westernmost segment of the profile, the *Mesozoic-Palaeozoic* "rift" disappears, being bounded by a sub-vertical fault truncating the entire pre-nappe sequence, with an uplifted position of the western block. This reverse fault is constrained by the observed gravity gradients, but the exact inclination cannot be properly constrained due to its position near the edge of the model. Following these constraints, this large scale fault must be reverse dipping westwards and, following

the truncated strata, must be Cretaceous or younger (see also Panea et al., 2005). This large scale feature provides the most important contrast in terms of both geophysical and geological characteristics. This is the boundary between a positive magnetic anomaly to the east when compared to a minimum located westwards. Geologically, this is the speculatively interpreted boundary of the Danubian nappes by Schmid et al (2008) with its Palaeozoic metamorphism, separating eastern areas of the Moesian Platform ("Dobrogean" block), where only latest Precambrian metamorphism, overlain unconformably by a thick Palaeozoic - Mesozoic sequence, is known. This spatial coincidence of geophysical and geological interpretations looks strikingly similar with the contrast between Palaeozoic Europe and East European Craton across the TTZ. Moreover, this change in the basement affinity corresponds with significant crustal thickening eastwards, in the "Dobrogean" block with 10-15km, which is very similar with the same order crustal thickening across TTZ in Central Europe.

These findings points once more on the particular evolution of the Moesian Platform and its sedimentary cover, which is non-standard by the typical ways of judging Palaeozoic Europe or East European Platform across the TTZ in the areas NW of the Carpathian chain. Although it contains a sedimentary sequence which is specific to the Palaeozoic Europe, its Precambrian metamorphosed basement yields a geophysical signal which is typical East-European (Figure 5.6). Only those areas of the Moesian Platform that contain Palaeozoic metamorphism, such as the described Danubian nappes, would yield a geophysical signal which is characteristic for Palaeozoic Europe (Figure 5.6). The Palaeozoic European "geophysical" crust is less dense and less magnetically susceptible, while the East European "geophysical" crust is denser and more magnetically susceptible (Figure 5.5).

Although the densities were treated as variables in the modelling process, the continuity of properties of these contrasting crustal blocks suggests that the distinct affinities of the East European "geophysical" and Palaeozoic European "geophysical" types of crust is robust.

5.5.2. Teisseyre Tornquist Zone

One important implication of the crustal affinities model is that the typical geophysical contrast associated with TTZ is localized beneath the south-eastern Carpathians. Looking at the large variety of subduction models defined for the post-collisional stage (11-0 Ma) in relationship with the Vrancea seismicity or the high velocity mantle anomalies (e.g., Wenzel et al., 1999; Martin et al., 2006), the gravity and magnetic modelling show no clear signs of a subduction-related suture zone on the path of the profile. However, a subduction (or better said major continental underthrusting) zone could be present at the same contact between blocks with different European affinities. The Miocene thrusting can presumably take

place beneath the Danubian nappes, as clearly demonstrated by geological studies in the South Carpathians (e.g., Iancu et al., 2005).

The specific results of this study, having to do with heterogeneity within the basement layer, integrated with previous seismic studies such as strong reflections in the upper crust (Panea et al., 2005) or within the whole crust (Enciu et al., 2008), Moho thickening (Hauser et al., 2007) or seismic attenuation (Russo et al., 2005) can be correlated with previous results on the nature of the TTZ (Znosko, 1979; Berthelsen, 1992a, b, 1998; Dadlez et al., 1994; Zielhuis and Nolet, 1994; Schweitzer, 1995; Kutek, 1997; Pharaoh et al., 1997; Winchester et al., 2001). Figure 5.7 presents the regional satellite gravity map of central Europe including the study area extracted from GRACE data results and the regional magnetic anomaly map extracted from the World Digital Magnetic Anomaly Map. Although the presence of TTZ in the present study area is not evident in the gravity map (Figure 5.7a) because of the peculiar characteristics of the Moesian Platform, there is a clear boundary in the magnetic map which can be correlated with the present interpretation (Figure 5.7b).

Other regional geophysical studies are in agreement with our interpretation. Atanasiu et al (2005) proposed the trace of the TTZ on the Romanian territory using) satellite gravity and magnetic data, focussing on the strong contrast between the highly magnetic East European Craton and the less magnetic Palaeozoic accreted terranes of central Europe and the large gravity gradient zone corresponding to the same boundary. Anomalous features from both potential fields indicate the signature of the TTZ. Szafian et al (2006) performed regional three-dimensional gravity modelling of the Carpatho-Pannonian area that mapped the Moho boundary and the intra-crustal density heterogeneities in which a transitional unit at the base of the crust associated with the TTZ was inferred, which in the present interpretation corresponds due to similar characteristics with the "Dobrogean" block.

The association of the previously documented seismic velocity body beneath south-eastern Carpathians with the crustal boundary reveals further correlations with previous observations about the TTZ. Schweitzer (1995) explained the attenuation of seismic energy to a low Q-structure within/below the TTZ, clearly affecting seismic waves down to at least 200 km depth. Russo et al (2005) recorded the same low Q values at stations above and near the Vrancea zone, and at stations in the Transylvanian Basin and explains it in terms of the presence of hot asthenosphere in these areas. The same study documents low attenuation (high Q) beneath the East European platform, the Scythian Platform and the Moesian Platform and excludes models of the area invoking lithosphere delamination (since the presence of a highly attenuative asthenospheric wedge is not seen). Therefore, a boundary zone is implied by observed Q values although the attenuation is not caused by hot asthenosphere but

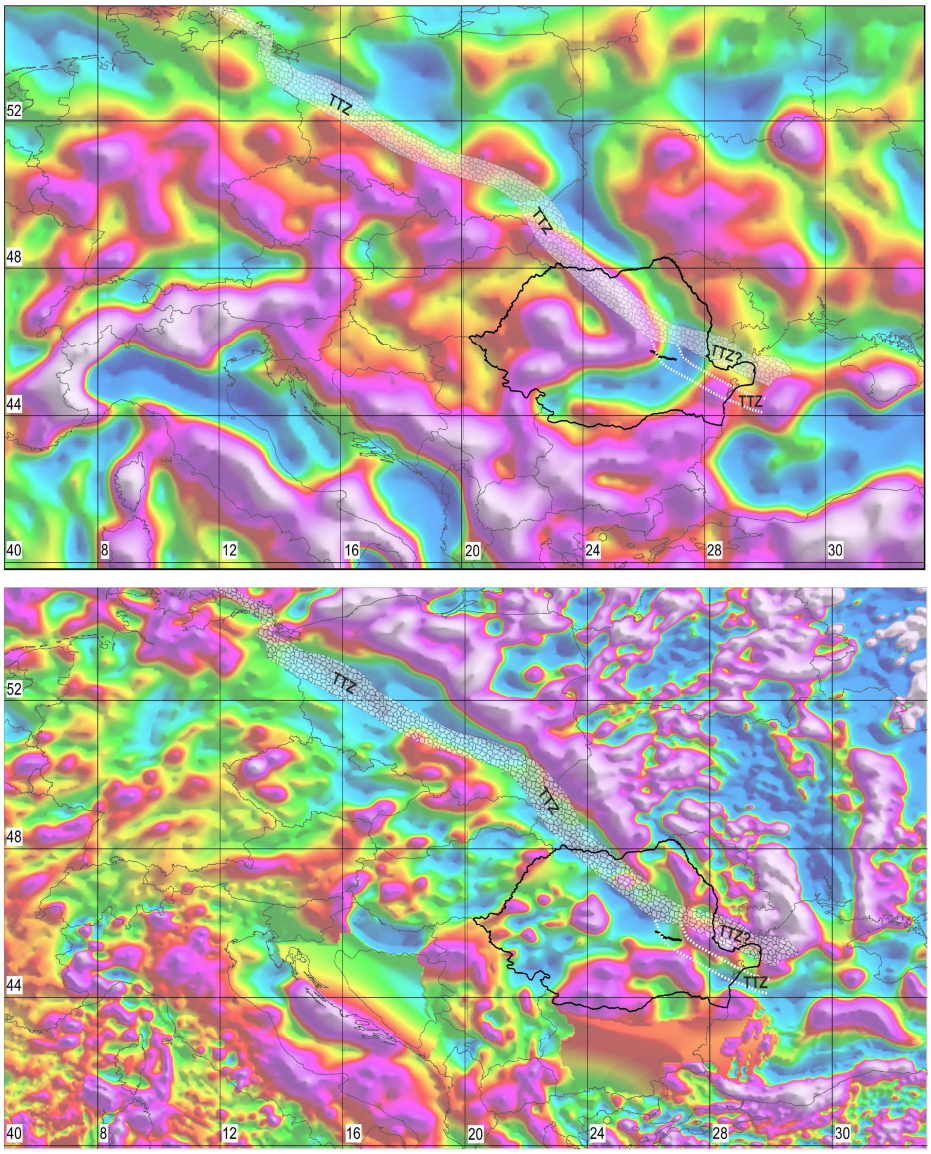

Fig.5.7. Correlation between local and regional gravity and magnetic interpretation a) Regional gravity anomaly map obtained from GRACE satellite missions; b) Regional magnetic map obtained from the World Digital Magnetic Anomaly Map. The potential fields profile is localised on the map. The position of TTZ conformably to Winchester et al (2002) (transparent hashed region) and conformably to this thesis (white dashed lines).

rather could be explained by a narrow highly heterogeneous deepening crustal structure associated with the TTZ. The results do not exclude models such as those invoking slab detachment that includes asthenospheric inflow or continental lithosphere delamination but suggest a new and different explanation for crustal (and sub-crustal) heterogeneities and their possible role in the unusual seismicity associated with the Vrancea Zone.

5.6. Conclusions

A well-resolved and robust potential field model, constructed in conjunction with constraints derived from the earlier seismic results, was obtained from a densely spaced gravity and magnetic field survey. This model has revealed heterogeneous relict structures of the underlying basement and has allowed new crustal tectonic information to be inferred.

The interpretation of potential field data of the DACIA PLAN GRAV MAN'S survey supports a number of conclusions that were already suggested by the previous seismic velocity models and interpretations:

1) The upper crustal structures of the nappe stack and the foreland basin are resolved with lithological constraints; the contact between these structures is mainly effected by an important crustal fault; the fault was previously interpreted as an active fault on the basis of crustal seismicity; the foreland basin thickness reaches approximate 12 km.

2) The ***supra-basement*** unit inferred in the previous seismic ray tracing model is constrained and its topography is determined; blocks within this structure located in the west part of the profile (beneath the south-eastern Carpathians) display 2 - 2.5 km uplift; the blocks beneath the foreland basin undergo subsidence; the lateral extent of this structure is bounded to the west by a crustal fault (previously inferred in the deep reflection ray tracing velocity model); the lithology used while modelling and inferred correlations indicate that Mesozoic sedimentary (or low-grade metamorphosed) rocks forms this unit.

3) The thickened Upper Palaeozoic - Lower Mesozoic sedimentary succession (***Palaeozoic - Mesozoic "rift")*** is considered to be responsible for middle crust strong reflections previously recorded by the deep seismic reflection and refraction lines; the lateral extent of this unit is bounded to the west by the crustal fault.

4) The modelled crystalline basement sectors geometry (spatial spread) confirms the shallower position (pronounced uplift) of the westernmost sector inferred by the previous deep seismic reflection ray tracing experiment; the same important bounding crustal fault is responsible for the pronounced uplift of the basement beneath the orogeny; the crust thickens eastwards with 10-15 km as was ascertained by the previous deep refraction seismic ray tracing velocity model (the information was used as a priori constrained by this study).

Though the conclusions mentioned above do not represent completely independent results they lead to further important implications and represent an advance in the interpretation of the south-eastern Carpathians and Focsani Basin area:

1) The modelling results shows that the Palaeozoic European "geophysical" crust is less dense and less magnetically susceptible, while the East European "geophysical" crust is denser and more magnetically susceptible, inferences that are correlatable with the results recorded in similar potential field studies.

2) The Moesian Platform contains a sedimentary sequence that is specific to the Palaeozoic Europe but its Precambrian metamorphosed basement yields a geophysical signal that is typical East-European; areas of the Moesian Platform which contain Palaeozoic metamorphism (specifically the Danubian block) yield a geophysical signal that is characteristic for Palaeozoic Europe.

3) Therefore, the typical geophysical contrasts and also the crustal affinities inferred in this study lead to the conclusion that the Teisseyre-Tornquist Zone is localized beneath the south-eastern Carpathians.

4) The gravity and magnetic modelling shows no clear signs of a subduction-related suture zone on the path of the profile but, nevertheless, a subduction or major continental underthrusting zone can be present at the same contact between blocks with different European affinities; Miocene thrusting can presumably take place beneath the Danubian nappes, as clearly demonstrated by geological studies in the South Carpathians.

Though the amount of densely spaced data is limited to local gravity and magnetic data, integration with previous complementary or independent studies has allowed a new interpretation of the south-eastern Carpathians and Focsani Basin in terms of active continental collision at the edge of the East European Craton. The results can be further constrained as new densely spaced data will be proposed for acquisition or future integration will be performed.

Acknowledgments

The students that participated to the DACIA PLAN GRAV MAN'S survey are thanked for their efforts and the many hours they spent in the field: Cristina Marin, Marian Iancu, Ioan Munteanu, Gabi Paal, Iulian Voinescu. Andre van der Hoeven is thanked for giving his support to manage and acquire the differential GPS and levelling data. The University of Utrecht and are thanked for offering the gravimeters. The GPS instruments and the geodetic leveller were lent by the University of Delft.

References

Andreescu, M., Demetrescu, C., 2001. Rheological implications of the thermal structure of the lithosphere in the convergence zone of the Eastern Carpathians, J. Geodyn. 31, pp. 373–391.

Atanasiu, L., Zugravescu, D., Mandea, M., Roharik, M., 2005. Trans-European Suture Zone over the Romanian territory in the light of new satellite data, Rév. Roum. Géol., Géophys. et Géogr., Geophysique, 43, Bucarest.

Bala, A., Radulian, M., Popescu, E., 2003. Earthquakes distribution and their focal mechanism in correlation with the active tectonic zones of Romania, Journal of Geodynamics, Volume 36, Issues 1-2, Active Faults: Analysis, Processes and Monitoring, Pages 129-145.

Balla, Z., 1987. Tertiary palaeomagnetic data for the Carpatho-Pannonian region in the light of Miocene rotation kinematics, Tectonophysics, Volume 139, Issues 1-2, Laurasian Paleomagnetism and Tectonic, Pages 67-98.

Berthulsen, A., 1992a. Mobile Europe, in: A continent revealed - The European Geotraverse, pp. 17 - 32, ed. Blundell, D., Freeman, R. & Cambridge University Press, Cambridge.

Berthelsen, A., 1992b. From Precambrian to Variscian Europe, in: A continent revealed- The European Geotraverse, pp. 153 - 164, ed. Blundell, D., Freeman, R & Mueler St., Cambridge University Press, Cambridge.

Berza, T., Iancu, V., 1994. Variscan events in the basement of the Danubian nappes (South Carpathians). In: Berza, T.(Ed.), Geological evolution of the Alpine–Carpathian–Pannonian system, ALCAPA II, field guidebook, Rom. J. Tect. Reg. Geol., 93–104.

Bielik, M., 1998. Analysis of the gravity field in the western and eastern Carpathian junction area: density modelling: Geologica Carpathica, 49, 2, 75-83.

Bielik, M., Makarenko, I., Starostenko, V., Legostaeva, O., Dérerová, J., Šefara, J., Pašteka, R., 2005. New 3D gravity modeling in the Carpathian-Pannonian basin region. In Contributions to Geophysics and Geodesy. Vol. 35, no. 1, p. 65-78.

Bocin, A., Stephenson, R., Tryggvason, A., Panea, I., Mocanu, V., Hauser, F., Matenco, L., 2005. 2.5 D seismic velocity modelling in the south-eastern Romainan Carpathians Orogen and its foreland, Tectonophysics, Volume 410, 273-291.

Bocin, A., Stephenson, R., Mocanu, V., Matenco, L., Architecture of the south-eastern Carpathians nappes and Focsani Basin (Romania) from 2D ray tracing of densely-spaced refraction data, Tectonophysics (2009), doi:10.1016/j.tecto.2009.07.027

Botezatu, R., Calota, C., 1983. Asupra anomaliei cimpului geomagnetic situata la nord-est de Suceava. Stud. Cerc. Geol. Geofiz. Geogr., Set. Geofiz. 9.

Cantini, P., Faggioni, O., Pinna, E., Soare, A., Stanica, D., Stanica, M., 1991. Structure of the transition from the Hercynian lithosphere to the East European platform in Romania (Tornquist–Teisseyre zone). Atti del 10 Convegno Annuale del Gruppo Nazionale di Geofisica della Terra Solida, Roma, 6–8 Novembre, pp. 601–613.

Chalot-Prat, F., Girbacea, R., 2000. Partial delamination of continental mantle lithosphere, uplift-related crust–mantle decoupling, volcanism and basin formation: a new model for the Pliocene–Quaternary evolution of the southern East-Carpathians, Romania. Tectonophysics 327, 83 – 107.

Christensen, N. I., Mooney, W. D., 1995. Seismic velocity structure and composition of the continental crust; a global view. J. Geophys. Res., 100, 9761– 9788.

Cloetingh, S. A. P. L., Burov, E., Matenco, L., Toussaint, G., Bertotti, G., Andriessen, P. A. M., Wortel M. J. R., Spakman, W., 2004. Thermo-mechanical controls on the mode of continental collision in the SE Carpathians (Romania). Earth and Planetary Science Letters, Volume 218, 57-76.

Cloetingh, S., Burov, E., Matenco, L., Toussaint, G., Bertotti, G., Andriessen, P.A.M., Wortel, M.J.R., Spakman, W., 2004. Thermo-mechanical controls on the mode of continental collision in the SE Carpathians (Romania). Earth Planet. Sci. Lett. 218, 57 – 76.

Cornea, I., Radulescu, F., Pompilian, A., Sova, A., 1981. Deep seismic sounding in Romania, Pure Appl. Geophys. 119, pp. 1144–1156.

Csontos, L., 1995. Tertiary tectonic evolution of the Intra-Carpathian area: a review. Acta Vulcanol. 7, 1–13.

Csontos, L., Voros, A., 2004. Mesozoic plate tectonic reconstruction of the Carpathian region, Palaeogeography, Palaeoclimatology, Palaeoecology, Volume 210, Issue 1, Pages 1-56.

Dadlez, R., Kowalczeski, Z., Znosko, J., 1994. Some key problems of the pre-Permian tectonics of Poland. Geol. Quart., 38 (2): 169–189.

Demetrescu, C., Wilhelm, H., Ene, M., Andreescu, M., Polonic, G., Baumann, C., Dobrica, V., Serban, D. Z., 2005. On the geothermal regime of the foreland of the Eastern Carpathians bend, Journal of Geodynamics, Volume 39, Issue 1, Pages 29-59.

Dicea, O., 1996. Tectonic setting and hydrocarbon habitat of the Romanian external Carpathians. In: P.A. Ziegler and F. Horváth, Editors, Peri-Tethys Memoir: 2. Structure and Prospects of Alpine Basins and ForelandsMém. Mus. Natl. Hist. Nat. vol. 170, Mémoires du Muséum National d'Histoire Naturelle, Publications Scientifiques, Diffusion, Paris, pp. 403–425.

Ellouz, N., Roca, E., 1994. Palinspastic reconstructions of the Carpathians and adjacent areas since the Cretaceous: a quantitative approach. In: F. Roure, Editor, *Peri-Tethyan Platforms*, Editions Technip, Paris, pp. 51–78.

Enciu, D. M., Knapp, C. C., Knapp, J. H., 2009. Revised crustal architecture of the southeastern Carpathian foreland from active and passive seismic data, Tectonics, 28, TC4013, doi:10.1029/2008TC002381.

Enescu, D., Danchiv, D., Bala, A., 1992. Lithosphere structure in Romania II. Thickness of the Earth crust. Depth-dependent propagation velocity curves for the P and S waves, Stud. Cercet. Geol. Geofiz. Geogr., Ser. Geofiz. 30, pp. 3–19.

Gardner, G. H. F., Gardner, L. W., Gregory, A. R., 1984. Formation velocity and density -The diagnostic basics for stratigraphic traps, Geophysics 39, 770-780.

Gee, D.G., Zeyen, H.J., (editors), 1996. EUROPROBE 1996 - Lithospheric dynamics: Origin and evolution of continents. Publ by the EUROPROBE Secretariate, Uppsala University, 138 pp.

Georgiev, G., Dabovski, C., Stanisheva-Vassileva, G., 2001. East Srednogorie–Balkan rift zone. In: P.A. Ziegler, W. Cavazza, A.H.F. Robertson and S. Crasquin-Soleau, Editors, Peri-Tethys Memoir 6: Peri-Tethyan Rift/Wrench Basins and Passive Margins. Mémoires du Muséum Nationale d'Histoire Naturelle, pp. 259–293.

Girbacea, R., Frisch, W., 1998. Slab in the wrong place: lower lithospheric mantle delamination in the last stage of the Eastern Carpathian subduction retreat. Geology 26, 611 – 614.

Grosse, S., Conrad, W., Behr, H. J., Heinrichs, T., 1990. Major gravity axes and anomalies in central Europe. The European Geotraverse: integrative studies1: 35–146. Rauischholzhausen, European Sc. Foundation, Strasbourg.

Guterch, A., Grad, M., Materzak, R., Perchuc, E., 1986. Deep structure of the Earth's crust in the contact zone of the Paleozoic and Precambrian platforms in Poland (Tornquist – Teisseyre Zone). Tectonophysics, 128, pp. 251–279.

Hauser, F., Raileanu, V., Fielitz, W., Bala, A., Prodehl, C., Polonic, G., Schulze, A., 2001. VRANCEA'99 – the crustal structure beneath the southeastern Carpathians and the Moesian Platform from a seismic refraction profile in Romania. Tectonophysics, 340, 233-256.

Hauser, F., Raileanu, V., Fielitz, W., Dinu, C., Landes, M., Bala A., Prodehl, C., 2007. Seismic crustal structure between the Transylvanian Basin and the Black Sea, Romania. Tectonophysics.Volume 430, 1-25.

Houseman, G.A., Gemmer, L., 2007. Intra-orogenic and extension driven by lithospheric gravitational instability: Carpathian–Pannonian orogeny, Geology 35 (12), pp. 1235–1238.

Hippolyte, J.C., Sandulescu, M., 1996. Paleostress characterization of the 'Wallachian phase' in its type area (southeastern Carpathians, Romania), Tectonophysics, Volume 263, Issues 1-4, Pages 235-248.

Hippolyte, J.C., 2002. Geodynamics of Dobrogea (Romania): new constraints on the evolution of the Tornquist-Teisseyre Line, the Black Sea and the Carpathians, Tectonophysics, Volume 357, Issues 1-4, Pages 33-53.

Iancu, V., Berza, T., Seghedi, A., Gheuca, I., Hann, H.P., 2005. Alpine polyphase tectono-metamorphic evolution of the South Carpathians: A new overview, Tectonophysics, Volume 410, Issues 1-4, The Carpathians-Pannonian Basin System - Natural Laboratory for Coupled Lithospheric-Surface Processes, Pages 337-365.

Ioane, D., Ion, D., 2005. A 3D crustal gravity modelling of the Romanian territory Journal of Balkan Geophysical Society, Vol.8, No 4, p.189-198

Ionesi., L., 1989. Geologia României: unitati de platforma si orogenul Nord Dobrogean (translated title: The geology of Romania: platform units and the North-Dobrogean orogen). Thesis, Univ. Al. I. Cuza, Iasi, Romania. 253 pp. (in Romanian).

Knapp, J.H., Knapp, C.C., Raileanu, V., Matenco, L., Mocanu, V., Dinu, C. 2005. Crustal constraints on the origin of mantle seismicity in the Vrancea Zone, Romania: the case for active continental lithospheric delamination. Tectonophysics, Volume 410, 311-323.

Królikowski, C., Petecki, Z., 1997. Crustal structure at the Trans-European Suture Zone in northwest Poland based on gravity data. In: Geol. Mag. vol. 134 (5), Cambridge Univ. Press, Cambridge, pp. 661–667.

Kutek, J., 1997. The Polish Permo-Mesozoic rift basin. In: IGCP Project No. 369 Comparative Evolution of Peri-Tethyan Rift Basins, Abstract Book, 4th Annual Meeting and Fieldtrip, 29 August–3 September 1997, Barcelona, Spain.

Landes, M., Fielitz, W., Hauser, F., Popa, M. & CALIXTO group, 2004. 3-D upper-crustal tomographic structure across the Vrancea seismic zone, Romania, Tectonophysics, 382, 85–102.

Leever, K.A., Matenco, L., Bertotti, G., Cloetingh, S.A.P.L., and Drijkoningen, G.G., 2006, Late orogenic vertical movements in the Carpathian Bend Zone - seismic constraints on the transition zone from orogen to foredeep: Basin Research, Volume 18, 521-545.

Ludwig, W. J., Nafe, J. E., Drake, C. L., 1970. Seismic refraction, in The Sea, A. E.Maxwell, (Editor) Vol. 4, Wiley-Interscience, New York, 53–84.

Martin, M., Ritter, J.R.R., the CALIXTO working group, 2005. High-resolution teleseismic body-wave tomography beneath SE Romania—I. Implications for three-dimensional versus one-dimensional crustal correction strategies with a new crustal velocity model, Geophys. J. Int. 162, pp. 448–460.

Martin, M., Wenzel, F., the CALIXTO Working Group, 2006. High-resolution teleseismic body wave tomography beneath SE - Romania – II. Imaging of a slab detachment scenario. Geophysical Journal International, 164: 579-595.

Matenco, L., Bertotti, G., Cloetingh, S., Dinu, C., 2003. Subsidence analysis and tectonic evolution of the external Carpathian–Moesian Platform region during Neogene times. Sedimentary Geology, Volume 156, Issues 1-4, 71-94.

Matenco, L., G. Bertotti, K. Leever, S. Cloetingh, S. Schmid, M. Tarapoanca, and C. Dinu, 2007. Large-scale deformation in a locked collisional boundary: Interplay between subsidence and uplift, intraplate stress, and inherited lithospheric structure in the late stage of the SE Carpathians evolution, Tectonics, 26, TC4011, doi: 4010.1029/2006TC001951.

Mocanu, V., Dinu, C., Radulescu, F., Diaconescu, M., 1996. Seismogeological features of the crust in România, in Wessely G. and Leibl. W.(eds.), "Oil and Gas in Alpidic Thrustbets and Basins of Central and Eastern Europe", EAGE Sp. Publ.No.5, p.289-299.

Morley, C.K., 1996. Models for relative motion of crustal blocks within the Carpathian region, based on restorations of the outer Carpathian thrust sheets. Tectonics 15, 4, pp. 885–904.

Mucuta, D., Knapp, C., Knapp, J., 2006. Constraints from Moho geometry and crustal thickness on the geodynamic origin of the Vrancea Seismogenic Zone (Romania), Tectonophysics, Volume 420, Issues 1-2, Seismic Probing of Continents and their Margins, Pages 23-36.

Oncescu, M. C., Bonjer, K.P., 1997. A note on the depth recurrence and strain release of large Vrancea earthquakes, Tectonophysics, Volume 272, Issues 2-4, Tectonics of the Alpine-Carpathian-Pannonian Region, II, Pages 291-302.

Panea, I., Stephenson, R., Knapp, C., Mocanu, V., Drijkoningen, G., Matenco, L., Knapp, J., Prodehl, K. 2005. Near-vertical seismic reflection image using a novel acquisition technique across the Vrancea Zone and Foscani Basin, south eastern Carpathians. Tectonophysics, Volume 410, 293-309.

Pharaoh, T. C., England, R.W., Verniers, J., Zelazniewicz, A., 1997. Introduction: geological and geophysical studies in the Trans-European Suture Zone. Geol. Mag., 134 (5): 585–590.

Pharaoh, T.C., Winchester, J.A., Verniers, J., Lassen, A., Seghedi, A., 2006. The Western Accretionary Margin of the East European Craton: an overview Geological Society, London, Memoirs, 32(1): 291 - 311.

Radulescu, D.P., Cornea, I., Săndulescu, M., Constantinescu, P., Rădulescu, F., Pompilian, A., 1976. Structure de la croûte terrestre en Roumanie. Essai d'interprétation des études séismiques profondes. Anu. Inst. Geol. Geofiz. 50, pp. 5–36 (in French).

Radulescu, F., Constantinescu, P., Pompilian, A., Ibadof, N., Sova, A., 1979. Crustal structure along the profile Galati-Oradea from seismic data. Studii tehnice si economice, seria D 12, 69–80.

Radulescu, F., 1981. Crustal seismic studies in Romania. Rev.Roum. Geol. Geophys. Geogr. Ser. Geophys., 25: 57-74.

Radulescu, F., 1998. Seismic models of the crustal structure in Romania. Rev. roum. géol. géophys., géogr. (Géophysique), 32, 13–17.

Raileanu, V., Diaconescu, C., Radulescu, F., 1994. Characteristics of Romanian lithosphere from deep seismic reflection profiling. Tectonophysics 239, pp. 165–185.

Raileanu, V., Bala, A., Hauser, F., Prodehl, C., Fielitz, W., 2005. Crustal properties from S-wave and gravity data along a seismic refraction profile in Romania. Tectonophysics, Volume 410, Issues 1-4, 251-272.

Russo, R.M, Mocanu, V., Radulian, M., 2005. Seismic attenuation in the Carpathian bend zone and surroundings. Earth and Planetary Science Letters, 237 (3-4): 695-709.

Saintot, A., Stephenson, R., Stovba, S., Brunet, M-F., Yegorova, T., Starostenko, V., 2006. The south margin of the East European continent: its evolution during the Paleozoic and Early Mesozoic, in: Gee D.G. and Stephenson R.A. (Eds.), European Lithosphere Dynamics, Geological Society of London, Memoir 32: 277-289.

Sandulescu, M., Stefanescu, M., Butac, A., Patrut, I., Zaharescu, P., 1981. Genetical and structural relations between flysch and molasse (The East Carpathians), Carp.-Balc. In: Assoc., XII Congr., Guide of Excursions vol. A5, Institute of Geology and Geophysics, Bucharest, 95 pp.

Sandulescu, M., 1984. In: Geotectonica Romaniei, Ed. Tehnica, Bucharest, 336.

Sandulescu, M., Visarion, M., 1988a. La structures des plateformes situées dans l'avant-pays et audessous des nappes du flysch des Carpathes Orientales, Stud. Teh. Econ. - Inst. Geol., Ser. D Prospect. Geofiz. 15, pp. 61–68.

Sandulescu, M., 1988b. Cenozoic tectonic history of the Carpathians. In: Royden, L.H., Horvath, F. (Eds.), The Pannonian Basin, A Study in Basin Evolution. AAPG memoir, pp. 17 – 25.

Sandulescu, M Visarion, M., 2000. Crustal structure and evolution of the Carpathianwestern Black Sea area. EAEG, First Break, 18, 3, 103–108.

Schmid, S., Bernoulli, D., Fügenschuh, B., Matenco, L., Schefer, S., Schuster, R., Tischler, M. and Ustaszewski, K., 2008. The Alpine-Carpathian-Dinaridic orogenic system: correlation and evolution of tectonic units. Swiss Journal of Geosciences, 101(1): 139-183.

Schweitzer, J., 1995. Blockage of regional seismic waves by the Teisseyre-Tornquist zone. Geophys. J. Int., 123: 260–276.

Seghedi, A., 2001. The North Dobrogea orogenic belt (Romania): a review. In: Ziegler, P.A., Cavazza, W., A.H.F. Robertson & Crasquin-Soleau, S. (eds) Peri-Tethys Memoir 6: Peri-Tethyan Rift/Wrench Basins and Passive Margins. Memoires du Museum National d'Histoire Naturelle, Paris, 186, 237-257.

Seghedi, I., Downes, H., Harangi, S., Mason, P.R.D., Pecskay, Z., 2005. Geochemical response of magmas to Neogene-Quaternary continental collision in the Carpathian-Pannonian region: A review, Tectonophysics, Volume 410, Issues 1-4, The Carpathians-Pannonian Basin System - Natural Laboratory for Coupled Lithospheric-Surface Processes, Pages 485-499.

Sliaupa, S., Fokin, P., Lazauskiene, J. Stephenson, R. A., 2006. Vendian–Early Palaeozoic Sedimentary basins of the East European Craton. In: GEE, D. G. & STEPHENSON, R. A. (eds) European Lithosphere Dynamics. Geological Society, London, Memoris, 32, 449–462.

Sperner, B., Lorenz, F.P., Bonjer, K.-P., Hettel, S., Muller, B., Wenzel, F., 2001. Slab break-off — abrupt cut or gradual detachment? New insights from the Vrancea Region (SE Carpathians, Romania). Terra Nova 13 (3), 172 – 179.

Sperner, B., Ioane, D., Lillie, R.J., 2004. Slab behavior and its surface expression: new insights from gravity modelling in the SE-Carpathians. Tectonophysics 382, 51– 84.

Stanica, D., Stanica, M., 1993. An electrical resistivity lithospheric model in the Carpathian Orogen from Romania, Phys. Earth Planet. Inter., 81, 99–105.

Stanica, M., Stanica, D., Marin-Furnica, C., 1999. The placement of the Trans-European Suture Zone on the Romanian territory by electromagnetic arguments. Earth Planets Space 51:1073–1078.

Stefanesc u, M., 1976. O noua imagine a structurii flisului intern din regiunea de curbura a Carpaților. Dari de Seama ale Institutului de Geologie si Geofizica LXII/5, p. 257-279.

Stefanescu, M., and Working Group, 1988. Geological cross sections at scale 1:200,000, Map A9-14, Inst. Geol. Geofiz., Bucharest.

Stefanescu, M, 2006. Subcarpathian Nappe - Analysis of Hydrocarbon Prospectivity in the Gresu and Nereju Blocks. Rompetrol E&P Report, Bucharest.

Stephenson, R.A., Mart, Y., Okay, A., Robertson, A., Saintot, A., Stovba, S., Khriachtchevskaia, O., 2004. TRANSMED Transect VIII: Eastern European Craton to Arabian Craton (Red Star to Red Sea). In: W. Cavazza, G. Stampfli and P. Ziegler, Editors, The TRANSMED Atlas—The Mediterranean Region from Crust to Mantle, Springer Verlag, Berlin.

Szafian P., Horvath F., 2006. Crustal structure in the Carpatho-Pannonian region: insights from three-dimensional gravity modelling and their geodynamic significance. Int. J. Earth Sci (Geol Rundsch) 95: 50–67.

Talwani, M, Worzel, JL, and Landisman, M, 1959. Rapid Gravity Computations for Two-Dimensional Bodies with Application to the Mendocino Submarine Fracture Zone, Journal of Geophysical Research, 64:49-61.

Talwani, M., Heirtzler, J.R., 1964. Computation of magnetic anomalies caused by two-dimensional structures of arbitrary shape. Computers in the Mineral Industries, George A. Parks (ed.), School of Earth Sciences, Stanford University (Publc.), 464-480,.

Tarapoanca, M., Bertotti, G., Matenco, L., Dinu, C., Cloetingh, S., 2003. Architecture of the Focsani Depression: a 13 km deep basin in the Carpathians Bend Zone (Romania). Tectonics, Volume 22, 1074.

Tarapoanca, M., 2004. Architecture, 3D geometry and tectonic evolution of the Carpathians foreland basin. PhD Thesys, Vrije Universiteit, Amsterdam, The Netherlands.

Tari, G., Dicea, O., Faulkerson, J., Georgiev, G., Popov, S., Stefanescu, M., Weir, G., 1997. Cimmerian and Alpine stratigraphy and structural evolution of the Moesian platform (Romania/Bulgaria). In: Robinson, A.G., Editor, , 1997. Regional and petroleum geology of the Black Sea and surrounding regions AAPG Memoir 68, pp. 63–90.

Vaida, M., 1999. Dating and correlation, on the basis of the palynological associations, of the metamorphic formations from the southern part of the Eastern Carpathians and the eastern part of the South Carpathians (in Romanian). Ph.D. Thesis, "Al. I. Cuza" University, Iasi, Romania.

Vaida, M., Seghedi, A., Verniers, J., 2005. Northern Gondwanan affinity of the East Moesian Terrane based on chitinozoans, Tectonophysics, Volume 410, Issues 1-4, The Carpathians-Pannonian Basin System - Natural Laboratory for Coupled Lithospheric-Surface Processes, Pages 379-387.

Veliciu, S., Visarion, M., 1984. Geothermal models for the East Carpathians, Tectonophysics 103, pp. 157–165.

Visarion, M., Veliciu, S., Stefanescu, M., Čermák, V., 1978. Thermal field in the Romanian Carpathian bend and some aspects of its interpretation Studia Geophysica et Geodaetica,Volume 22, Issue - 2,196-200.

Visarion, M., Sandulescu, M., Stanica D., Veliciu, S., 1988a. Contributions a la connaissance de la structure profonde de la platforme Moesienne en Roumanie, Stud. Teh. Econ. - Inst. Geol., Ser. D Prospect. Geofiz. 15, pp. 211–222.

Visarion, M., 1998b. Gravity anomalies on the Romanian territory, CERGOP "South Carpathians" monograph vol. 7 (37) (1998), pp. 133–138 Warszawa.

Wenzel, F., Achauer, U., Enescu, D., Kissling, E., Russo, R., Mocanu, V., 1998a. The final stage of plate detachment: international tomographic experiment in Romania aims to a high-resolution snapshot of this process. EOS.

Wenzel, F., Lorenz, F.P., Sperner, B., Oncescu, M.C., 1998b. Seismotectonics of the Romanian Vrancea area. In: Wenzel, F., Lungu, D. (Eds.),Vrancea Earthquakes. Kluwer Academic Publishers, Dordrecht, Netherlands.

Wenzel, F., Lungu D., Novak, O.,1999. Vrancea earthquakes: tectonics, hazard and risk mitigation, Kluwer Academic Publishers, Netherlands.

Wenzel, F., Sperner, B., Lorenz, F., Mocanu, V., 2002. Geodynamics, tomographic images and seismicity of the Vrancea region (SE-Carpathians, Romania). EGU Stephan Mueller Special Publication Series, 3, 95-104.

Williamson, J.P., Pharaoh, T.C., Banka, D., Thybo, H., Laigle, M., Lee, M.K., 2002. Potential field modelling of the Baltica-Avalonia (Thorn-Torquist) suture beneath the southern North Sea. Tectonophysics, 360, 1, 47–60.

Winchester, J. A., The PACE TMR Network Team, 2002. Palaeozoic amalgamation of Central Europe: new results from recent geological and geophysical investigations. Tectonophysics, Volume 360, Issues 1-4, 5-21.

Won, I.J., Bevis, M.G., 1987. Computing the gravitational and magnetic anomalies due to a polygon: Algorithms and Fortran subroutines. Geophysics, 52, 232-238.

Wortel, M.J.R., Spakman, W., 2000. Subduction and slab detachment in the Mediterranean–Carpathian Region. Science 290, 1910 – 1917.

Yegorova, T.P., Starostenko, V.I., 2002. Lithosphere structure of European sedimentary basins from regional three-dimensional gravity modelling. Tectonophysics, Volume 346, Issues 1-2, 5-21.

Ziegler, P.A., 1981. Evolution of sedimentary basins in northern Europe. In: L. Illing and G.D. Hobson, Editors, Petroleum Geology, The Petroleum Institute, London, pp. 3–39.

Ziegler, P.A., 1990. Geological Atlas of Western and Central Europe, Shell International Petroleum Mij. B.V. dist. Geol. Soc. (2nd Ed.), Publishing House Bath, London, 239 pp.

Zielhuis, A., Nolet, G., 1994. Shear-wave variations in the upper mantle beneath Central Europe, Geophys. J. Int., 117, 695-715.

Zonenshain, L.P., Kuzmin, M.I., Natapov, L.M., 1990. Geology of the USSR: A plate tectonic synthesis. Geodynamic Series vol. 21, American Geophysical Union, Washington, 242 pp.

Znosko, J., 1979. Teisseyre-Tornquist tectonic zone: some interpretative implications of recent geological and geophysical investigations. Acta Geol. Pol., 29: 365–382.

Zweigel, P., Ratschbacher, L., Frisch, W., 1998. Kinematics of an arcuate fold–thrust belt: the southern Eastern Carpathians (Romania), Tectonophysics 297 (1–4), pp. 177–207.

CHAPTER VI
CONCLUSIONS

"Under normal conditions the research scientist is not an innovator but a solver of puzzles, and the puzzles upon which he concentrates are just those which he believes can be both stated and solved within the existing scientific tradition."

Thomas Kuhn

The general objectives of this thesis were stated in the *Introduction* chapter as to conduct novel methods of geophysical data acquisition and processing, to model the data using geophysical forward or inverse methods and to integrate the results from different sets of data to infer interpretations of crustal structure in the area of the south-eastern Carpathians, Vrancea Zone and Focsani Basin. In this final chapter the particular solutions to the problem statements for each study of the correspondent chapters (tomography, ray tracing and gravity and magnetic from acquisition to interpretation) are summarized, after which an outlook for further research is proposed. The PhD research of this thesis was accomplished in the framework of the ISES Pannonian-Carpathian programme and the results were partly integrated or correlated with results from different projects performed in the same framework.

6.1. Synthesis

6.1.1. Seismic tomography modelling results

The seismic tomography technique was a novel approach to DACIA PLAN seismic datasets where first arrival travel times were inverted in order to obtain an accurate upper crustal velocity model of the south-eastern Carpathians, Vrancea Zone and Focsani Basin. The 2.5D seismic velocity model coverage and its power of resolution offered a considerable amount of significant information related to depth to basement and lateral structural heterogeneities at the basement level and beneath the Focsani Basin. A pre-Tertiary basement in the Vrancea Zone was determined to be shallower (<5 km) than previously deduced in published geological cross-sections (where it is taken to be as deep as 8–10 km) and indeed shallower than the less resolved basement "uplift" in the same and surrounding areas inferred from the 3D regional upper crustal tomographic model (CALIXTO – VRANCEA99 and VRANCEA2001). Also, complexities observed in the travel time data and their implications for the velocity modelling suggest that basement material is involved in Carpathian thrusting. A low velocity structure was identified within the model but its origins were unclear at the time the tomographic inversion was performed. Now the low velocity deepening anomaly in the model is interpreted as being the Subcarpathians nappe underlain by the Upper Sarmatian-Quaternary sediments of the Focsani Basin. The velocity perturbations (basement domain) in the eastern extremity of the model are interpreted as being the results of basement involved deformation on or near the Peceneaga-Camena fault, as also implied by a number of previous seismic industry lines. The depth of the velocity depression correspondent to Focsani Basin is also correlatable with previous studies.

6.1.2. Seismic ray tracing modelling results

The forward seismic ray tracing was performed in order to constrain the velocity structures inferred by the previous tomographic experiment and to derive a better, layered model with greater potential for a structural and geological interpretation. The methodology used in the approach allowed constraints on the model by introducing geological and structural features into a seismological tool and, as such, represented a new concept of handling seismic datasets. Also, two new notions were defined in the modelling procedure: "*long wavelength*" anomalies that incorporate information from 5 to 15 studied shots (20-40 km), representing robust features of the model; and "*short wavelength*" anomalies that bear seismic information from 2 to 3 shots (5-10 km), perturbing the velocity locally. A comparison between the tomographic model and the ray tracing model was performed and explained in Chapter III. The conclusion was that a number of structures are quite robust but that

performing ray tracing could lead to a better structural (resolution) understanding of their origins and occurrences.

But the seismic ray tracing did not represent only a reiterative velocity modelling procedure and, indeed, it confirmed and resolved a number of partly new issues and led to new discoveries about the basement structure beneath the south-eastern Carpathian nappe stack and Focsani Basin. The seismic velocity ray tracing modelling results shows (here are mentioned briefly as they are presented in greater detail in Chapter III): velocity anomalies at the base of the supra-basement layer associated with faults or systems of faults; reverse faulting allowing crystalline rocks or highly metamorphosed sedimentary cover to be elevated to quite shallow levels (3.5-4 km); crustal earthquakes associated with some of the fault traces; the Carpathian Vrancea Zone uplift through mapped faults coupled with the adjacent Focsani Basin subsidence on normal faults and flower structures; the seismic activity on the traces of the inferred faults revealing that the topographic evolution in the area is coupled with a coevally synchronous uplift-subsidence within the larger regional Pannonian-Carpathian system.

6.1.3. Gravity and magnetic modelling results

Crustal scale gravity and magnetic modelling was performed using densely spaced sets of data acquired on the same path as the seismic experiments (coinciding with the DACIA PLAN seismic profile for 71 km) but intentionally lengthened to the west by a few kilometres in order to cover the targeted shallower positioned basement material previously constrained by the seismic methods. The interpretation of the modelling results focused on three depth levels: first, the relatively shallower but very well constrained nappe complex and foreland basin; second, the supra-basement and relict pre-orogenic rifted basin partially constrained from previous seismic data but so far impossible to map in the direction of the profile; and third, the crustal units beneath the thick succession of structures, their base (Moho topography) being constrained by previous refraction seismic models. The modelling technique included a set of a priori conditions, being mainly the constraints coming from the previous seismic deep reflection or refraction experiments.

The implications of the results are discussed in greater detail in Chapter V but some important conclusions are reiterated here. The supra-basement layer is coevally present until a certain, inferred lateral boundary; its upper and lower boundaries, along with fractures that offset these, represented important signals whilst modelling. The presence of the thickened Upper Palaeozoic - Lower Mesozoic sedimentary succession (***Palaeozoic - Mesozoic "rift")*** and its thickness and lateral extent (same boundary as the ***supra-basement*** unit) was required by the gravity and

magnetic anomaly shapes and gradients. The modelling results shows that the Palaeozoic European "geophysical" crust is less dense and less magnetically susceptible, while the East European "geophysical" crust is denser and more magnetically susceptible, inferences that are correlatable with the results recorded in similar potential field studies. The Moesian Platform contains a sedimentary sequence that is specific to the Palaeozoic Europe but its Precambrian metamorphosed basement yields a geophysical signal that is typical East-European while areas of the Moesian Platform which contain Palaeozoic metamorphism (specifically the Danubian block) yield a geophysical signal that is characteristic for Palaeozoic Europe. Consequently, the crustal affinities and geophysical contrasts inferred in this study lead to the conclusion that the Teisseyre-Tornquist Zone is localized beneath the south-eastern Carpathians. The interpretation was tested within a regional context by analysing schematically the gravity and magnetic anomalies compiled from satellite or other sources and a new path of the Teisseyre Tornquist Zone in the south-eastern Carpathians area was proposed.

6.2. Integration and discussion

The seismic modelling results show basement material being uplifted (2 to 2.5 km) on crustal faults whilst the thick sedimentary succession undergoes accentuated subsidence (~ 12 km). Some of the identified crustal faults are also presently active, as is constrained by recorded seismic activity along the traces of the faults where the uplift-subsidence processes occur. The imaging result of the gravity and magnetic modelling correlates very well with the seismic interpretation in part because some of the seismic information was used as a priori constraint but also because of the robust signal given by the modelled structures regardless of physical significance (Fig 6.1). The ***Palaeozoic - Mesozoic "rift"*** identified while interpreting the seismic stack of the DACIA PLAN seismic survey is also recovered by the potential field modelling. The fundamental contrast between the strongly magnetic crust of the East European Craton and the less magnetic crust of Phanerozoic-accreted Europe (strong gravity gradient zone) that has been modelled lead to the conclusion that the Teisseyre-Tornquist Zone is localized beneath the south-eastern Carpathians. Though the gravity and magnetic modelling did not revealed a subduction-related suture zone on the path of the profile, the subduction or a major continental underthrusting zone can be present at the same contact between blocks with different European crustal affinities and can take place beneath the Danubian nappes (previously demonstrated by other studies).

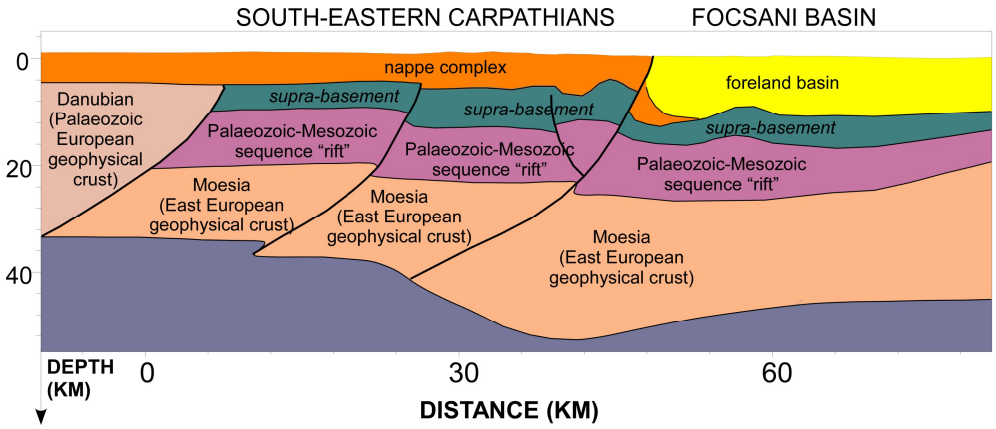

Fig. 6.1. Simplified crustal scale cross-section inferred from seismic, gravity and magnetic data modelling. The vertical scale exaggeration is 1.7. For further lithospheric details and the geometry of the Vrancea slab see Figure 1.5 and Martin et al. (2006). Note the crustal displacement of the Moesia blocks (East European geophysical crust) and the Moho topography.

A possible scenario for the tectonic evolution in the area of the south eastern Carpathians and the Focsani Basin, that is consistent with the geophysical inferred crustal structure and lithospheric heterogeneities, is proposed in the following paragraphs. This scenario contains three scenes: the first scene is related to the eastern Moesian Platform units being accreted to the south western margin of the East European craton; the second scene represents the behaviour of the accreted Moesian Platform units while subduction of an oceanic plate to its western margin is consumed (slab roll back and following detachment); and third scene the post subduction and ongoing collision tectonics and neotectonics.

The first scene suggests that the Moesian Platform units were accreted to the East European craton. From here on two tectonic interpretations could be forwarded: the first suggests a divergent passive margin whereas the Variscan orogeny represents a soft collision, a transitional crust is formed (distal Moesian blocks) and the allochtoon mantle is being accreted to Baltica; the second refers to an abrupt transtensional margin where the Baltica westward extension is limited, a rifted crust is formed and a rifted mantle between the accreted and Baltica mantle is formed too. Both scenes development are very much in agreement with other previous studies about the crustal and lithospheric processes along the Teisseyre Tornquist Zone.

The second scene will follow the classical scenario of an oceanic slab subduction, whereas an oceanic plate developed between the Danubian Moesian Platform unit and the accreted to Baltica Moesian Platform units (one of the previous interpretation) is subducted. The Danubian Moesian Platform unit is accreted to the upper plate at the end of the Cretaceous.

The third scene starts during Late Miocene when the subducted slab has been rolled back and portions of it are partially detached. The continental collision starts to deform the lower plate whereas crustal thrust begin to appear. The lower plate role in this case is played by the previously accreted to Baltica Moesian Platform units. The gradual accretion of the lower plate or the collisional coupling/foreland coupling* is concordant with crustal thickening towards the lower plate.

Therefore this scenario in three scenes correlates/accommodates well with the lithospheric heterogeneities, the crustal thickening or the lower plate uplift recorded in the area of the south eastern Carpathians and its foreland. Furthermore, the units implicated in this scenario gives the right geophysical signature correspondent to a contact between units of Baltican and Phanerozoic Europe origins. The tectonic scenario that was presented here tough it does not go into further tectonic details presents otherwise a possible evolution at crustal and litosperic scale of the south eastern Carpathians and its foreland.

6.3. Future directions

The different studies presented in this thesis represent a foundation for future research. Further progress can potentially be achieved by improving various techniques that were used in the processing, modelling and interpretation processes applied to the DACIA-PLAN data. New processing techniques applied to the DACIA PLAN or similar datasets that filters the multiples or ground-roll could increase the signal to noise ratio and therefore the quality of the seismic inputs and improved seismic stack and their interpretations can increase considerably. The 2D ray tracing modelling can be performed with a different algorithm in order to be able to model back-thrusts (NORSAR 2D and 3D modelling programs, for example, techniques that were not in our possession at the time the present work was undertaken). The seismic interpretation would benefit if new datasets were to be acquired on parallel profiles such that lateral heterogeneities of the mapped structures could be imaged.

The degree of detail present on the existing compiled gravity and magnetic maps are barely sufficient and this study demonstrated that important structures and boundaries of various scale can be missed. The added value of densely spaced measurement is obvious especially in the case of the old compiled Romanian aeromagnetic map compared to the profile data and WDMAM map. The gravity and magnetic reduction methodology could be become more efficient if further proficient

* *Matenco, L., Krezsek, C., Merten, S., Schmid, S., Cloetingh, S. And Andriessen, P.A.M., 2010. Characteristics of collisional orogens with low topographic build-up: an example from the Carpathians. Terra Nova, in press.*

Microsoft Excel macros were to be created or the formulas would be imported and developed under the Oasis Montaj Software formulas editor. The acquisition of commercial software for correcting (Oasis Montaj module for terrain correction) the data can also offer a solution.

The acquisition of new data is crucial for future interpretations. Therefore, new potential field profiles should be projected to cover the main geological units or contact zones and their correlation with seismic data is imperative. The gravity and magnetic data were used already for performing automatic interpretations, Euler and Werner deconvolutions or Analytical Analysis, but further modelling is required. The results are not presented here as further filtering and modelling of the data needed to be performed and, coincidentally, did not represent one of the objectives of this thesis. The Geosoft software modules can efficiently perform such automatic interpretations and a standalone study is planned that will further constrain the present results. Another direction for improving the interpretation is to construct a 3D crustal structure model in the south-eastern Carpathians and its foreland basin based on all the accessible information that could support, in a robust way, gravity stripping, for example, at different depths or surfaces. This process is in development but the 3D crustal structure model is not yet complete due to insufficient data being available at this time. Further seismic data and structures inferred from these types of data and geological cross-sections are needed in order to obtain and integrate the crustal scale structure model. The gravity stripping procedure will be conducted in order to constrain also the presence of any subducted slab, hypothesised by some authors to be in the upper mantle in the study area. The interpretation of the results can be improved by performing further correlations with previous studies and especially by placing them in a regional context through integration with new studies and hypotheses as they are done and proposed to explain the geology and geodynamics of the south-eastern Carpathians and the Vrancea Zone.